2019

Thermo- and Zero-Valent Iron-Activated Persulfate Oxidation of 3,5,6-Trichloro-2-pyridinol in an Aquatic System

Roaa Mogharbel
University of Central Florida

THERMO- AND ZERO-VALENT IRON-ACTIVATED PERSULFATE OXIDATION OF 3,5,6-TRICHLORO-2-PYRIDINOL IN AN AQUATIC SYSTEM

by

ROAA MOGHARBEL
B.S. Taibah University, Saudi Arabia, 2008
M.Sc. Florida Institute of Technology, Melbourne, 2013

A dissertation submitted in partial fulfillment of the requirements
for the degree of the Doctor of Philosophy
in the Department of Chemistry
in the College of Sciences
at the University of Central Florida
Orlando, Florida

Fall Term
2018

Major Professor: Cherie L. Yestrebsky

ABSTRACT

The compound 3,5,6-trichloro-2-pyridinol (TCPy), a metabolite of the broad-spectrum organophosphorous insecticide chlorpyrifos, is both more persistent and more water soluble than its parent compound. This difference, which allows TCPy to more readily leach into surface water and groundwater, has led to widespread contamination of TCPy in soils and aquatic environments. In this study, the degradation of TCPy by sulfate radicals was evaluated using zero valent iron-activated persulfate systems and heat activated persulfate system in aqueous media. Response surface methodology coupled with Box-Behnken design was applied in these studies to evaluate the effects of the independent variables on the mineralization of TCPy by both systems. In each system, the interactions, coefficients, and residuals of these variables were statically evaluated by Analysis of variance. Results indicate that both systems can effectively oxidized TCPy in water. While ZV/PS exhibited a high mineralization rate of TCPy up to 81.1%, TCPy was completely mineralized in heat activated PS system. The reaction kinetics of the degradation process were examined as functions of experimental parameters in each system and the result revealed that the oxidation of TCPy in both systems followed a pseudo-first-order model under all conditions tested. Radical scavenging tests indicated that sulfate radicals are the predominated species in zero valent iron activated persulfate system, whereas hydroxyl radicals are the predominated species in heat activated persulfate system. The presence of chloride, sulfate and phosphate anions showed negligible effects on TCPy oxidation by heat activated PS system. The degradation pathways of TCPy were proposed based on the products identified by GC-MS. Calculated ΔG values using density functional theory agreed with the proposed experimental pathway.

To my parent,
For their unconditional love and continuous prayers.
I know they are proud and pleased with this achievement.

To my husband, Mohammed,
For his care, endurance, and endless love.
I wouldn’t have made it this far without you!

To my siblings,
For filling my journey with continuous encouragement.

To my kids, Malik and Abd al-Rahman,
Since you were born, my life is greater than myself.
You are the reasons I strive to be better.

ACKNOWLEDGMENTS

My first and foremost sincere thanks and praise go to Allah for giving me the opportunity, knowledge, strength and patience needed to complete this doctoral journey.

I owe an incredible debt of thanks and appreciation to my research advisor, Prof. Cherie Yestrebsky, without her inspiration, support, and generous guidance, this doctoral research would not have been accomplished. Dr. Yestrebsky, you are an amazing professor, but first and foremost you are an amazing person; I am honored to have you as my advisor.

Sincere appreciation is also necessary to my exceptional committee members; Drs. Andrew Randall, Melanie Beazley, Shengli Zou and Tamra Legron-Rodriguez for their time, patience and consideration in reviewing my research efforts.

To my colleagues in the Industrial/Environmental Laboratory at UCF. I gained a lot from the experience and the time we had. Special thanks to Dr. Fiona Zullo, Nia Hurst, Muquiong Liu for their valuable help and to Charles Lewis for time he happily and graciously assisted throughout the process.

My sincere appreciation goes to my good friends Dr. Adibah Almutairi and Mohra Albalwi. The doctoral program is a challenging undertaking, full of difficulties and recurring, stressful deadlines. Your presence as friends and fellow aspirants made it enjoyable and it has truly filled my memory with unforgettable moments. Thank you for your unique friendship!

I am also thankful to my mother in law, Wafaa Satih for her prayers and support.

My heartfelt gratitude to my beloved husband Mohammed, your encouragement has supported me throughout these many years, and your understanding has kept me whole. I am very grateful you have been with me to make these the best years of my life. I love you!

I am infinitely thankful to my parents, Talaat Mogharbel and Nadyah Edreec, for giving me their unconditional love and teaching me the value of hard work and dedication to my aspirations and achievements. Dad and mom, nothing makes me happier than knowing you are proud of me! This is the culmination of our dreams, and it was only possible because you chose to give me the best education you could.

I hold deep appreciation to my brothers and sisters for their love and caring. Mohammed, Bander, Fahad, Amal, Ahmed, Rawan, Razan, Reham, Al-Hanoof and Abdulazeez, thank you for believing in me and foreseeing that I can achieve this. Special thank goes to my sister Amal, she has been alongside me on this journey and has always been supportive and positive, without her this work would have been much harder. I love you all!

Thanks to my kids Malik and Abd al-Rahman for fulfilling my life with everlasting joyful and happy moments. I love you to the moon and back.

TABLE OF CONTENTS

LIST OF FIGURES

LIST OF TABLES

LIST OF ACRONYMS/ABBREVIATIONS

ACN	Acetonitrile
ANOVA	Analysis of variance
AOPs	Advanced oxidation process
BBD	Box-Behnken design
CP	Chlorpyrifos
DFT	Density functional theory
EPA	Environmental Protection Agency
EtOH	Ethanol
HR	Hydroxyl radical
ISCO	*In situ* chemical oxidation
k_{obs}	Pseudo-first order apparent rate constant
k_{ow}	Octanol–water partition coefficient
MTBSTFA	N-tert-Butyldimethylsilyl-N methyltrifluoroacetamide
OCs	Organic contaminants
OPs	Organophosphates
PCM	Polarizable Continuum Model
PS	Persulfate
RSE	Reaction stoichiometric efficiency
RSM	Response surface methodology
SR	Sulfate radical
SR-AOP	Sulfate radical based advanced oxidation process

T	Temperature
TBA	Tert-butyl alcohol
TCPy	3,5,6-Trichloro-2-pyridinol
TOC	Total organic carbon
WHO	The World Health Organization
ZVI	Zero valent iron
ZVI/PS	Zero valent iron activated persulfate

CHAPTER ONE: GENERAL INTRODUCTION

Organophosphate Insecticides

Organophosphates (OPs) are a class of insecticides which were first synthesized in 1937 [1]. Organophosphate compounds have become widely used in agriculture, homes, gardens, and veterinary practices. Although OPs have played an important role in the protection of food and feed crops, their excessive use and persistence have caused many environmental concerns[2]. Because of possible effects of some OPs on human health and the environment, their production has been discontinued in the United States, such as parathion [2]. Additionally, residential use of chlorpyrifos was banned in the United States in the year 2000 [3].

The basic chemical structure of OP is presented in Figure 1. Most OP compounds are esters, amides, or thiol derivatives of the phosphoric, phosphonic, phosphoramidic, phosphorothioic, or phosphonothioic acids. The R_1 and R_2 are usually the aryl or alkyl group which can be directly bonded to the phosphorous atom (phosphinates), attached to the phosphorous atom via oxygen (phosphates), or linked to phosphorous via sulphur (phosphothioates). In phosphoramidates, either R_1 or R_2 is attached with un-, mono- or di-substituted amino groups. In phosphonates or thion phosphonates, phosphorus is bonded directly with R_1 while it is connected to R_2 through an oxygen or sulfur atom. The X group can be of many different types, such as aliphatic, aromatic, or heterocyclic groups.

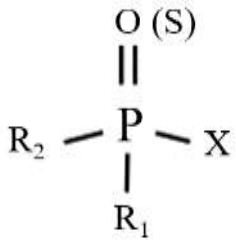

Figure 1: General formula of organophosphate pesticides.

The environmental behavior of OPs is controlled by their physical and chemical properties. The majority of OPs have a high octanol–water partition coefficient (k_{ow}), moderate water solubility, and low vapor pressures. At high temperature, phosphorothioates are oxidized to a toxic agent phosphate which is more volatile than its parent compounds. Under ultraviolet radiation, many organophosphate insecticides have been shown to be oxidized to byproducts that have more toxicity than their parent compounds. The hydrolysis of OPs is accelerated in basic pH [4]. Today, more than 200 different organophosphate insecticides are regularly manufactured. Among them, the common used OP compounds are triaziphos, chlorpyrifos, and fenitrothion

Chlorpyrifos

Chlorpyrifos (O,O-diethyl-O-3,5,6-trichloro-2-pyridyl phosphorothionate; CP) is a broad-spectrum insecticide which has been used for agriculture worldwide since 1965, though residential use was banned in the United States in the year 2002. Although CP has played an important role in the protection of food and feed crops, its excessive use and persistence have caused many environmental concerns, including CP contamination of soil and aquatic environments and measurable CP levels on products for human consumption.

The World Health Organization (WHO) has identified CP as moderately hazardous to humans. For instance, many studies have shown adverse effects on fetal development as a result of the exposure of expectant mothers to CP. Additionally, carcinogenicity studies of CP exposure suggested development of lung cancer and prostate cancer as the result of exposure to CP [5-6].

According to the United States Environmental Protection Agency (USEPA), there is a significant association between CP exposure and neurodevelopmental outcomes. For instance, studies on infants and children who were exposed to organophosphates during gestation have shown mental development delay, attention disorder and intelligence decrements in infants, early childhood and school age children, respectively [7].

Additionally, many studies have shown specific adverse effects (e.g. mental delay, psychomotor delay, attention disorder attention deficit hyperactivity disorder, and pervasive developmental disorders) were developed as the result of children's exposure to CP [7].

CP has been released into the environment through agricultural application, improper disposal, and industrial runoff [8]. Once in the environment, the phosphoester bond of CP is hydrolyzed to 3,5,6-trichloro-2-pyridinol (TCPy), which is the primary by product of CP (Figure 2). Also, photodegradation and microbial degradation of CP both demonstrate the formation of TCPy.

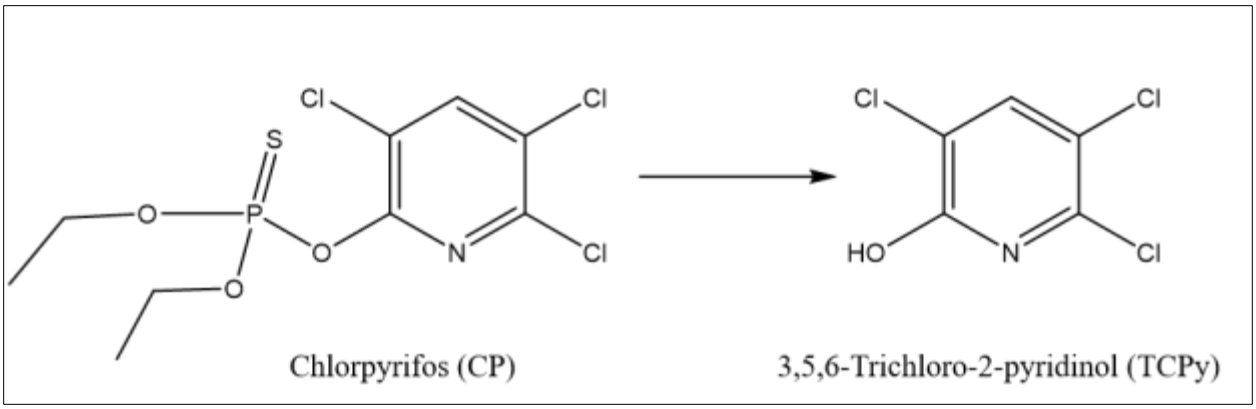

Figure 2: Chlorpyrifos and its hydrolysis product, 3,5,6-Trichloro-2-pyridinol (TCPy)

3,5,6-Trichloro-2-pyridinol (TCPy)

3,5,6-Trichloro-2-pyridinol (TCPy) is the main degradation byproduct of the widely used insecticide, chlorpyrifos. TCPy has been detected in many places where CP was applied. For instance, TCPy has been identified in such diverse sources as spinach, cauliflower, and potato crops; golf course leachate; and human urine. As one would expect, TCPy has been confirmed to be present in wastewater streams from both chlorpyrifos and methyl-chlorpyrifos manufacturing plants [9].

TCPy is more water soluble than its parent compound, and it is persistent compound according to the USEPA [10], which significantly increases its ability to leach into surface water and groundwater, causing widespread contamination in soils and aquatic environments [11-12].

Treatment Methods for Chlorpyrifos

Several treatment technologies have been used to degrade chlorpyrifos. For instance, a photocatalytic technology successfully achieved complete mineralization of chlorpyrifos using a UV/TiO_2/H_2O_2 process [13]. Also, a $CoFe_2O_4$@TiO_2/rGO nanocomposite was used to treat CP, and

was able to effectively degrade CP [14]. In addition to photocatalysis, CP was effectively degraded by using an ultrasonic method, and up to 82% of CP was degraded after two hours treatment [15]. Furthermore, electrochemical oxidation using a boron-doped diamond anode successfully degraded CP [16].

In situ chemical oxidation (ISCO) is becoming an effective technology for the remediation of contaminated soil and ground water. Among the different ISCO oxidants, persulfate has been intensively used due to its advantages such as its chemical stability at ambient temperature and its high aqueous solubility with a strong redox potential (Eq. 1.1)

$$S_2O_8^{2-} + 2e^- \rightarrow 2SO_4^{2-} \qquad E^0 = 2.01\ V \qquad (1.1)$$

However, for remediation applications, the activation of PS to generate highly reactive oxidants called sulfate radicals ($SO_4^{\bullet-}$, SR) with strong redox potential (E^0 = 2.5 - 3.1 V) is particularly significant.

Many activation methods have been developed to activate PS such as heat, UV, basic conditions, and transition metal ions [17].

$$S_2O_8^{2-} + heat/uv \rightarrow 2SO_4^{\bullet-} \qquad (1.2)$$

$$S_2O_8^{2-} + Me^{n+} \rightarrow SO_4^{2-} + SO_4^{\bullet-} + Me^{(n+1)+1} \qquad (1.3)$$

Iron [as iron (II), Fe^{2+}] is becoming favored over other common transition metals used in persulfate activation because it is nontoxic, cost effective and environmental friendly [18] (Eq 1.4). However, rapid scavenging of $SO_4^{\bullet-}$ occurred with excessive Fe^{2+}, which in turn reduces the efficiency of Fe^{2+}/ PS on contaminant degradation (Eq 1.5).

$$S_2O_8^{2-} + Fe^{2+} \rightarrow SO_4^{2-} + SO_4^{\bullet-} + Fe^{3+} \qquad (1.4)$$

$$Fe^{2+} + SO_4^{\bullet-} \rightarrow Fe^{3+} + SO_4^{2-} \qquad (1.5)$$

Recently, zero valent iron (ZVI) has been developed as an alternative activator of PS to overcome such a disadvantage. ZVI not only acts as a smooth releasing method of Fe^{2+}, but is also able to generate sulfate radicals directly (Eqs 1.6 and 1.7).

$$Fe^0 + 2H_20 \rightarrow Fe^{2+} + 2OH^- + H_2 \quad (1.6)$$

$$Fe^0 + 2S_2O_8^{2-} \rightarrow 2SO_4^{2-} + 2SO_4^{\bullet -} + Fe^{2+} \quad (1.7)$$

Thermally-activated PS has been applied to many environmental pollutants [17]. The applied temperature (30 ℃ – 99 ℃) plays an important role in the oxidation efficiency of the pollutants. Higher temperature provides more activation energy to rupture the peroxide bond of PS molecules and generate more SRs as described in Eq 1.2, as well as hydroxyl radicals in an indirect way (Eqs. 1.8 and 1.9) [17]. The high temperature also thermodynamically promotes the chemical reactions between reactive species and contaminants [19].Therefore, high temperature leads to dramatically enhanced degradation of the selected contaminant in water.

$$SO_4^{\bullet -} + H_2O \rightarrow OH^{\bullet} + SO_4^{2-} + H^+ \quad (1.8)$$

$$SO_4^{\bullet -} + OH^- \rightarrow OH^{\bullet} + SO_4^{2-} \quad (1.9)$$

SR based AOPs (SR-AOPs) have been shown to be effective in mineralizing a variety of organic contaminants (OCs) in water and wastewater effluents such as herbicides, industrial chemicals, and pharmaceuticals [17]. Therefore, ZVI and thermal activation are employed in this study to activate PS in order to degrade the TCPy.

Research Objectives

Chlorpyrifos (CP) is a broad-spectrum organophosphorous insecticide which has been widely used in agriculture since 1965. Although CP has played an important role in the protection of food and feed crops, its excessive use and persistence have caused many environmental concerns, including CP contamination of soil and aquatic environments and measurable CP levels on products for human consumption [20]. This issue is of such concern that the EPA delivered a proposal on October 30, 2015 recommending that chlorpyrifos use be completely ceased. In 2017, EPA declined to revoke chlorpyrifos tolerances. However, as of 9th August 2018, the 9th Circuit Court of Appeals has given the EPA 60 days to revoke all food tolerances and cancel all registrations for the widely used insecticide CP. The primary product of its microbial and photodegradation, 3,5,6-trichloro-2-pyridinol (TCPy), has been listed as a persistent and mobile pollutant by the USEPA[10]. TCPy is more water soluble than its parent compound, which significantly increases its ability to leach into groundwater and surface water, causing widespread contamination in soils and the aquatic environment. Therefore, it is critical that a method be developed to degrade TCPy to compounds that are more readily biodegradable and less toxic to humans and the environment.

SR-AOPs are a very promising and attractive advanced oxidation technology to decompose organic contaminates of concern. There are many activation methods of persulfate; however, activating PS by heat and iron for ISCO applications is currently used [17]. Therefore, the overall objective of this research is to evaluate the oxidation efficiency of TCPy by means of SR based AOPs at the laboratory scale.

In chapter two, the degradation of TCPy by sulfate radicals was evaluated using zero-valent iron-activated persulfate (ZVI/PS) in aqueous media. Response surface methodology and Box-Behnken design were applied in this study to assess the effects of the experimental parameters (concentration of ZVI, concentration of PS, and pH) on the mineralization of TCPy by ZVI/PS system. The interactions, coefficients, and residuals of these parameters were statically evaluated by analysis of variance (ANOVA). The reaction kinetics of the degradation process were examined as functions of ZVI concentration, PS concentration, and pH.

The desirability function was performed to specify the optimum conditions for the system which were further validated by performing duplicate experiments. The kinetics of the optimized condition were studied.

Comparison studies of persulfate activation by heat or catalysis concluded that thermally-activated PS exhibited higher oxidation efficiency [17]. Therefore, assessing the role of thermally-activated PS for the oxidation of TCPy in aqueous systems is the primary objective in chapter three. This objective includes studying the effect of operational parameters, such as initial PS dose, solution pH, and temperature on the degradation kinetics of TCPy. Optimization of the experimental factors was carried out by means of Response Surface Methodology based on Box-Behnken design with TCPy mineralization after 30 minutes chosen as the response. The predominant oxidizing species responsible for TCPy oxidation in this condition were identified by radical quenching experiments. Also, the optimized condition was further studied to evaluate the performance of the proposed method in the presence of scavenger ions.

In an oxidation reaction using persulfate where PS concentration is kept almost constant during the reaction, a steady-state sulfate free-radical concentration would occur which results in

difficult quantification of the radicals. However, if persulfate is present in a high amount compared to TCPy, more SR are produced in the system. Therefore, by fixing the concentrations of PS and TCPy, the kinetics of these parameters can be studied, thus determining the reaction kinetics order. Therefore, in chapter four, a detailed study of the reaction kinetic orders in a thermally-activated PS system is performed. This study involved performing further kinetics experiments where one of the reactants was kept at a constant concentration while varying the concentration of the other one. The half-lives method was employed to explore the kinetic orders.

In chapter five, the transformation intermediates and by-products of TCPy oxidation by ZVI and heat-activated PS were identified by GC-MS. The favorable reaction sites of SR with TCPy were investigated by density functional theory. The degradation pathways of TCPy in both systems were proposed based on the identified products and the calculated ΔG values using DFT were compared with the proposed experimental pathway.

CHAPTER TWO: OXIDATION OF 3,5,6-TRICHLORO-2-PYRIDINOL BY ZERO VALENT IRON(ZVI) ACTIVATED PERSULFATE

Introduction

Chlorpyrifos (O,O-diethyl-O-3,5,6-trichloro-2-pyridyl phosphorothionate; CP) is a broad-spectrum insecticide which has been used for agriculture worldwide since 1965, though residential use was banned in the United States in the year 2000 [3]. Although CP has played an important role in the protection of food and feed crops, its excessive use and persistence have caused many environmental concerns, including CP contamination of soil and aquatic environments and measurable CP levels on products for human consumption [20]. CP has been released into the environment through agricultural application, improper disposal, and industrial runoff [8]. Once in the environment, the phosphoester bond of CP is hydrolyzed to 3,5,6-trichloro-2-pyridinol (TCPy), which is the primary by product of CP. Also, photodegradation and microbial degradation of CP both demonstrate the formation of TCPy. TCPy is more persistent and more water soluble than its parent compound, according to the United States Environmental Protection Agency (USEPA) [10] which significantly increases its ability to leach into surface water and groundwater, causing widespread contamination in soils and aquatic environments [11-12]. TCPy has been detected in many places where CP was applied. For instance, TCPy has been identified in such diverse sources as spinach, cauliflower, and potato crops; golf course leachate; and human urine. As one would expect, TCPy has been confirmed to be present in wastewater streams from both chlorpyrifos and methyl-chlorpyrifos manufacturing plants [9].

In the past two decades, advanced oxidation processes (AOPs) have been proven to be effective for the degradation of a wide range of persistent organic contaminants. In accordance

with their varied natures, AOPs oxidize the original contaminants of concern to form various byproducts and eventually to carbon dioxide and water.

Persulfate (PS) has been explored as a suitable oxidizing agent for AOPs that can be activated to generate highly reactive sulfate radicals ($SO_4^{\bullet-}$, SR), which bear a strong redox potential (E^0 = 2.5-3.1 V, depending on pH). SR based AOPs have been shown to be effective in mineralizing a variety of organic contaminants in water and wastewater effluents such as herbicides, industrial chemicals, and pharmaceuticals [17]. Many activation methods have been developed to activate PS such as heat, UV, basic conditions, and transition metal ions[17].

$$S_2O_8^{2-} + heat/uv \rightarrow 2SO_4^{\bullet-} \quad (2.1)$$

$$S_2O_8^{2-} + Me^{n+} \rightarrow SO_4^{2-} + SO_4^{\bullet-} + Me^{(n+1)+1} \quad (2.2)$$

Iron [as iron (II), Fe^{2+}] is becoming favored over other common transition metals used in persulfate activation because it is nontoxic, cost effective and environmental friendly [18] (Eq 2.3). However, rapid scavenging of $SO_4^{\bullet-}$ occurred with excessive Fe^{2+}, which in turn reduces the efficiency of Fe^{2+}/ PS on contaminant degradation (Eq 2.4).

$$S_2O_8^{2-} + Fe^{2+} \rightarrow SO_4^{2-} + SO_4^{\bullet-} + Fe^{3+} \quad (2.3)$$

$$Fe^{2+} + SO_4^{\bullet-} \rightarrow Fe^{3+} + SO_4^{2-} \quad (2.4)$$

Recently, zero valent iron (ZVI) has been developed as an alternative activator of PS to overcome such a disadvantage. ZVI not only acts as a smooth releasing method of Fe^{2+}, but is also able to generate sulfate radicals directly (Eqs 2.5 and 2.6).

$$Fe^0 + 2H_20 \rightarrow Fe^{2+} + 2OH^- + H_2 \quad (2.5)$$

$$Fe^0 + 2S_2O_8^{2-} \rightarrow 2SO_4^{2-} + 2SO_4^{\bullet-} + Fe^{2+} \quad (2.6)$$

This chapter evaluated the removal efficiency of TCPy by means of SR based AOPs via laboratory-scale. The primary objective of this study was to investigate ZVI-activated persulfate (ZVI/ PS) for the oxidation of TCPy in aqueous system, determined by HPLC/MS. This objective included studying the effect of operational parameters, such as initial PS dose, initial ZVI dosage, and solution pH on the degradation kinetic of TCPy. The process was optimized by using the Box-Behnken experimental design (BBD) and response surface modeling (RSM) of TCPy degradation by ZVI/PS.

Experimental

Chemicals

Neat TCPy, ammonium acetate ($C_2H_7NO_2$, ≥ 98%), sodium hydrogen carbonate ($NaHCO_3$, 99.5-100.5%), ferrous sulfate ($FeSO_4$.$7H_2O$), 1,10-phenanthroline ($C_{12}H_8N_2$, ≥ 99%), hydroxylamine hydrochloride ($NH_2OH.HCl$, 98.0%), N-tert-Butyldimethylsilyl-N methyltrifluoroacetamide (MTBSTFA (with 1% t-BDMCS)) were purchased from Sigma Aldrich (USA). Sodium persulfate ($Na_2S_2O_8$, ≥ 98.0%), potassium iodide (KI, ≥ 99%), HPLC grade solvent; acetonitrile (CH_3CN, >99.9%), formic acid (HCOOH, ≥99.5 %), tert-butyl alcohol (TBA) ($C_4H_{10}O$, > 99%) and chloroform ($CHCl_3$, 99.8%) were purchased from Fisher Scientific. Iron particles were purchased from provectus environmental products.

Experimental Procedure

These experiments were conducted in 20 mL amber glass vials. A predetermined mass of ZVI particles was added to each of the vials, followed by the addition of TCPy stock solution to a final concentration of 10 mg/ L (50 μM) and varying concentrations of PS (2.5 – 25 mM). Then,

the vials were placed on a Thermo Scientific MaxO 4000 orbital shaker table operated at 200 rpm at room temperature for an appropriate amount of time. At designated time points, samples were removed from the shaker table and quenched in ice bath.

To evaluate the effects of the initial concentration of ZVI on TCPy degradation, additional batch experiments were performed with different ZVI concentrations (0.25, 0.5, 1.0 and 2.5 g/L) under the same experimental conditions as described above, but with predetermined concentration of PS.

To study the influence of the initial reaction pH at various pH values (3.0 - 12.0), the initial pH of the TCPy solution was adjusted by adding small amounts of 0.1 M H_2SO_4 or 0.1 M NaOH to the desired value before starting the experiment. To prevent potential side reactions between $SO_4^{\bullet-}$ and other species, buffers were not employed in the present study. All solutions were prepared daily using deionized water. All experiments were performed in duplicate.

Analysis

The analysis of the TCPy was performed on an Agilent 6230 TOF LC-MS instrument with an Agilent Zorbax SB-C18 analytical column. A mixture of Acetonitrile (ACN) and water was used as the mobile phase at ACN: H_2O ratio of 60:40% (v:v) and at a flow rate of 1.0 mL/min in LC-MS.

An ultraviolet-visible light (UV-VIS) spectrometer (Agilent 8453 UV Visible Spectrophotometer equipped with deuterium (UV) and tungsten (visible) lamps) was used to determine the concentration of PS and ferrous ions. The concentration of PS anion was determined following the procedure developed by Liang *et al.*[21]. Ferrous ions were measured with 1,10-phenanthroline at a wavelength of 510 nm for ferroin absorbance [22].

Shimadzu TOC-L Analyzer (Shimadzu Instruments, Kyoto, Japan) was used to determine nonpurgeable organic carbon (TOC) concentration. Samples were acidified to pH 2-3 with sulfuric acid prior to analysis.

Brunauer–Emmett–Teller analysis of surface area and porosity was accomplished using a Micromeritics ASAP 2020. Iron was placed in a pre-weighed ASAP tube and heated to 100 °C at a rate of 5 deg/min under ultra-high vacuum and left for 12 hours. The tube was then allowed to slowly cool back down to room temperature and re-weighed to obtain the activated sample mass. The tube with the sample was attached to the ASAP analysis port and a nitrogen adsorption isotherm was run at 77 K. A Rouquerol analysis was performed and used to determine the BET surface area of the compound.

Experimental Design

To specify the optimum conditions for the system, the design of the experiment was structured to determine the common relationship between several process variables that influence the system. Response surface methodology, which is an effective and useful statistical method for improving, developing, and optimizing processes, was employed in this study to process the optimization. In the experimental procedure, Box-Behnken design, a widely used form of RSM, was employed. The Design-Expert (10.0.3) statistical software package was used to determine the total number of experimental runs necessary (N). For development of BBD, N is defined as:

$$N = 2k\,(k-1) + C_0 \tag{2.7}$$

Where k is the number of variables and C_0 is the number of central points. The experimental design consisted of 17 experiments calculated from Eq 2.7 which included twelve factorial points with five center points. The independent variables were set at three different levels, low (-1),

medium (0) and high (+1). The ranges and coded levels of the TCPy degradation variables studied are given in Table 1.

The predicted response (Y) as a function of the main independent variables was expressed by using a second order polynomial regression model equation:

$$Y = \beta_0 + \sum_{i=1}^{k} \beta_i X_i + \sum_{i=1}^{k} \beta_{ii} X_i^2 + \sum_{i=1}^{k} \sum_{j=1}^{k} \beta_{ij} X_i X_j + \epsilon \quad (2.8)$$

Where β_0, β_i, β_{ii}, and β_{ij} are the regression coefficients representing the constant, the linear, the square, and the interactive effect terms, respectively. The terms X_i and X_j are the coded independent variables while ϵ is random error.

The parameters that affect the oxidation of TCPy by ZVI/PS, their interactions, coefficients, and residuals were statically evaluated by ANOVA which provides an overall summary for the full model.

Table 1: Experimental ranges and levels of the independent test variables.

Variables	Unit	Coded variable level		
		-1	0	1
Persulfate (PS)	mM	5	12.5	20
pH	-	3	7.5	12
ZVI	g/L	0.5	1.5	2.5

Results and Discussion

Effect of Parameters on TCPy Removal and Kinetic Studies

Effect of PS concentration

The concentration of PS is an essential factor that affects the oxidation of the contaminants in the ZVI/PS system. Increasing PS concentration is associated proportionally with an increase in SR formation, hence improving the oxidation efficiency. The removal of normalized TCPy concentration over time in a ZVI/PS system with various PS concentrations up to 25 mM is presented in Figure 3. For the range of PS doses employed, TCPy removal was significantly faster with higher PS dose up to 15 mM; further increasing the concentration of PS in the solution decreased the overall removal efficiency of TCPy. In the absence of PS, only 5% of TCPy was removed after 40 minutes of reaction. Although a sudden decrease in the concentration of TCPy occurred in all PS containing systems, complete TCPy removal was not achieved at 2.5 mM PS and 56% of TCPy remained in the system. As the concentration of PS increased from 5 mM to 15 mM, the reaction time for TCPy removal was reduced and TCPy was successfully oxidized in 30 mins and 25 mins, respectively. High PS dosage enhances TCPy degradation due to the higher amount of radicals produced (Eq 2.6). However, when the concentration of PS further increased to 20 mM, the reaction time increased and TCPy was removed after 40 mins of the reaction. Further increasing of the PS concentration to 25 mM lowered the degradation efficiency of TCPy and almost 20% of TCPy remained in the system. This trend can be attributed to the greater production of SR by excess PS which results in radical-radical reactions (Eq 2.9). Moreover, PS may scavenge SR as demonstrated in Eq 2.10 [23-24].

$$SO_4^{\bullet -} + SO_4^{\bullet -} \rightarrow S_2O_8^{2-} \quad (2.9)$$

$$SO_4^{\bullet -} + S_2O_8^{2-} \rightarrow SO_4^{2-} + S_2O_8^{\bullet -} \quad (2.10)$$

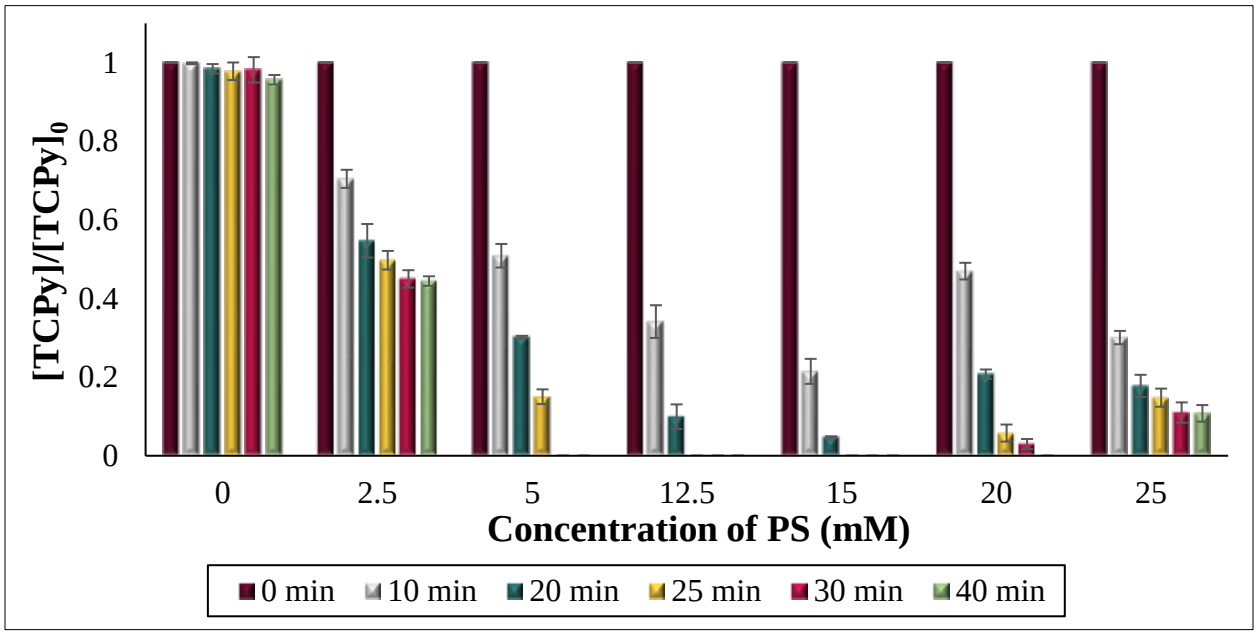

Figure 3: Effects of PS concentration on TCPy degradation by ZVI activated PS. Experimental conditions: $[TCPy]_0$ = 50 µM; [PS]0=2.5-20 mM; [ZVI]0= 1.5 g/L; pH = 7.5.

Figure 4 presents the normalized rate constants of TCPy removal at different concentrations of PS. For any specific concentration of PS, TCPy removal exhibited pseudo-first-order kinetics ($R^2 > 0.98 \pm 0.002$), which could be described as follow:

$$\ln([TCPy]/[TCPy]_0) = -k_{obs} \cdot t \quad (2.11)$$

Where k_{obs} (min^{-1}) is the pseudo-first-order rate constant. [TCPy] and $[TCPy]_0$ are the molar concentration of TCPy at times t and 0, respectively. The value of the observed rate constant (k_{obs}) of TCPy removal increased from 2.9×10^{-2} min^{-1} to 1.4×10^{-1} min^{-1} as the concentration of PS increased from 2.5 mM to15 mM. As PS concentrations increased to 20 mM, the k_{obs} decreased

to 7.9×10^{-2} min^{-1} due to the side reaction of SR with higher concentrations of PS as described by Eqs 2.9 and 2.10.

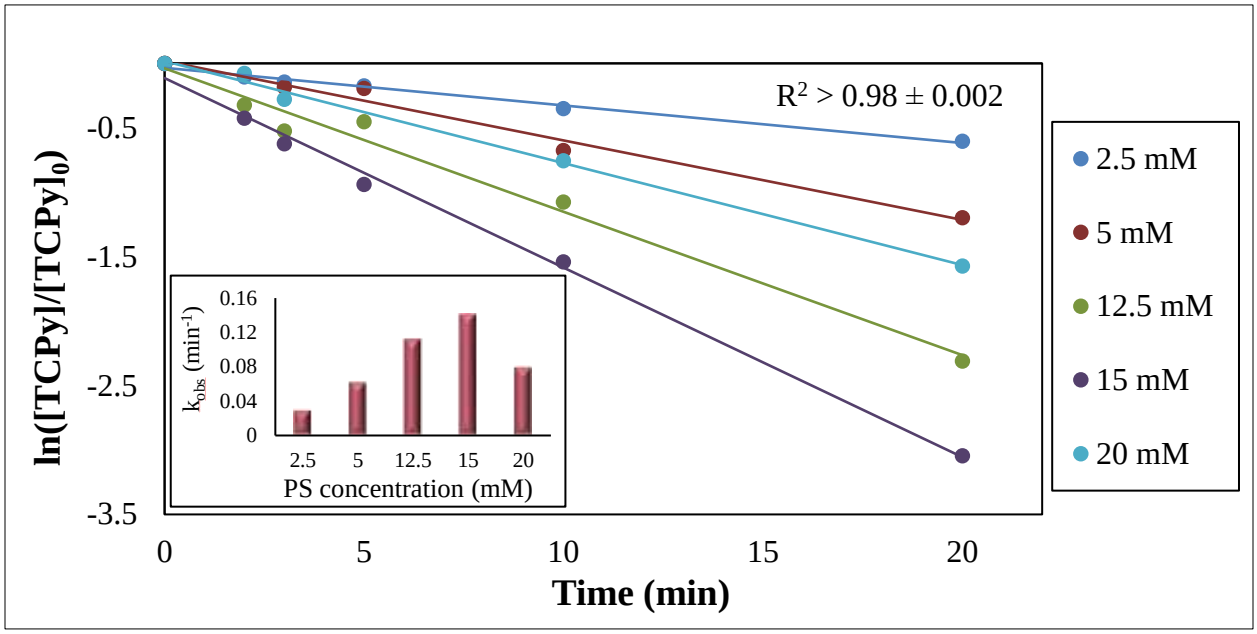

Figure 4: Pseudo-First-Order kinetics of TCPy degradation at different concentrations of PS in ZVI/PS system. Inset: the corresponding rate constants of TCPy removal. Experimental conditions: $[TCPy]_0$ = 50 µM; $[PS]_0$=2.5-20 mM; $[ZVI]_0$= 1.5 g/L; pH = 7.5.

The consumption of PS during the oxidation of TCPy by ZVI/PS for all PS concentrations used is presented in Figure 5. While all PS was consumed ($[PS]_0$ = 2.5 mM) at 30 min, 66% of PS was consumed with a higher initial concentration of PS ($[PS]_0$ = 15 mM) in the same time. At initial PS concentration of 12.5 mM and 15 mM, almost 68% and 64% of PS were consumed respectively after 25 mins, in which TCPy was completely removed. The PS consumption results demonstrated that the consumption of PS was faster at the beginning of the reaction with higher PS concentration.

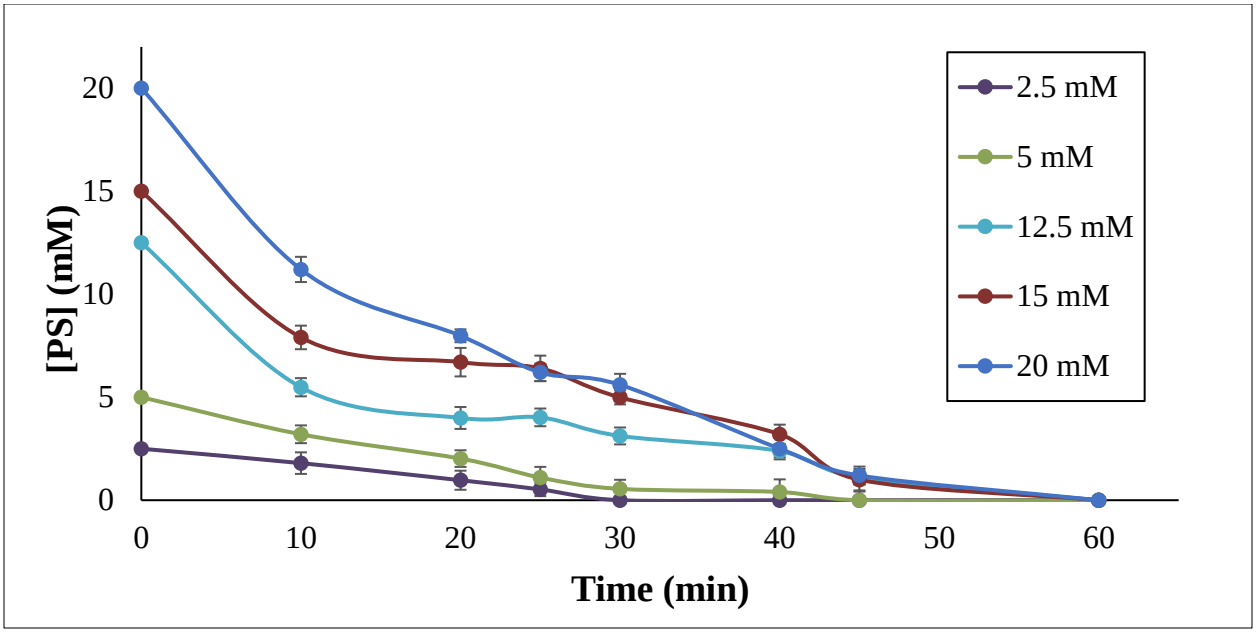

Figure 5: PS consumption during the reaction. Experimental conditions: $[TCPy]_0$ = 50 µM; $[PS]_0$=2.5-20 mM; $[ZVI]_0$= 1.5 g/L; pH = 7.5.

The reaction stoichiometric efficiency (RSE), which is the ratio of the molar concentration of oxidized TCPy to the consumed PS, is used in this study to evaluate the utilization efficiency of PS. Actual RSE was calculated for each PS concentration after TCPy was oxidized completely while RSE average was the mean for each concentration of PS at all sampling times, both are presented in Figure 6. The results showed that for both actual and average RSE, the highest values were observed for the lowest concentration of PS. For instance, RSE% was increased from 0.571% to 2.25% as the initial PS concentration decreased from 20 mM to 5 mM.

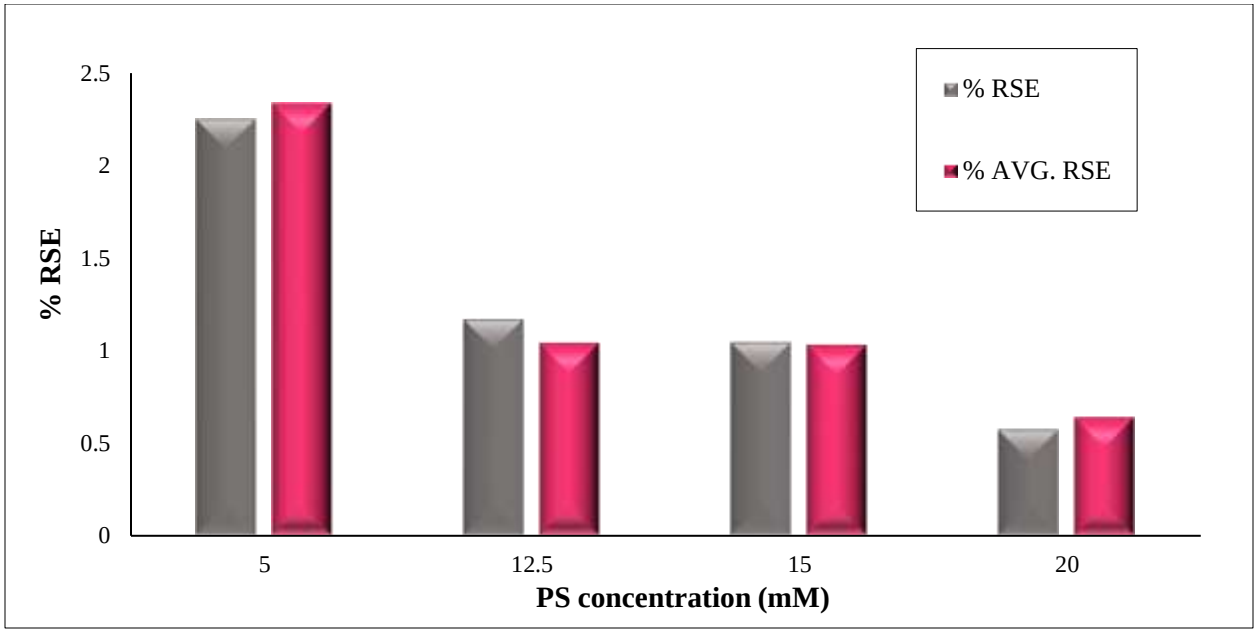

Figure 6: The reaction stoichiometric efficiencies during the TCPy degradation. Experimental conditions: $[TCPy]_0$ = 50 µM; $[PS]_0$=2.5-20 mM; $[ZVI]_0$= 1.5 g/L; pH = 7.5.

While the concentration of ZVI is the same in all experiments, increasing the PS concentrations contributed to produce more Fe^{2+} in the system (Eq 2.6). Figure 7 shows that the concentration of Fe^{2+} released after 10 minutes of reaction increased from 4.4 x 10^{-1} mg/L at 5 mM PS to 2.19 mg/L at 20 mM PS. Similarly, more iron ions were released at higher PS concentrations throughout the course of the experiment. Accordingly, at higher PS concentration, more sulfate free radicals would be generated in response to the greater formation of Fe^{2+} activators. This favors the radical reaction with Fe^{2+}, SR, and H_2O (Eqs 2.4, 2.9, and 2.12, respectively). However, for lower PS concentration, SR generation is less prevalent due to the lower amount of iron ions produced, side reactions are therefore disfavored and the calculated RSE is increased [23-24].

$$SO_4^{\bullet -} + H_2O \rightarrow HSO_4^- + OH^{\bullet} \quad (2.12)$$

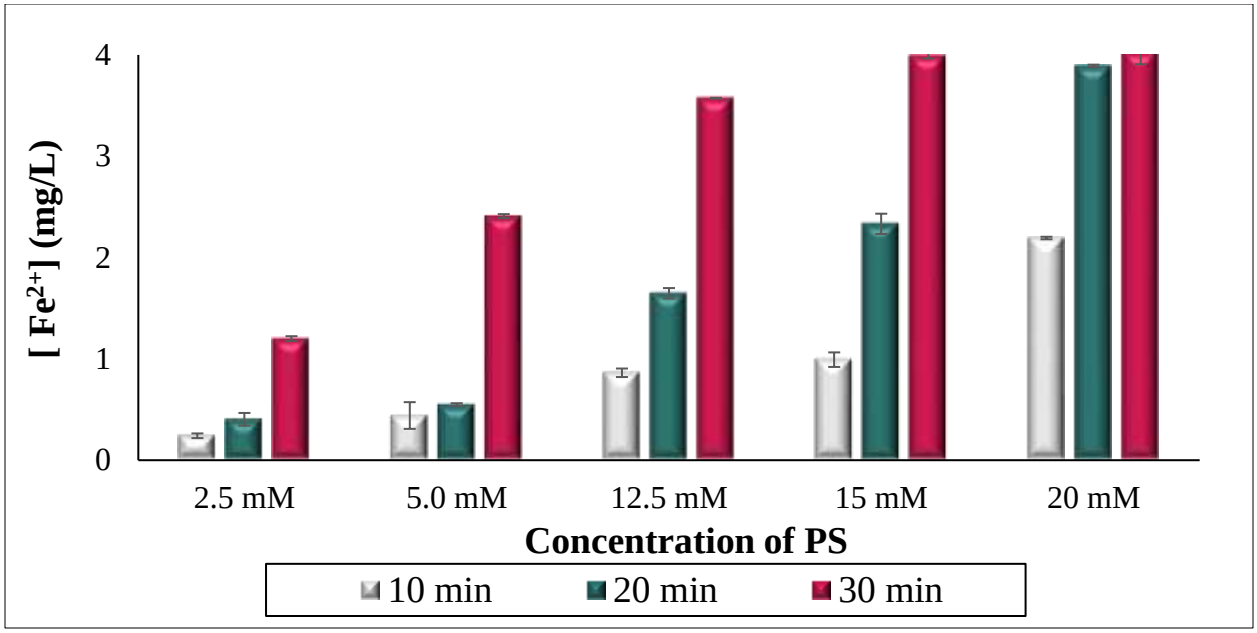

Figure 7: The concentration of Fe2+ at 10, 20 and 30 min of the reaction. Experimental conditions: $[TCPy]_0$ = 50 µM; $[PS]_0$=2.5-20 mM; $[ZVI]_0$= 1.5 g/L; pH = 7.5.

Effect of ZVI

ZVI concentration is another essential parameter which influences the degradation efficiency of PS activated by ZVI. Figure 8 shows the role of initial ZVI dosage on the oxidation of TCPy in the ZVI/PS system. It was found that varying the ZVI concentration from 0.5 g/L to 2.5 g/L has a strong impact on TCPy oxidation. As ZVI dosage increased from 0.5 g/L to 2.0 g/L, the removal efficiency of TCPy increased from 77% to 100% after 22 mins of the reaction. However, increasing the ZVI concentration to 2.5 g/L decreased removal efficiency and increased the removal time. For example, at 2.5 g/L ZVI, TCPy was completely removed after 35 mins of the reaction.

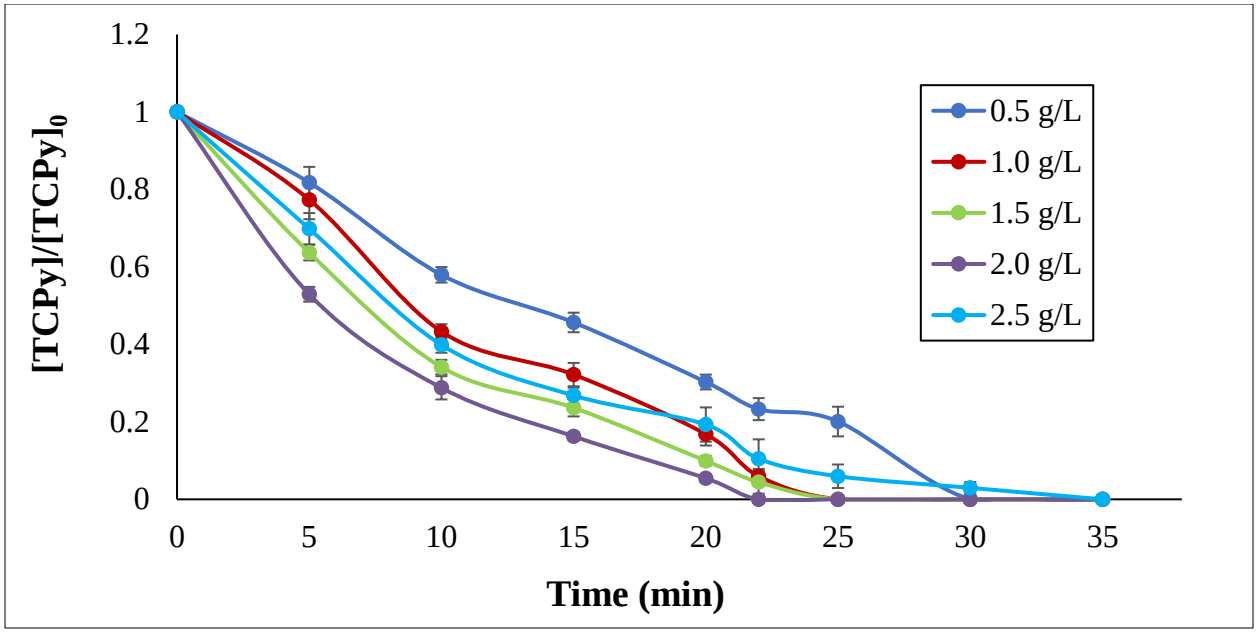

Figure 8: Effect of ZVI concentration on TCPy degradation by ZVI activated PS. Experimental conditions: $[TCPy]_0$ = 50 µM; $[PS]_0$=12.5 mM; $[ZVI]_0$= 0.5-2.5 g/L; pH = 7.5.

As shown in Figure 9, the degradation of TCPy is well fitted to a pseudo-first-order kinetics pattern, and the oxidation rate of TCPy was significantly affected by ZVI loading. The degradation of TCPy is well fitted to a pseudo-first-order kinetics pattern, and the oxidation rate of TCPy was significantly affected by ZVI loading (Figure 9). The observed first-order rate constants (k_{obs}) went up from 6.4 x 10^{-2} min^{-1} to 1.4 x 10^{-1} min^{-1} as the concentration of ZVI increased from 0.5 to 2.0 g/L. However, increasing the ZVI concentration to 2.5 g/L decreased the k_{obs} to 1.1 x 10^{-1} min^{-1}.

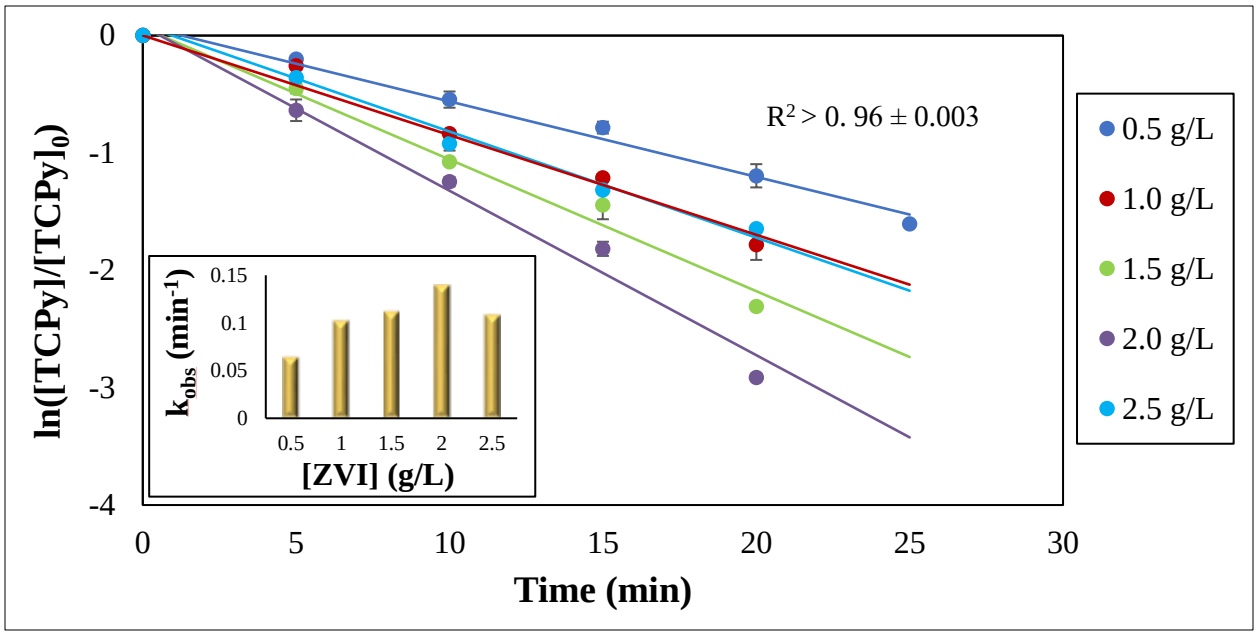

Figure 9: Pseudo-First-Order kinetics of TCPy degradation. Inset: plot of kobs vs ZVI concentration. Experimental conditions: $[TCPy]_0$ = 50 µM; $[PS]_0$=12.5 mM; $[ZVI]_0$= 0.5 - 2.5 g/L; pH = 7.5.

To explore the role of ZVI in ZVI/PS system, the concentration of ferrous ions released during the reaction was investigated. Figure 10 illustrates the released concentration of Fe^{2+} in the ZVI/PS system as a function of reaction time. As the concentration of applied ZVI increased, the concentration of Fe^{2+} in the system increased. For example, at ZVI load (1.0 g/L), a concentration of only 1 mg/L Fe^{2+} was found after 20 mins of the reaction while 8 mg/L Fe^{2+} was found for the highest ZVI load (2.5 g/L). PS is activated by these Fe^{2+} to generate sulfate radicals that subsequently accelerate the oxidation of TCPy, which can explain the findings in Figure 8. However, increasing the ZVI load causes the release of excessive Fe^{2+} over time, which scavenge the produced sulfate radicals (Eq 2.4), thus reducing the degradation efficiency. The Fe^{2+} release data demonstrates that ZVI plays an integral role in generation Fe^{2+} in the system. There are many possible routes for the generation of Fe^{2+} in the ZVI/PS system, one being a direct electron transfer from ZVI to persulfate in a Fenton-like reaction incorporating a Haber–Weiss like mechanism [25].

ZVI acts as a reducing agent (E^0= -0.44 V) to provide electrons which reductively decompose persulfate to form sulfate radicals. This direct interaction with persulfate oxidizes iron, resulting in corrosion of ZVI and the release of Fe^{2+} ions (Eq 2.6). Alternatively, Fe^{2+} may be formed as a direct product of corrosion of iron metal under aerobic or anaerobic conditions as described in Eqs 2.5 and 2.13.

$$Fe^0 + H_2O + 0.5\,O_2 \rightarrow Fe^{2+} + 2OH^- \quad (2.13)$$

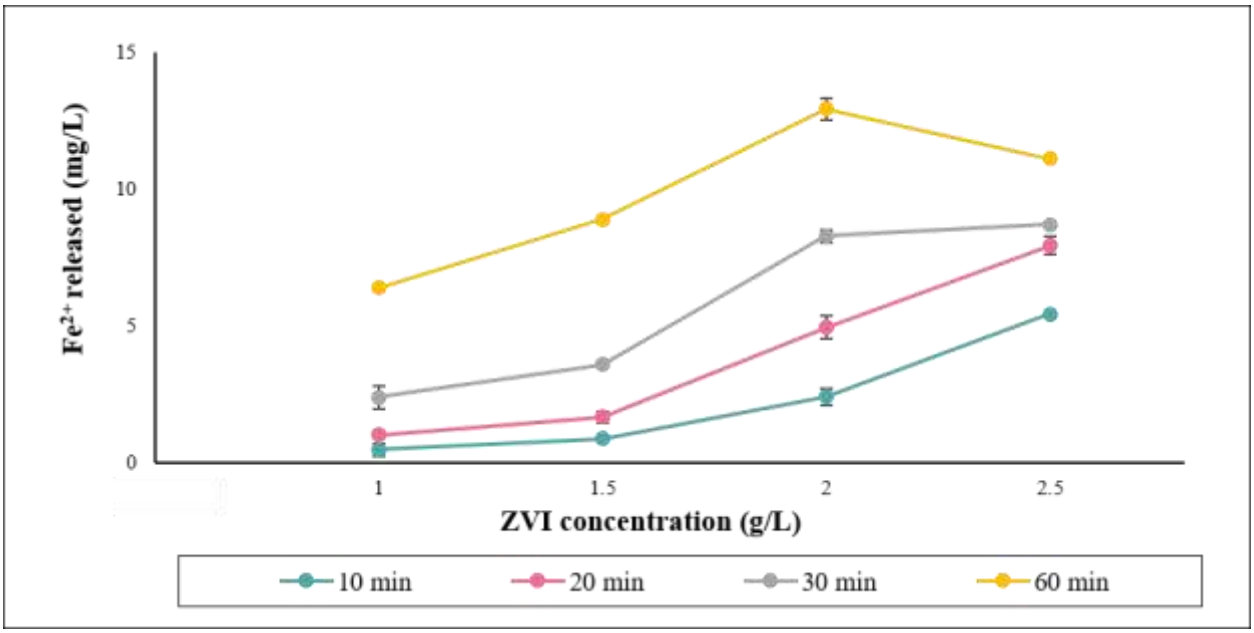

Figure 10: Concentration of Fe^{2+} during the reaction. Experimental conditions: $[TCPy]_0$ = 50 µM; $[PS]_0$=12.5 mM; $[ZVI]_0$= 0.5-2.5 g/L; pH = 7.5.

The consumption of PS during the reaction at the different applied ZVI dosage is shown in Figure 11. The results indicate that a higher concentration of ZVI consumed more PS. This was likely due to the reaction between PS and Fe^{2+}, which was produced in more quantity with higher ZVI dosage, or the reaction between PS and ZVI itself. The corresponding RSE values are

presented in Figure 12. The RSE was enhanced by increasing the concentration of ZVI from 0.5 g/L to 1.0 and 1.5 g/L. However, further increasing ZVI decreased the RSE% which is likely due to the scavenging of SRs by Fe^{2+} (Eq 2.3).

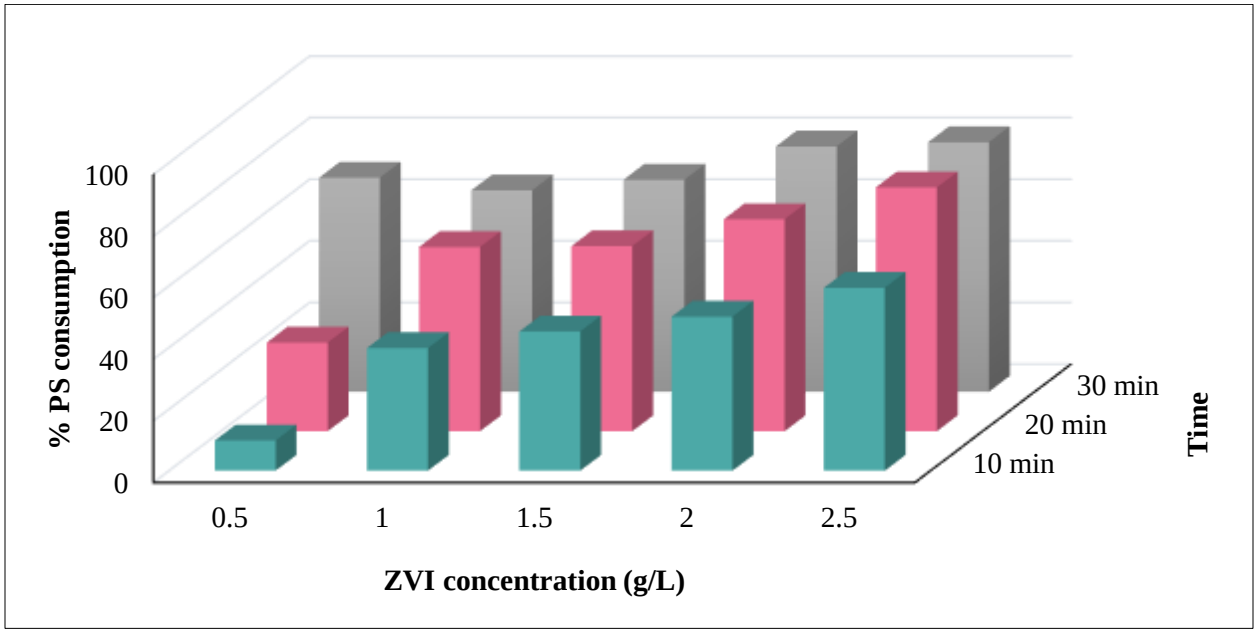

Figure 11: Consumption of PS at different ZVI concentrations. Experimental conditions: $[TCPy]_0$ = 50 µM; $[PS]_0$=12.5 mM; [ZVI]= 0.5-2.5 g/L; pH = 7.5.

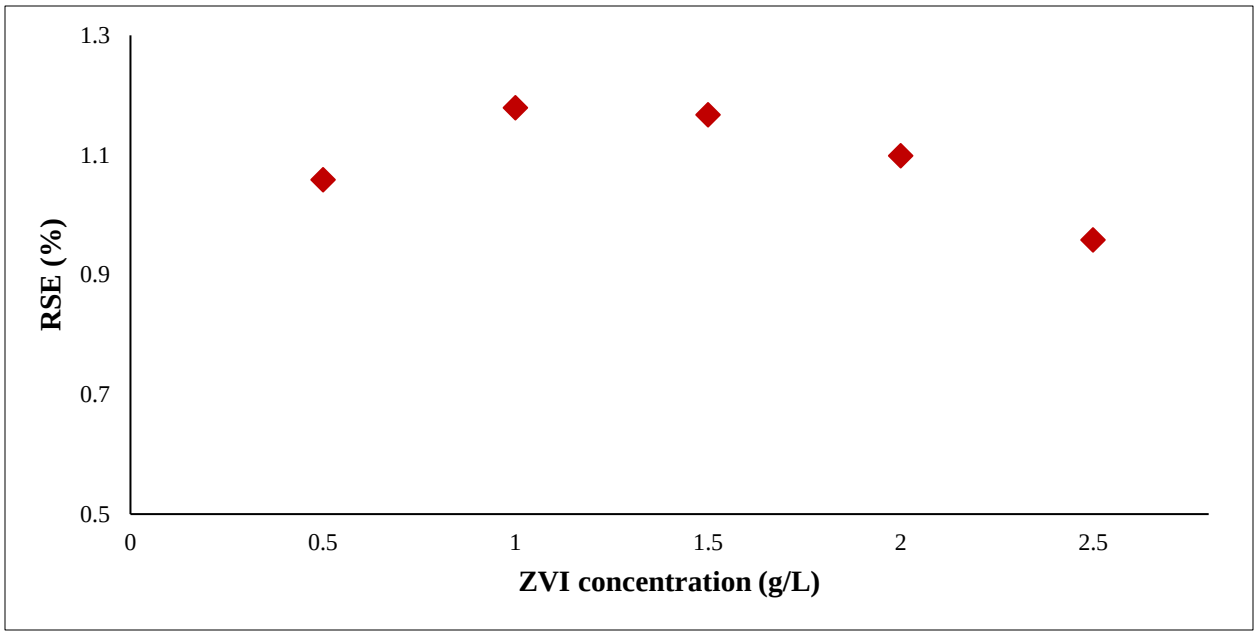

Figure 12: RSE (%) at different ZVI concentrations. Experimental conditions: $[TCPy]_0$ = 50 µM; $[PS]_0$=12.5 mM; [ZVI]= 0.5-2.5 g/L; pH = 7.5.

Effect of pH

Solution pH is an important environmental parameter which may significantly affect the pollutant's degradation as well as the formation of radicals [26]. In the ZVI/PS system, as the solution pH changes the dominant oxidizing species changes. At all pH values, sulfate radicals react with water forming hydroxyl radicals (HR) (Eq 2.14). Under acidic conditions, sulfate radicals are the primary reactive species; however, all sulfate radicals are converted into hydroxyl radicals in basic conditions (Eq 2.15) [26].

$$SO_4^{\bullet -} + H_2O \rightarrow SO_4^{2-} + OH^{\bullet} + H^+ \quad (2.14)$$

$$SO_4^{\bullet -} + OH^- \rightarrow SO_4^{2-} + OH^{\bullet} \quad (2.15)$$

This radical conversion is mainly controlled by Eq 2.15 since the rate constant for the reaction in Eq 2.14 (k [H_2O] < 2 X 10^{-3} s^{-1}) is low compared to the reaction of SR with other organic contaminants [27].

Figure 13 shows the change in normalized TCPy concentrations over time at various initial solution pH values in the range of 3.0 –12.0. The oxidation of TCPy in acidic pH resulted in significantly higher efficiency of removal compared to that of basic pH. Complete TCPy removal was achieved after 20, 22 and 30 minutes reaction at pH 3, 5, and 7.5, respectively. The results indicated that acidic conditions are more favorable for TCPy degradation than neutral condition. This favorability might be ascribed to the formation of more Fe^{2+} in acidic solution because of the iron corrosion (Eq 2.16) which in turn generates more SR and enhances the oxidation efficiency.

$$Fe^0 + 2H^+ \rightarrow Fe^{2+} + H_2 \quad (2.16)$$

Interestingly, enhancement of TCPy oxidation by the ZVI/PS system was observed after increasing the solution pH to 9.0 and the removal of TCPy was achieved after 22 minutes. However, removal efficiencies of TCPy with ZVI/PS system remain poor at higher pH (pH= 12).

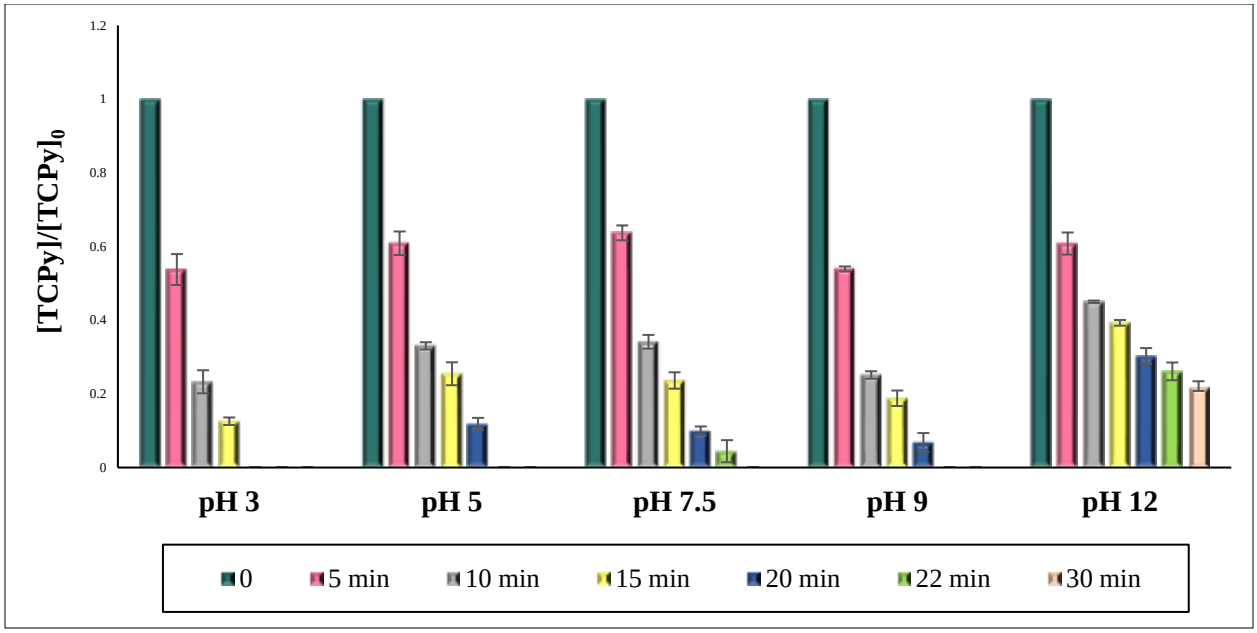

Figure 13: Oxidation of TCPy by ZVI/PS at different pH. Experimental conditions: $[TCPy]_0$ = 50 µM; $[PS]_0$=12.5 mM; [ZVI]= 1.5 g/L; pH =3-12.

As mentioned previously, the dominant oxidizing species change in response to changing pH. Therefore, radical scavenger tests were used to explore the involvement of SR and HR species in the oxidation of TCPy at different pH. Radical scavengers such as ethanol (EtOH) and tert-butyl alcohol (TBA) are usually used to identify the contribution of SRs and HRs to organic contaminants degradation in the SR- AOPs. EtOH with α-H was reported as an active reactant with both SRs and HRs at rate constant of $((1.6\text{-}7.7) \times 10^7\ M^{-1}\ S^{-1}$ and $(1.2\text{-}2.8) \times 10^9\ M^{-1}\ S^{-1})$, respectively [27]. In contrast, TBA can mainly scavenge HR at second-order rate constant $((3.8\text{-}7.6) \times 10^8\ M^{-1}\ S^{-1})$ approximately 1000-fold higher than that with SR $((4.0\text{-}9.1) \times 10^5\ M^{-1}\ S^{-1})$ [27]. Therefore, these two alcohols were used as quenching agent and the oxidation of TCPy was measured at different pH.

As shown in Figure 14, in the quencher free system, complete removal of TCPy was achieved at pH 3 while treatment with EtOH resulted in poor degradation efficiency of 13.1%. However, treatment with TBA resulted in higher TCPy removal than treatment with EtOH, indicating that in acidic solution SRs were the predominant species. The same trend was observed at pH 5 and pH 7.5. The removal efficiency of TCPy in the presence of TBA decreased as the solution pH increased to 9, indicating the presence of both SR and HR in the system. However, at pH 12 the inhibition of TCPy degradation levels are closed by both TBA and EtOH indicating a greater generation of HR in the system.

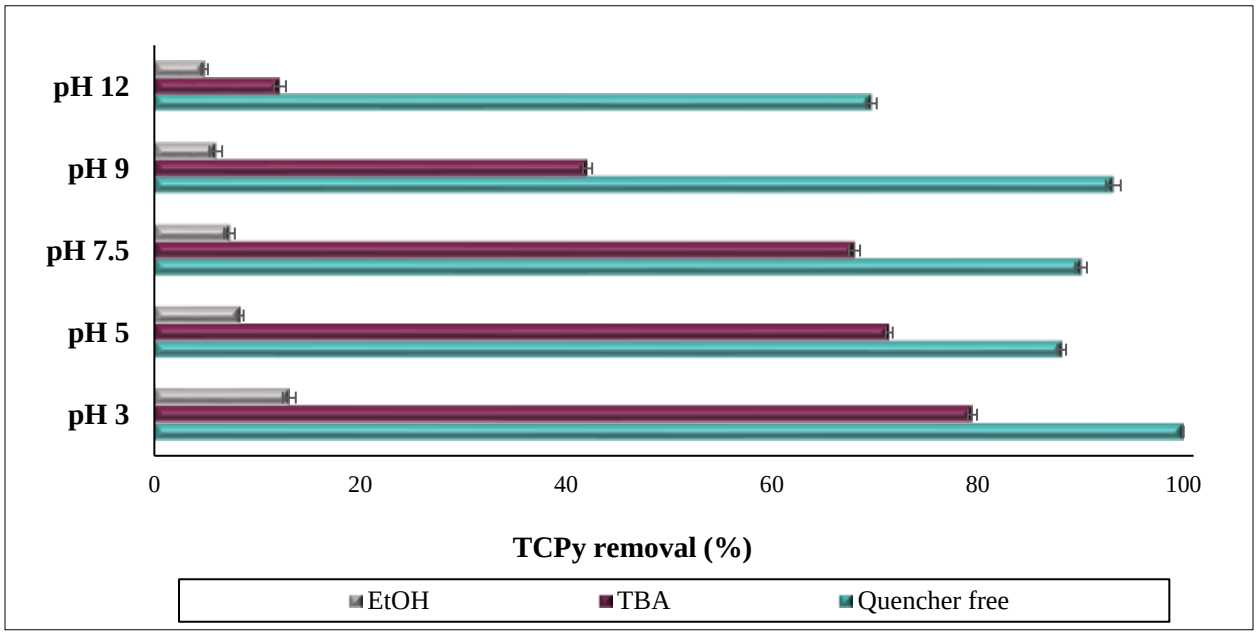

Figure 14: TCPy degradation in the absence and in the presence of radical scavengers at different pH in ZVI/PS system. Experimental conditions: $[TCPy]_0$ = 50 µM; $[PS]_0$=12.5 mM; [ZVI]= 1.5 g/L; pH =3-12.

The predominant oxidizing species at different pH values is presented in Table 2. According to the radical scavenger test, SR is the predominant species at pH ≤ 7.5, while HR is

the predominant species at pH ≥ 9. These results are in agreement with Liang, C. & Su, H. W., who identified the presence of SR and HR by using a chemical probe method on heat activated PS system. Their results indicated that in basic conditions, HR is the predominant radical, while at near neutral pH, both SR and HR are present. In acidic conditions with pH less than 7, SR is the predominant radical [27].

Table 2: The predominant species for TCPy oxidation at different pH.

pH	Predominant species
3	SR
5	SR
7.5	SR
9	HR
12	HR

This observation can explain the findings in Figure 13. The highest degradation efficiency occurring in acidic conditions can be attributed to the presence of SR. At pH 9, there is increased HR presence which has a higher redox potential than SR. The increase of HR along with the presence of SR can explain the enhanced degradation efficiency at pH 9. Furthermore, the reactivity of PS would increase in alkaline conditions, which could account for the enhancement of TCPy removal at higher pH [28]. The poor removal efficiency of TCPy at pH 12 can be attributed to the excessive amount of HR which contributed to the reaction of HR with itself, leading to quick loss of the radicals in the solution (Eq 2.17).

$$OH^{\bullet} + OH^{\bullet} \rightarrow H_2O_2 \qquad (2.17)$$

Although the rate constant for TCPy removal is higher at pH 9 than pH 5 and 7.5, the mineralization efficiency of TCPy after one hour of the reaction is lower at pH 9 (Figure 15). This is likely due to the formation of an oxide layer on the surface of ZVI which inhibits the complete mineralization of TCPy.

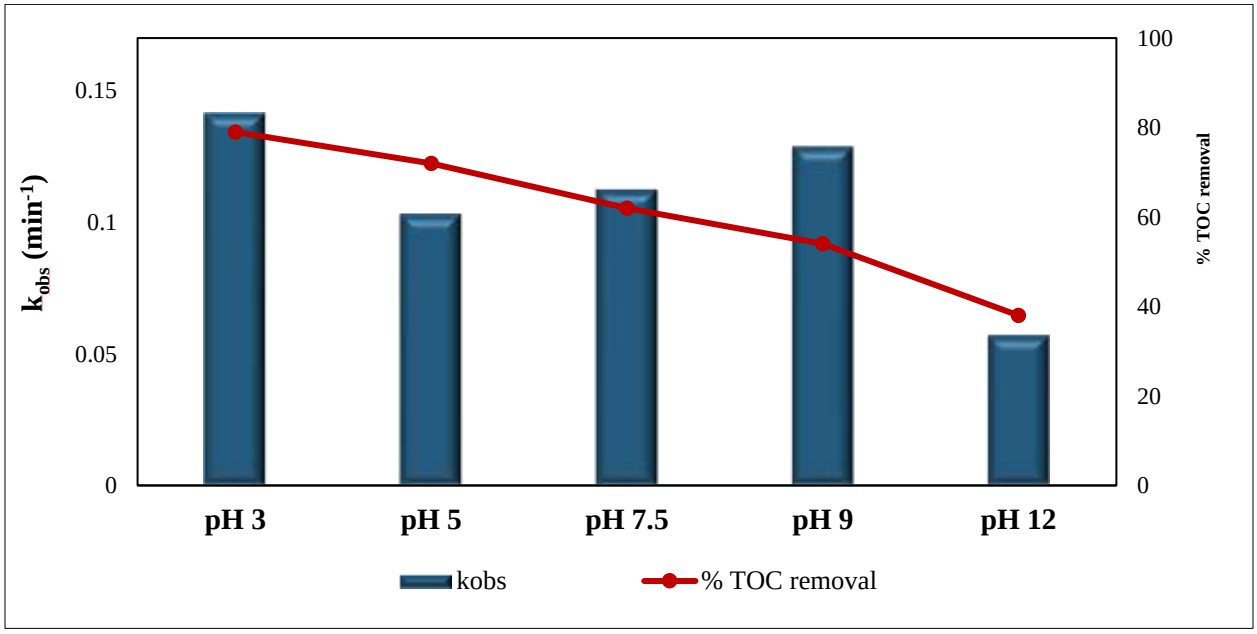

Figure 15: Plot of k_{obs} vs pH and %TOC removal after 2 hours of the reaction at different pH. Experimental conditions: $[TCPy]_0$ = 50 µM; $[PS]_0$=12.5 mM; [ZVI]= 1.5 g/L; pH =3-12.

Regression Model Representation

As discussed previously in the effect of parameters on TCPy removal, the removal efficiency of TCPy in ZVI/PS depends on various parameters. Therefore, RSM with BBD was applied in this study to evaluate the effects of the independent variables ([PS], [ZVI], and pH) and to assess the relationships between them on the mineralization of TCPy by ZVI/PS system. Although the complete removal of TCPy by ZVI/PS was achieved after 25 mins of reaction, only partial mineralization of TCPy (4.0 – 32.1%) occurred, depending on process parameters as shown in Table 14 in Appendix A. Thus, mineralization after two hours treatment (up to 81% mineralization) was chosen as an appropriate measure for evaluating the combined effect of the selected parameters by RSM.

The experimental design matrix using three factors as independent variables and the responses based on experimental runs proposed by BBD are summarized in Table 3. Design-Expert Software indicated that the quadratic model is the most applicable model for the degradation of TCPy by ZVI/PS due to its higher R^2 value as well as lower standard deviation relative to other models. The final predicted model in terms of coded factors can be described by the following Eq:

$$Y= 70.5 + 13.875\ A - 20.7125\ B + 4.2875\ C - 6.6\ AB + 3.4\ AC + 7.625\ BC - 37.8875\ A^2 - 0.9625\ B^2 - 11.6125\ C^2 \quad (2.18)$$

Where Y represents the % mineralization of TCPy at 120 min. A, B, and C are the coded values of the initial concentration of PS, pH, and the concentration of ZVI, respectively.

Table 3: The BBD design matrix and experimental results for TCPy degradation by ZVI/PS.

Run	Independent variables (coded)			TOC removal (%)	
	PS (mM)	pH	ZVI (g/L)	Exp	Pred
1	0	1	-1	20.30	25.30
2	0	0	0	70.20	70.50
3	0	-1	-1	81.10	81.97
4	0	0	0	70.40	70.50
5	1	0	1	39.80	42.56
6	0	0	0	69.8	70.50
7	1	-1	0	70.60	72.84
8	0	0	0	71.40	70.50
9	0	-1	1	80.30	75.30
10	0	0	0	70.70	70.50
11	0	1	1	50.00	49.12
12	1	1	0	20.10	18.21
13	-1	1	0	5.90	3.66
14	1	0	-1	30.30	27.19
15	-1	0	1	4.90	8.01
16	-1	0	-1	9.00	6.24
17	-1	-1	0	30.0	31.89

Statistical Analysis (ANOVA)

ANOVA was used to assess the significance of the fitting of the second order quadratic model for TCPy degradation by ZVI/PS as shown in Table 4. The sufficiency of the model was confirmed by a model F-value of 92.49 with (Prob > F) less than 0.0001 as presented in Table 4. As shown in the ANOVA table, A, B, C, AB, BC, A^2, and C^2 were determined to be statistically significant model terms. All the studied factors, [PS], pH, and [ZVI], had a significant influence on TCPy degradation by ZVI/PS. Moreover, the interaction between PS or ZVI and pH played an important role in the system for the degradation of TCPy. The coefficient of determination (R^2) in the present study for TCPy mineralization (0.9917) indicates that the fitted polynomial equations have a significant relationship with the model. The values of predicted R^2 and adjusted R^2 (0.8682 and 0.9809, respectively) illustrated a reasonable agreement with less than 0.2 difference which confirmed the model's good predictability. Moreover, the model is adequate because the signal to noise ratio obtained in this study is 26.396, which is significantly greater than the minimum desirable value of 4.

Table 4: ANOVA for response surface quadratic model of TCPy mineralization.

Source	Sum of square	Degree of freedom	Mean square	F-value	P-value	
Model	12456.41	9	1384.05	92.49	< 0.0001	significant
A	1540.13	1	1540.13	102.92	< 0.0001	
B	3423.06	1	3432.06	229.36	< 0.0001	
C	147.06	1	147.06	9.83	0.0165	
AB	174.24	1	174.24	11.64	0.0113	
AC	46.24	1	46.24	3.09	0.1222	
C^2	232.56	1	232.56	15.54	0.0056	
A^2	6044.05	1	6044.05	403.91	< 0.0001	
B^2	3.90	1	3.90	0.2607	0.6254	
C^2	567.79	1	567.79	37.94	0.0005	
Residual	104.75	7	14.96			

Residual analysis was used to further validate this model. First, a normal probability plot of the residuals was generated, which, according to Teh, *et al.* must approximate a straight line to be valid; this condition is satisfied [29] as shown in Figure 16. Additionally, the residuals are well-distributed around the mean response, indicating satisfactory random distribution. Second, predicted responses were plotted against actual responses to confirm good predictability Figure 17.

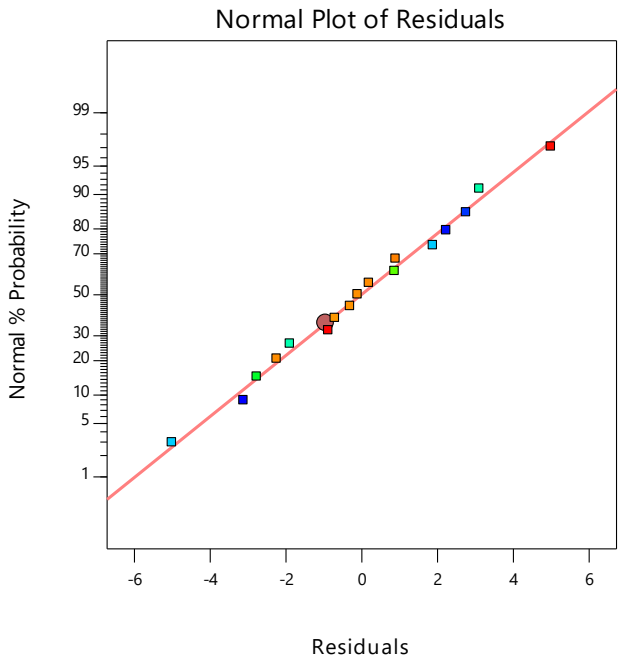

Figure 16: Normal probability plot of the residuals in ZVI/PS system.

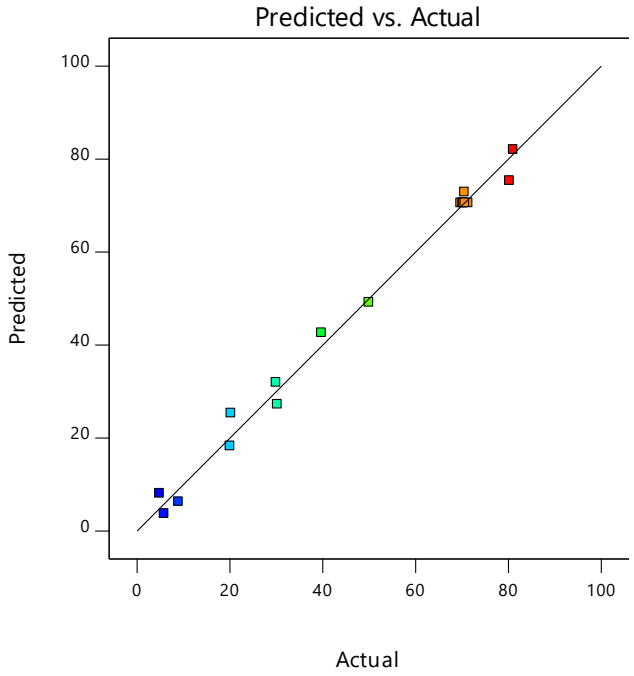

Figure 17: Predicted response versus actual response for TCPy mineralization in ZVI/PS system.

One Factor Effect on TCPy Mineralization

Based on the quadratic model, the influence of a single factor on the mineralization of TCPy by ZVI/PS was investigated while all other factors were kept constant at coded value 0, and the results are shown in Figure 18. Figure 18a indicates that the TCPy degradation efficiency increases as the concentration of PS increases. However, above a certain PS concentration, the mineralization of TCPy was decreased as PS concentration increased. A similar trend was observed with the effect of ZVI concentration on TCPy mineralization (Figure 18b). For instance, lower mineralization efficiency was observed with both low and high concentrations of ZVI. For fixed concentration of PS and ZVI, as illustrated in Figure 18c. the TCPy degradation efficiency decreases by almost 36% as the pH increases from 3 to 12. Hence, the best TCPy mineralization is found to occur at lower pH. These observations are similar to the finding in the effect of these parameters on TCPy removal which were discussed previously.

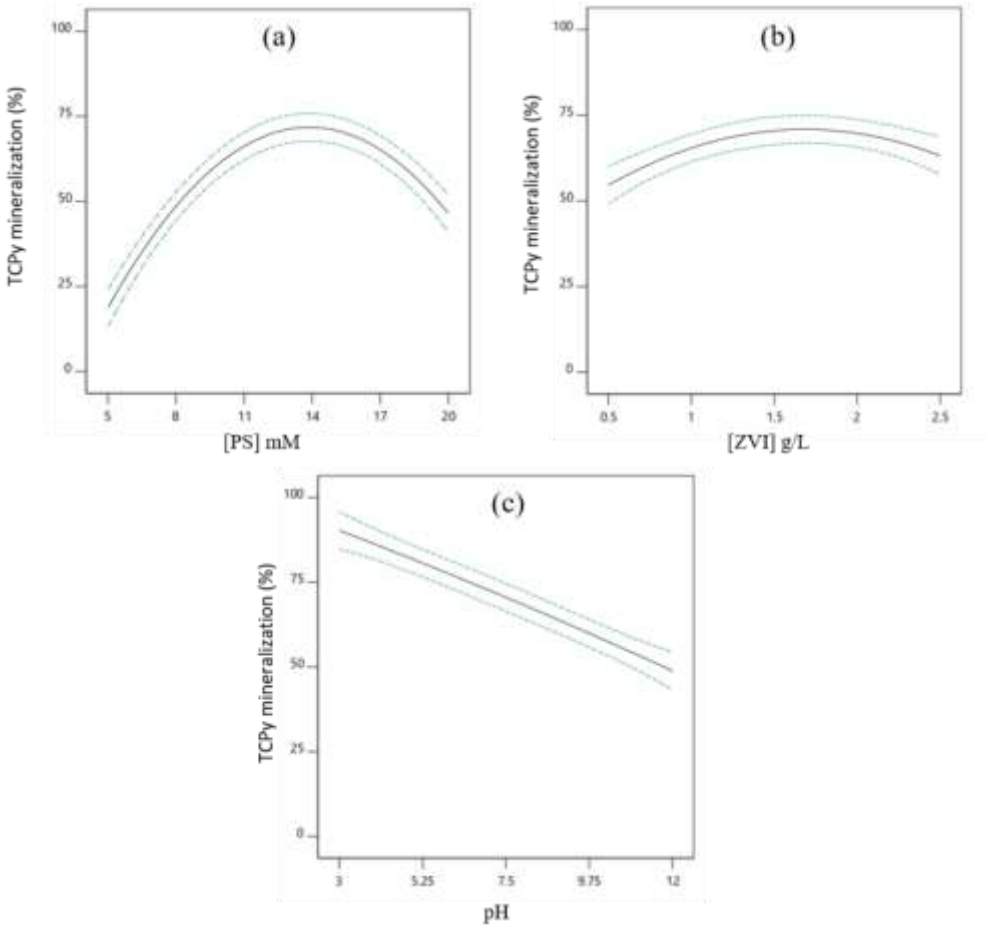

Figure 18: The influence of single factors on the mineralization of TCPy by ZVI/PS.

Response Surface Plotting for TCPy Mineralization

The following 3D response surface plots with the corresponding contour plots demonstrate the significant interactions between experimental variables by varying two variables at a fixed value while keeping the other variable at the center level (0) [30]. The 3D plots which were generated by using the developed quadratic model are presented in Figure 19. These surfaces illustrate that the interaction between ZVI and pH and between pH and PS have stronger influence on TCPy

mineralization than the interaction between ZVI and PS. Additionally, pH has greater influence on TCPy mineralization than ZVI and the highest removal efficiency was observed under acidic conditions. As PS concentration increased from a low to a moderate value within the experimental range, the mineralization of TCPy increased; however, higher PS concentration decreased the mineralization efficiency. At low PS concentration, even under acidic conditions, poor mineralization of TCPy was observed indicating that the influence of PS on TCPy mineralization is greater than that of pH.

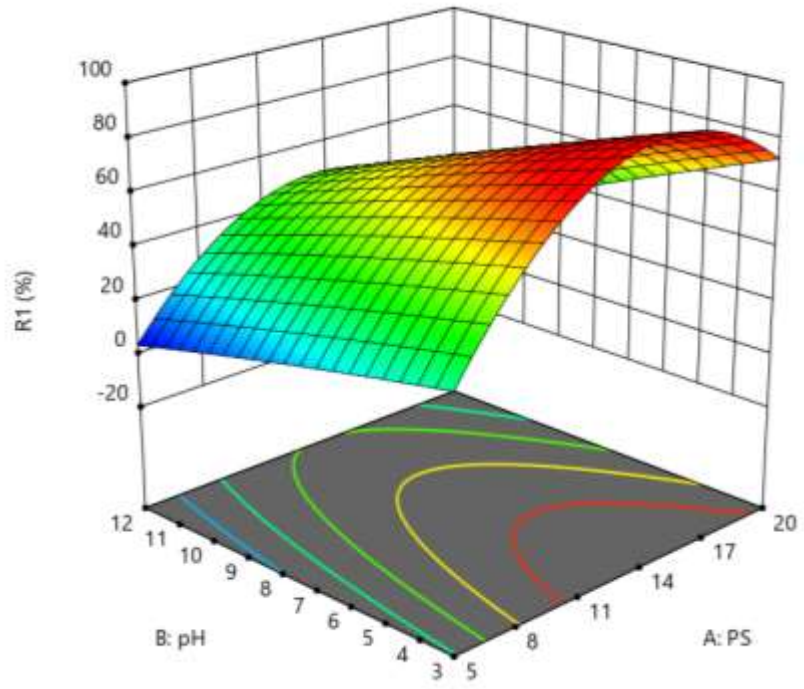
R1 (%)
100
80
60
40
20
0
-20
12
11
10
9
8
7
6
5
4
3
B: pH
5
8
11
14
17
20
A: PS

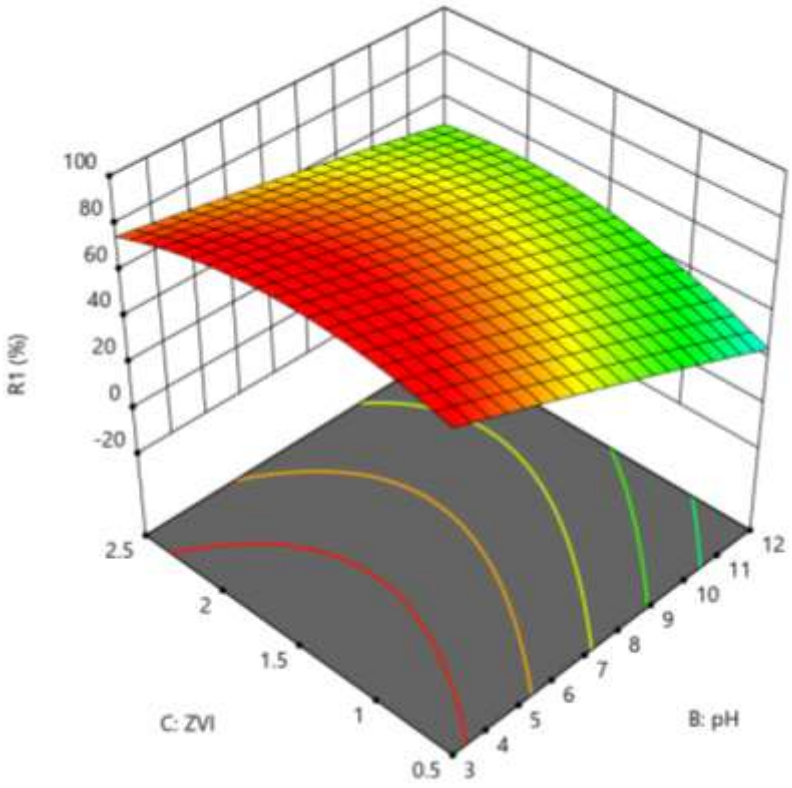
R1 (%)
100
80
60
40
20
0
-20
2.5
2
1.5
1
0.5
C: ZVI
3
4
5
6
7
8
9
10
11
12
B: pH

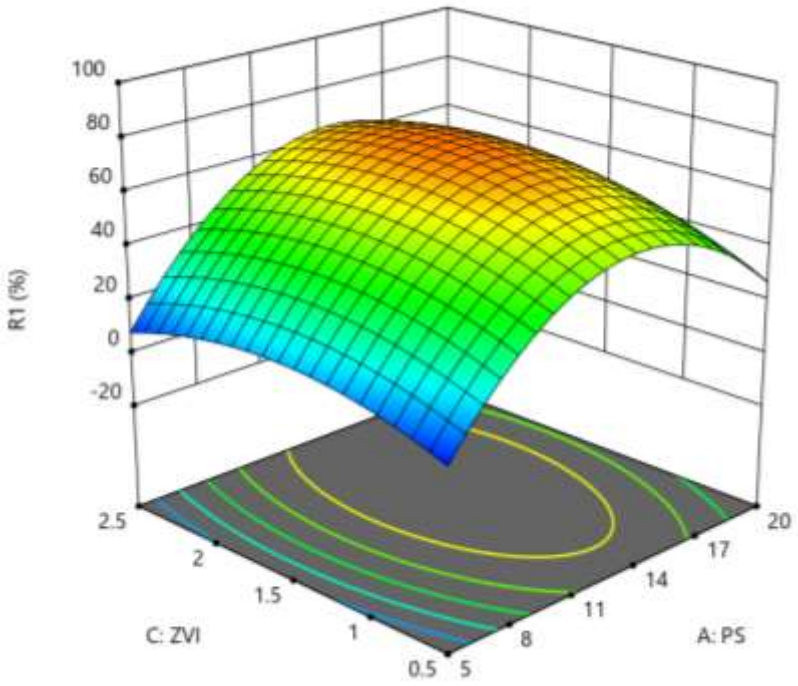

Figure 19: Response surface graphs of TCPy mineralization by ZVI/PS.

Optimization of the TCPy Mineralization Using Desirability Function

Numerical optimization was carried out using Design-Expert Software to determine the optimum conditions for the highest mineralization efficiency of TCPy (Figure 20). All parameters were selected to be within the experimental range while the response was set to maximum. The optimum conditions that led to maximum TCPy mineralization observed in this study (81.1%) were determined to be 10.4 mM PS concentration, 1.2 g/L initial ZVI concentration, and an initial pH of 3.2 with desirability function value of 1.000. To validate the prediction, an additional experiment was performed in duplicate using the predicted optimal condition. The values of TCPy mineralization obtained in these experiments were 72% and 79.4% with an average of 75.7%. The

obtained experimental values and predicted response values were in close agreement indicating the validity of this prediction.

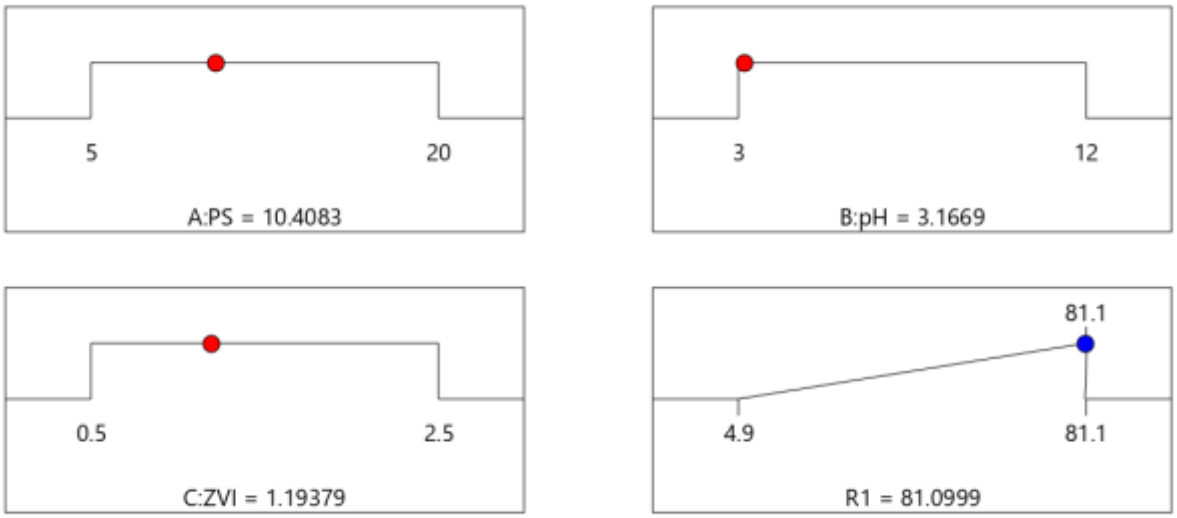

Figure 20: Desirability ramp for numerical optimization of the TCPy mineralization.

The degradation of TCPy by ZVI/PS under the optimum conditions suggested by the RSM was studied and the results are presented in Figure 21. Complete TCPy removal was achieved after 20 mins of reaction and the TCPy removal exhibited pseudo-first-order kinetics with k_{obs} of 1.254 × 10^{-1} min^{-1} (Figure 21).

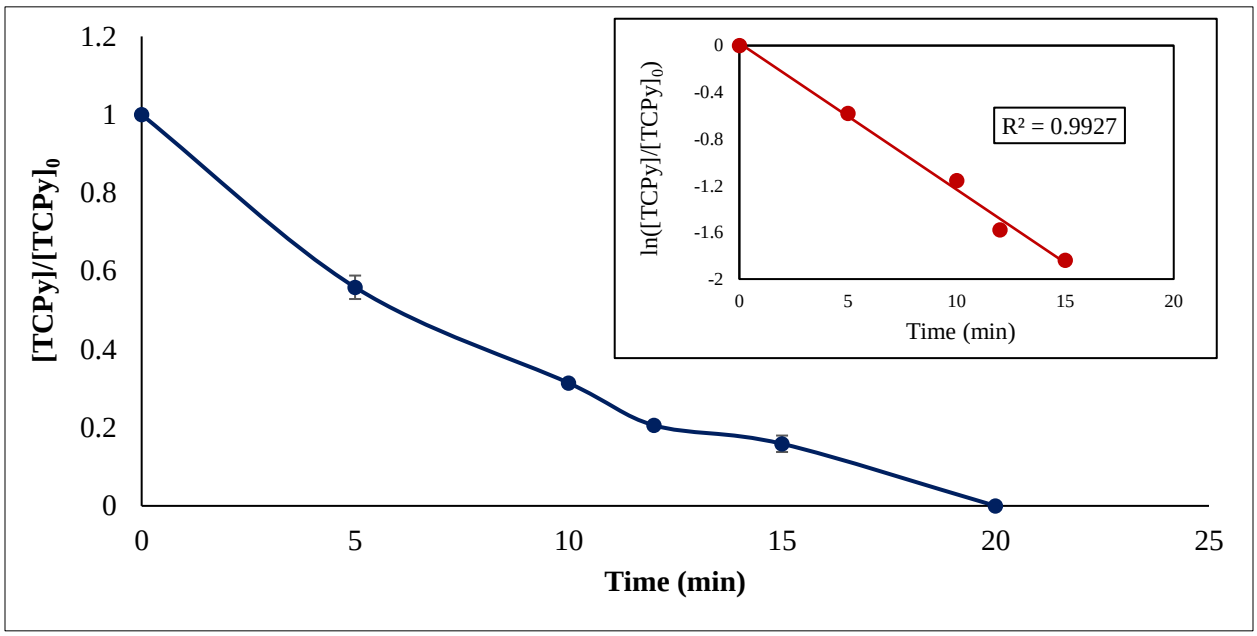

Figure 21: TCPy oxidation by ZVI/PS at optimal condition. Inset: Pseudo-First-Order kinetics of TCPy degradation.

Conclusion

ZVI is an effective method to activate persulfate for degradation of TCPy in water. Increasing the concentration of ZVI and PS increases the rate of TCPy removal, however, higher [PS] or [ZVI] decreased the TCPy oxidation rate. Acidic pH is more favorable toward the TCPy degradation rate than basic pH. For any particular [PS], [ZVI] and pH the removal of TCPy in ZVI/PS exhibited a pseudo-first-order kinetics pattern. Process optimization of the experimental factors ([PS], [ZVI], and pH) was carried out by means of Response Surface Methodology based on Box-Behnken design with TCPy mineralization after one hour chosen as the response. The significance of the fit for the second order quadratic model for TCPy mineralization was obtained by ANOVA yielding coefficient of determination (R^2) of 0.9917. The 3D plots show TCPy mineralization was influenced by the combined effect of ZVI and pH as well as between PS and pH. To determine the optimum conditions for the system, desirability function was performed and maximum TCPy mineralization (80.1%) was found at optimum process conditions (10.4 mM PS concentration, 1.2 g/L initial ZVI concentration, and an initial pH of 3.2). These values were further validated by performing duplicate experiments and were found to agree with model predictions. The kinetics of the optimized condition was studied and showed the oxidation of TCPy at this condition is well fitted to a pseudo-first-order model (R=0.99) with removal rate (k_{obs}) of $1.25 \times 10^{-1} min^{-1}$.

CHAPTER THREE: THERMOACTIVATED PERSULFATE OXIDATION OF 3,5,6-TRICHLORO-2-PYRIDINOL IN AQUATIC SYSTEM

Introduction

Chlorpyrifos (O,O-diethyl-O-3,5,6-trichloro-2-pyridyl phosphorothionate; CP) is a broad-spectrum insecticide which has been used for agriculture worldwide since 1965, though its registration for residential use was discontinued in the United States in the year 2000 [3]. Although CP has played an important role in improving agricultural productivity, its excessive use and persistence have caused many environmental concerns and adverse human health effects. The World Health Organization (WHO) has identified CP as moderately hazardous to humans. For instance, many studies have shown adverse effects on fetal development as a result of the exposure of expectant mothers to CP. Additionally, specific adverse effects (e.g. mental delay, psychomotor delay, attention disorder attention deficit hyperactivity disorder, and pervasive developmental disorders) were developed as the result of children's exposure to CP [7]. CP has also exhibited endocrine-disrupting activity, and some carcinogenicity studies of CP exposure suggested development of lung cancer and prostate cancer as the result of exposure to CP [5-6]. According to the United States Environmental Protection Agency (USEPA), there is a significant association between CP exposure and neurodevelopmental outcomes [7]. Once CP is released into the environment by agricultural application, it is hydrolyzed to its primary product 3,5,6-trichloro-2-pyridinol (TCPy). TCPy has been listed as a persistent and mobile pollutant by the USEPA [10]. Because of the high water solubility of TCPy, its leaching into ground water and surface water has resulted in widespread contamination in water and soil [11-12, 31].

In recent years, using persulfate (PS) as an oxidant for *in situ* chemical oxidation (ISCO) technology for the removal of organic contamination from soils, sediments, and ground water has received extensive attention [18, 26]. The activation of PS results in producing a strong oxidant sulfate radical ($SO_4^{\bullet-}$, SR), with a redox potential of (E^0 = 2.5-3.1 V, depending on pH). Many activation methods have been developed to activate PS including heat, microwave, alkaline conditions, UV, and transition metal ions [17].

$$S_2O_8^{2-} + heat/uv \rightarrow 2SO_4^{\bullet-} \quad (3.1)$$

$$S_2O_8^{2-} + Me^{n+} \rightarrow SO_4^{2-} + SO_4^{\bullet-} + Me^{(n+1)+1} \quad (3.2)$$

Among the above methods, the use of thermally activated persulfate is considered a highly effective and clean method and has been increasingly utilized in ISCO processes for the treatment of hazardous organic pollutant-contaminated water [17-18].

Therefore, this chapter evaluates the removal efficiency of TCPy by means of SR-based AOPs at the laboratory scale. The primary objective of this study was to investigate the degradation of TCPy by thermally-activated persulfate, as quantified by HPLC/MS. The influence of operational parameters such as temperature (T), initial PS concentration, and solution pH on the degradation kinetics of TCPy was assessed. Response surface modeling (RSM) based Box-Behnken experimental design (BBD) was used to optimize the degradation process of TCPy by thermally-activated persulfate.

Experimental

Chemicals

Neat TCPy, ammonium acetate ($C_2H_7NO_2$, ≥ 98%), sodium hydrogen carbonate ($NaHCO_3$, 99.5-100.5%), and N-tert-butyldimethylsilyl-N-methyltrifluoroacetamide (MTBSTFA) with 1% t-BDMCS were purchased from Sigma Aldrich (USA). Sodium persulfate ($Na_2S_2O_8$, ≥ 98.0%), sodium phosphate (Na_2HPO_4), potassium iodide (KI, ≥ 99%), HPLC grade acetonitrile (CH_3CN, >99.9%), sodium sulfate (Na_2SO_4), formic acid (HCOOH, ≥99.5 %), tert-butyl alcohol (TBA) ($C_4H_{10}O$, > 99%) and chloroform ($CHCl_3$, 99.8%) were purchased from Fisher Scientific.

Experimental Procedure

These experiments were conducted in 20 mL amber glass vials. An appropriate volume of the prepared stock solution of TCPy and deionized water (DI) were added together into vials. Vials were immersed into a thermo-regulated water bath until reaching the working temperature, when appropriate volumes of the stock solution of PS were then transferred into the vials. To clarify the effect of temperature (T) on the degradation kinetics of TCPy, experiments at different temperatures (20 ˚C - 80˚C) were set up. All other experimental parameters were held constant. At designated time points, samples were removed from the water bath and quenched in an ice bath.

To evaluate the effects of the initial concentration of PS on TCPy degradation, additional batch experiments were performed with different PS concentrations (2.5 mM – 20 mM) under the same experimental conditions as described above, but with a single predetermined temperature.

To study the influence of the initial reaction pH at various pH values (3.0 - 12.0), the initial pH of the TCPy solution was adjusted by adding small amounts of 0.1 M H_2SO_4 or 0.1 M NaOH to the desired value before starting the experiment. To prevent potential side reactions between $SO_4^{\bullet-}$ and other species, buffers were not employed in the present study.

The effect of chloride, phosphate, and sulfate anions on TCPy degradation was assessed by adding a known amount of the anions to the vials contain TCPy, before the addition of persulfate. All solutions were prepared daily using deionized water. All experiments were performed in duplicate.

Analysis

An Agilent 6230 TOF LC-MS with an Agilent Zorbax SB-C18 analytical column was used for TCPy analysis. An acetonitrile (ACN) and water mixture with a ratio of 60:40 (v ACN:v H_2O) was used as the mobile phase at a flow rate of 1.0 mL/min.

To determine the concentration of persulfate, an ultraviolet-visible light (UV-VIS) spectrometer (Agilent 8453 UV Visible Spectrophotometer equipped with deuterium (UV) and tungsten (visible) lamps) was used, following the spectrophotometric method developed by Liang, *et al.*[21].

A Shimadzu TOC-L Analyzer (Shimadzu Instruments, Kyoto, Japan) was used for nonpurgeable organic carbon (TOC) analysis. Prior to analysis, samples were acidified to pH 2-3 with sulfuric acid.

Experimental Design

Design Expert software (10.0.3) was used in this study to perform the experimental design as well as process the optimization for the system. Response surface methodology (RSM) is an efficient statistical method useful for describing the relationships and interactions between the experimental variables in order to specify the optimum conditions of the system. The relationship between the independent variables and the predicted response is described by a second order polynomial model:

$$Y = \beta_0 + \sum_{i=1}^{k} \beta_i X_i + \sum_{i=1}^{k} \beta_{ii} X_i^2 + \sum_{i=1}^{k} \sum_{j=1}^{k} \beta_{ij} X_i X_j + \epsilon \quad (3.3)$$

The most commonly used designs of RSM are the Box-Behnken design (BBD) and the central composite design (CCD). The few required experiments, less time, and lower costs to build the model equation by using BBD compared to CCD make the former more favorable. Therefore, in this study, BBD and RSM were applied for the optimization of the experimental parameters and to evaluate the relationships between them. The independent variables (T, PS concentration, and pH) were set at three different levels; their ranges and their coded levels are given in Table 5.

Analysis of variance (ANOVA) was used to statically evaluate the significance of the experimental parameters and the fit between the experimental data and the model.

Table 5: Experimental ranges and levels of the independent test variables.

Variables	Unit	Coded variable level		
		-1	0	1
Persulfate (PS)	mM	2	11	20
pH	-	3	6.5	10
Temperature	°C	40	60	80

Results and Discussion

Parameter Effects on TCPy Removal

Effect of temperature

The oxidation efficiency of organic contaminants is strongly affected by the applied temperature. Higher temperature provides more activation energy to cleave the peroxide bond of PS molecules, which results in generating more SRs (Eq 3.1). The high temperature also thermodynamically promotes the chemical reactions between reactive species and contaminants. Therefore, the enhancement of the degradation of environmental contaminants was observed with high temperature [17].

The oxidation of normalized TCPy concentration over time in a thermally-activated PS system with various temperature (20 °C - 80 °C) is presented in Figure 22. For the range of the applied temperature, the degradation of TCPy was significantly faster with higher temperature up to 80 °C. At 20 °C, only 0.02% TCPy degradation was observed after 6 hours of reaction. As temperature increased from 40 °C to 80 °C, the removal efficiency of TCPy increased from 2% to

100% after 7 mins of the reaction. Complete TCPy removal was achieved after 120 min, 60 min, and 15 min at 50 °C, 60 °C and 70 °C, respectively, while partial removal of TCPy (79%) was observed at 40 °C after 6 hours of the reaction (Figure 23).

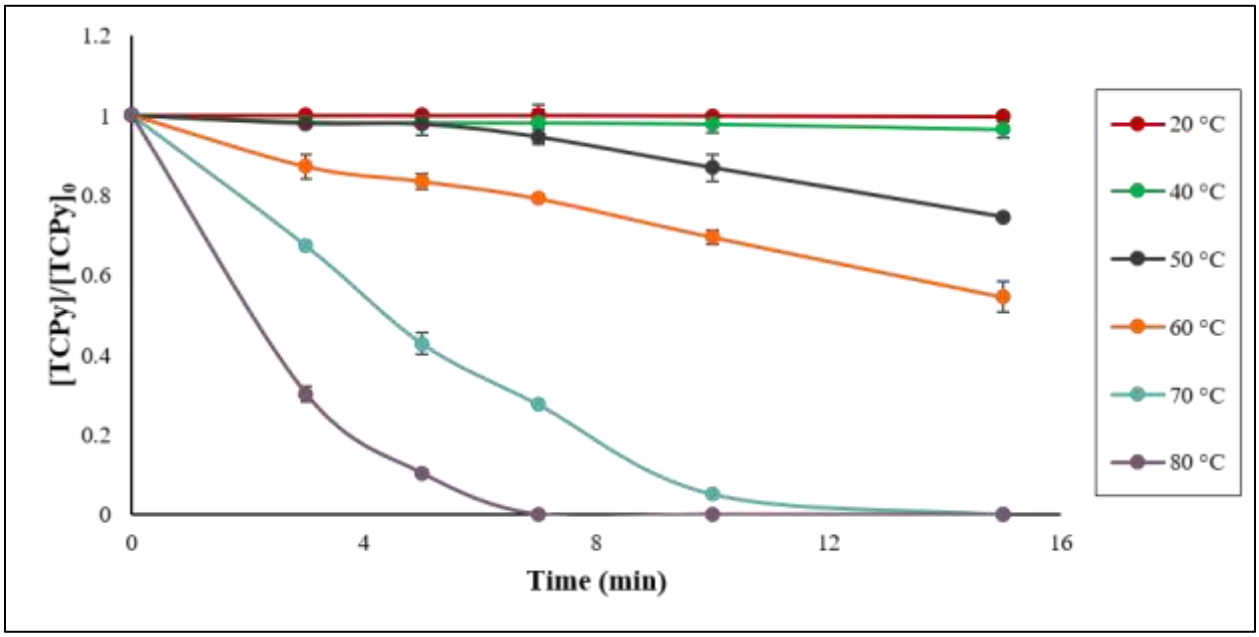

Figure 22: Influence of temperature on TCPy oxidation by heat activated persulfate. Experimental conditions: $[TCPy]_0$ = 50 µM; $[PS]_0$=10 mM; pH = 7

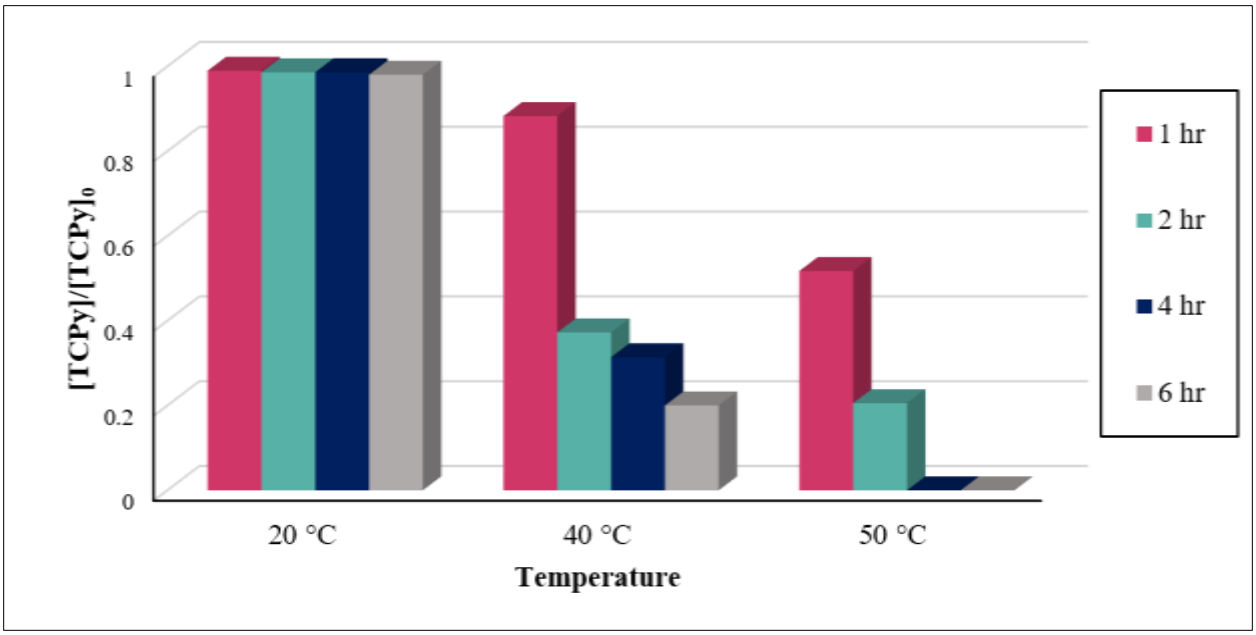

Figure 23: Extended oxidation time of TCPy at 20 °C, 40°C, and 50°C.

The normalized rate constants of TCPy removal at different temperature are presented in Figure 24. At all the applied temperatures except of 20 °C, TCPy removal exhibited pseudo-first-order kinetics. Therefore, the overall rate law for the oxidation of TCPy can be described by following equation

$$-\frac{d[TCPy]}{dt} = k\,[PS][TCPy]_0 = k_{obs}[TCPy] \qquad (3.4)$$

Increasing the temperature from 40 °C to 80 °C increased the rate constant (k_{obs}) of TCPy removal from 4.5×10^{-2} min^{-1} to 3.0×10^{-1} min^{-1}. The observed values of rate constants and the calculated half-lives ($t_{1/2}$) are presented in Table 6. As shown in this table, the half-lives of TCPy oxidation in thermally activated PS decreased from 91.2 min to 3.78 min as the temperature increased from 50 °C to 70 °C. Further incrementing the temperature to 80 °C significantly decreased the half-life to 1.5 min.

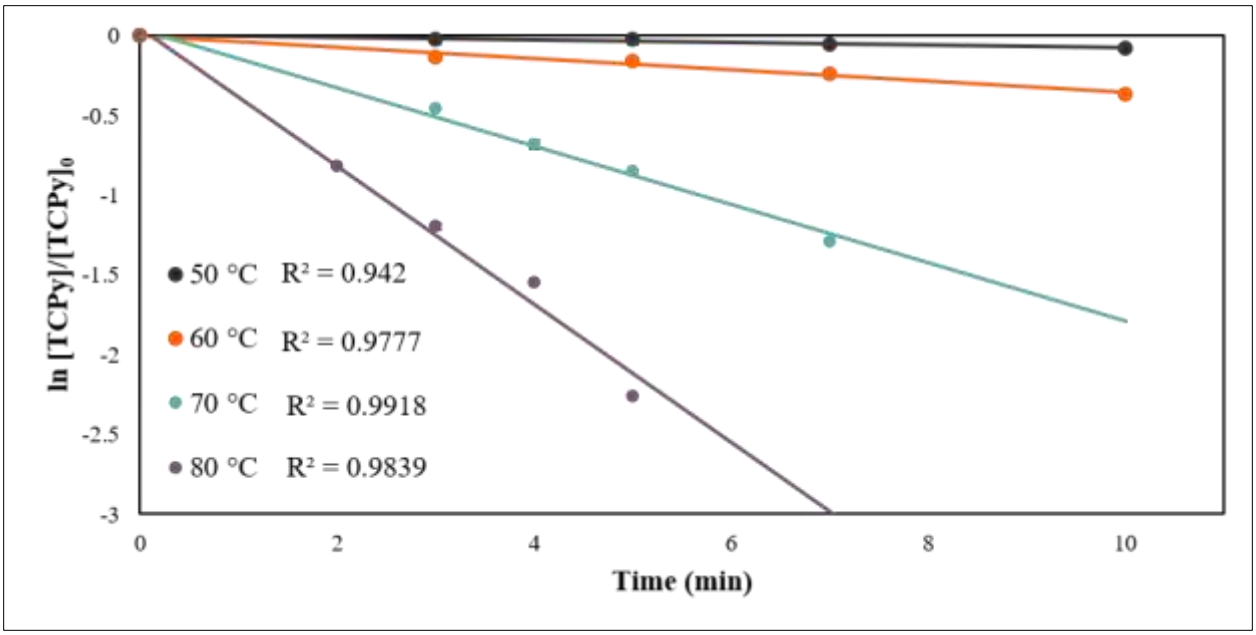

Figure 24: Pseudo-First-Order kinetics of TCPy degradation by heat activated PS at different temperatures.

Table 6: Comparison of TCPy degradation as a function of temperatures.

Temp (°C)	k_{obs} (min^{-1})	$t_{1/2\ (min)}$	R^2
50	7.6×10^{-3}	91.18	0.94
60	3.47×10^{-2}	19.97	0.98
70	1.83×10^{-1}	3.79	0.99
80	4.34×10^{-1}	1.60	0.98

The temperature-dependence of k_{obs} was further evaluated by the Arrhenius equation:

$$\ln k_{obs} = \ln A - \frac{E_a}{RT} \quad (3.5)$$

Where A is the pre-exponential factor, Ea is the apparent activation energy, R is the universal gas constant (8.314 J mol^{-1} K^{-1}), and T is the absolute temperature. The slope of the linear plot of ln (k_{obs}) *vs.* (1/T) ($R^2 > 0.99$) showed activation energy of 128 ± 0.6 kJ mol^{-1} (Figure 25).

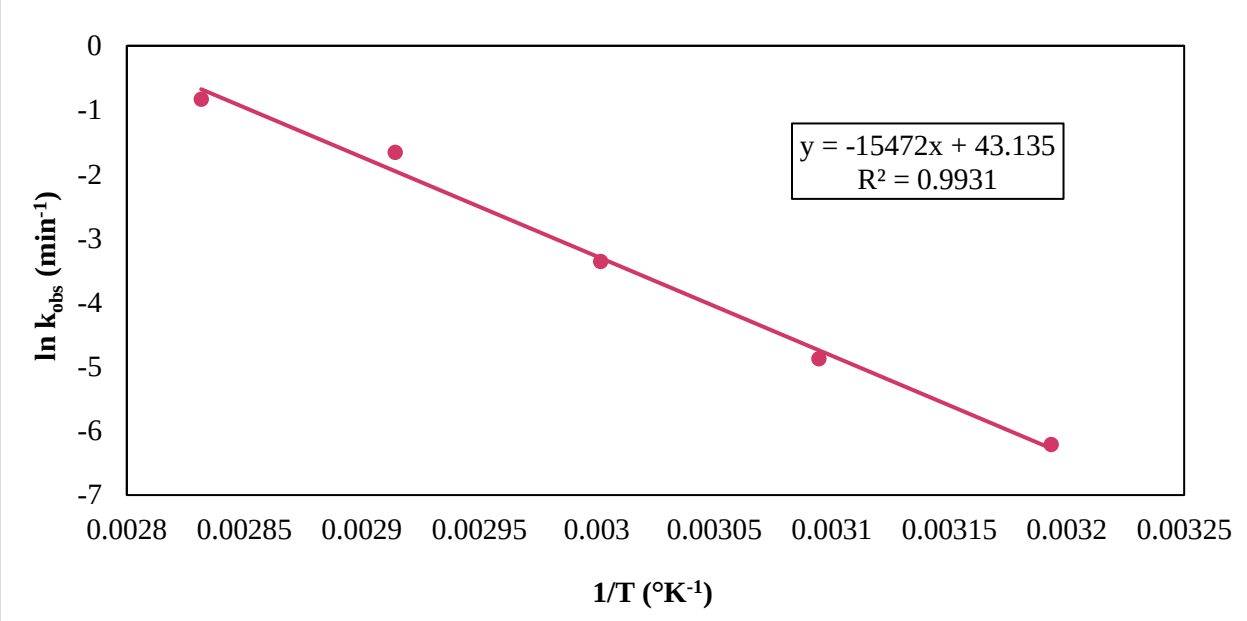

Figure 25: The Arrhenius plot for TCPy degradation.

Effects of PS concentration

The concentration of PS is another essential factor since it is the source of SRs. High PS dosage can enhance contaminant oxidation due to the higher amount of radicals produced. The effect of initial PS concentration on the oxidation of TCPy in a heat-activated PS system is presented in Figure 26. As shown in this figure, the degradation efficiency of TCPy increased with increasing concentration of PS. In the absence of PS, no oxidation of TCPy was observed. However, with the highest applied PS dosage (20 mM) TCPy was successfully oxidized after 12 min of reaction. Increasing the PS dose reduced the reaction time, and complete TCPy removal was achieved within 20, 15, and 12 mins, as the concentration of PS increased from 5, to 10, to 20 mM, respectively. This can be attributed to the higher amount of radicals produced as a result of higher concentrations of PS, which in turn oxidized more TCPy.

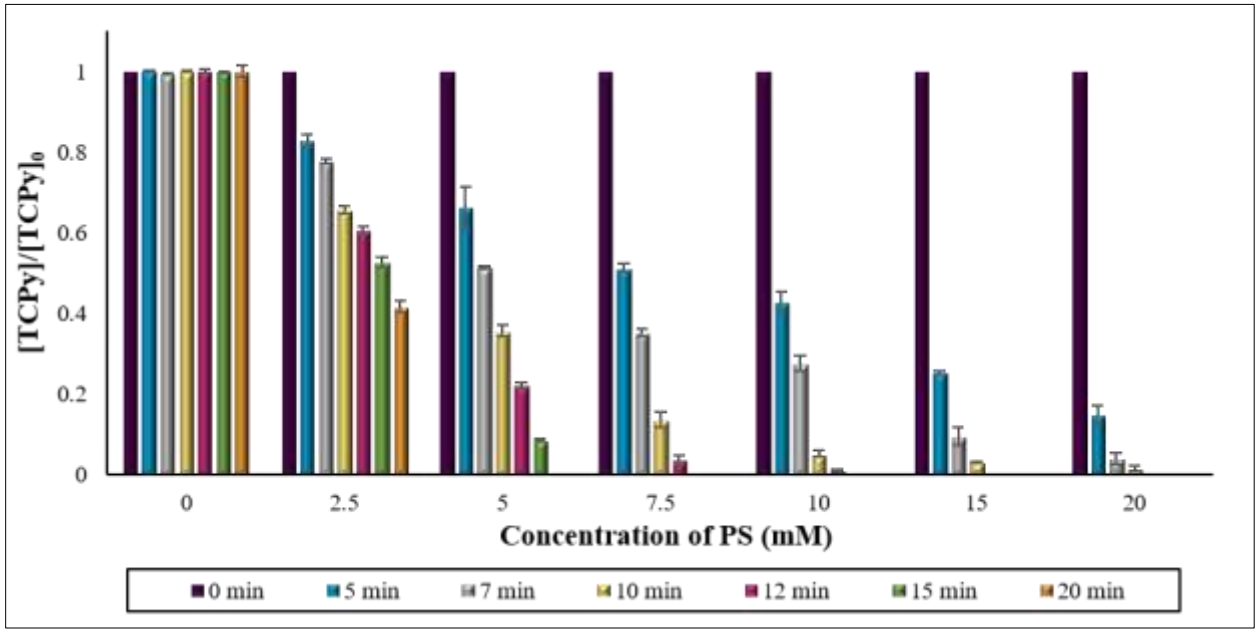

Figure 26: Effect of PS concentration on TCPy degradation by heat activated PS. Experimental conditions: $[TCPy]_0$ = 50 µM; T= 70 °C; pH = 7

The normalized rate constants of TCPy removal at different concentrations of PS are presented in Figure 27. For any specific concentration of PS in the thermally-activated PS system, TCPy removal exhibited pseudo-first-order kinetics (R^2 > 0.98 ± 0.04). Increasing the concentration of PS from 2.5 mM to 20 mM increased the value of the observed rate constant (k_{obs}) of TCPy removal from 4.1 × 10^{-2} min^{-1} to 4.2 ×10^{-1} min^{-1}. The calculated half-life of TCPy removal clearly indicates the enhancement of TCPy removal with increasing PS concentration (Table 7) as the $t_{1/2}$ value decreased from 16.5 to less than 2 min by increasing the PS concentration from 2.5 to 20 mM. The plot of k_{obs} vs the different initial concentrations of PS showed a good linear relationship indicating that the oxidation of TCPy in a heat-activated system is proportional to PS dosage (Figure 28).

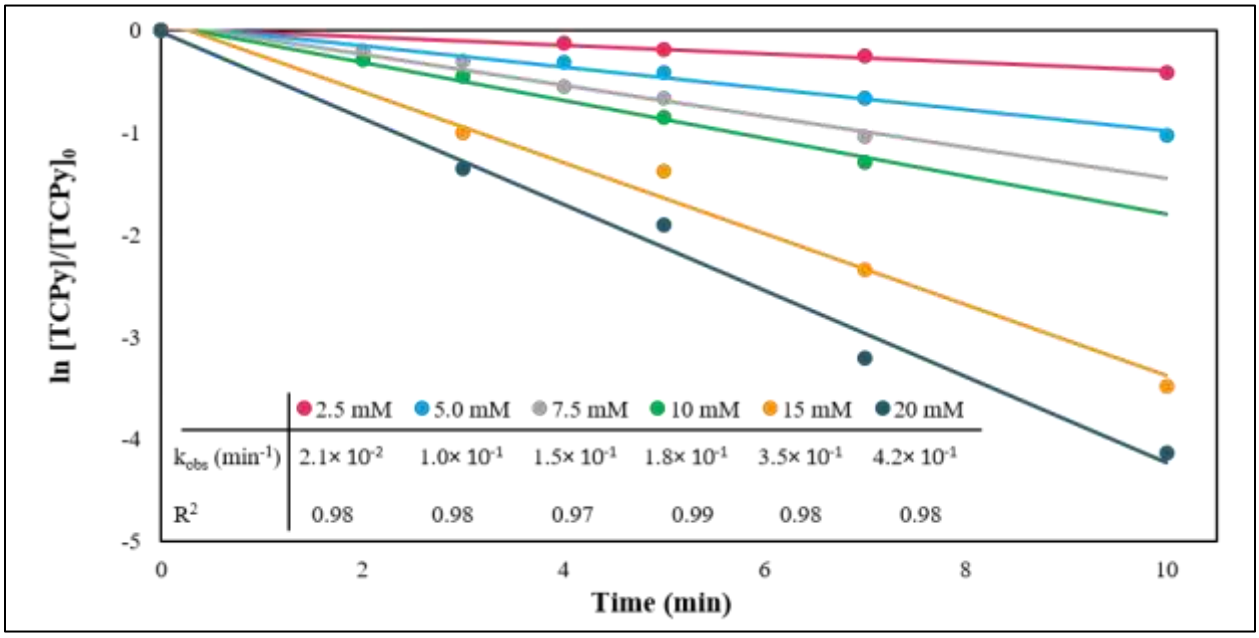

Figure 27: Rate constants of TCPy removal at different concentrations of PS in thermally activated PS system.

Table 7: Variation of pseudo-first-order rate constant as a function of initial PS concentrations for TCPy degradation by heat-activated PS oxidation. Experimental conditions: $[TCPy]_0$ = 50 µM; $[PS]_0$ = 10 mM; T= 70 °C

$[PS]_0$ (Mm)	k_{obs} (min^{-1})	R^2	$t_{1/2}$ (min)
2.5	2.1×10^{-2}	0.98	16.6
5	1.038×10^{-1}	0.98	6.7
7.5	1.522×10^{-1}	0.97	4.6
10	1.847×10^{-1}	0.99	3.8
15	3.465×10^{-1}	0.98	2.0
20	4.202×10^{-1}	0.98	1.6

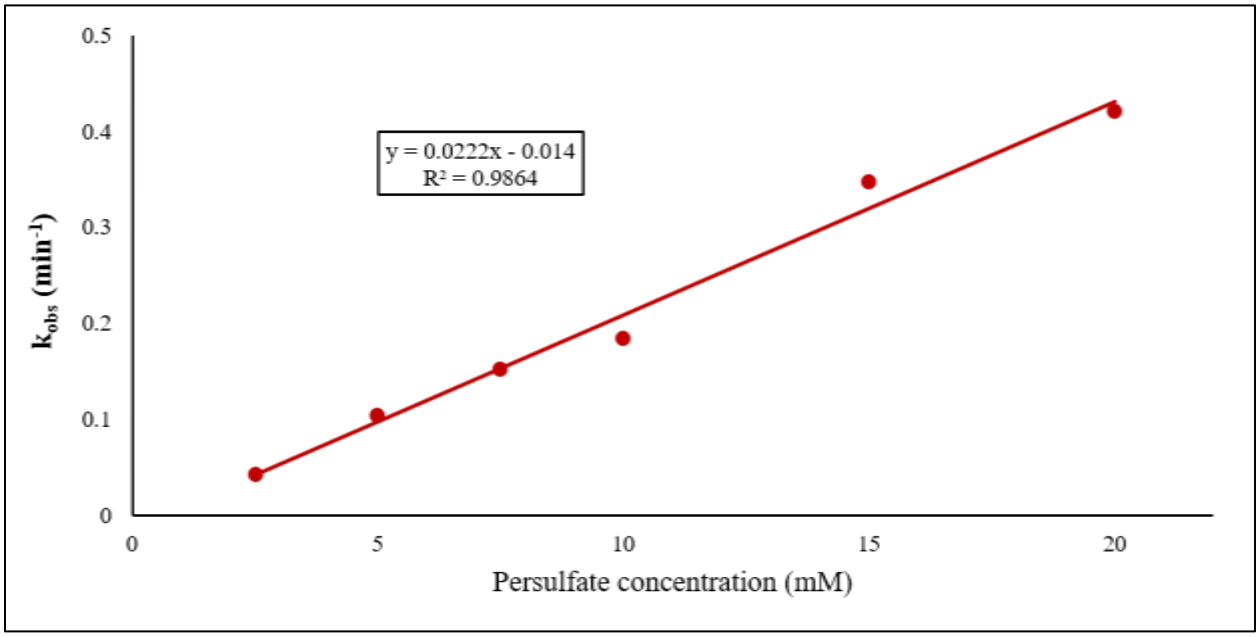

Figure 28: Plot of k_{obs} vs PS concentration in heat activated PS system.

Although TCPy was completely removed by 15 mM and 20 mM PS by the same time point, the rate constant of TCPy removal is higher at 20 mM PS (Figure 26). Similarly, 10 mM PS exhibits a higher removal rate of TCPy than 7.5 mM PS, although both were able to completely oxidize the TCPy after 15 min of reaction. This is likely due to the generation of more SRs with increasing PS dosage. As presented in Figure 29, the consumption of PS increased with increasing PS concentration. At 20 mM PS, up to 18.5% of the initial PS concentration was consumed within 12 min while 6.4% was consumed with the lowest initial concentration of PS ($[PS]_0$ = 2.5 mM) in the same time. The reaction stoichiometric efficiency (RSE), was evaluated when TCPy was completely removed at the different PS concentration. As shown in Figure 30, the RSE of the system decreased when increasing PS concentration from 5 mM to 10 mM. However, further increment of PS concentration to 15 mM and 20 mM enhanced the calculated RSE to 22.5% and 37.1%, respectively.

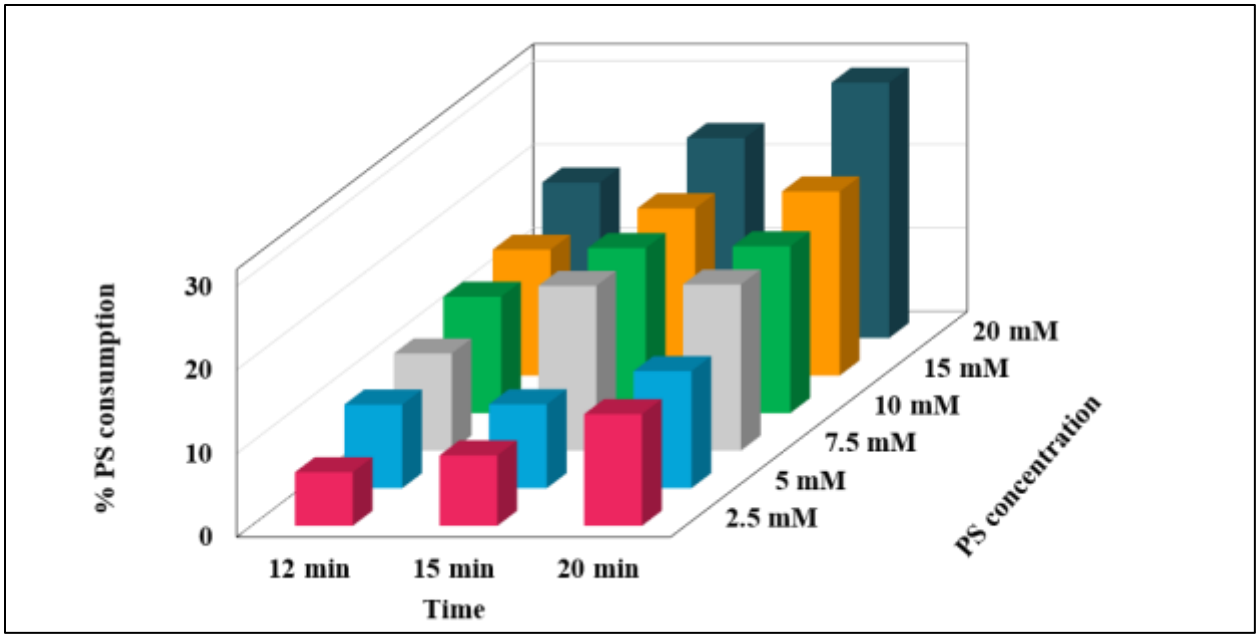

Figure 29: PS consumption during the reaction with different PS concentrating in heat activated PS system.

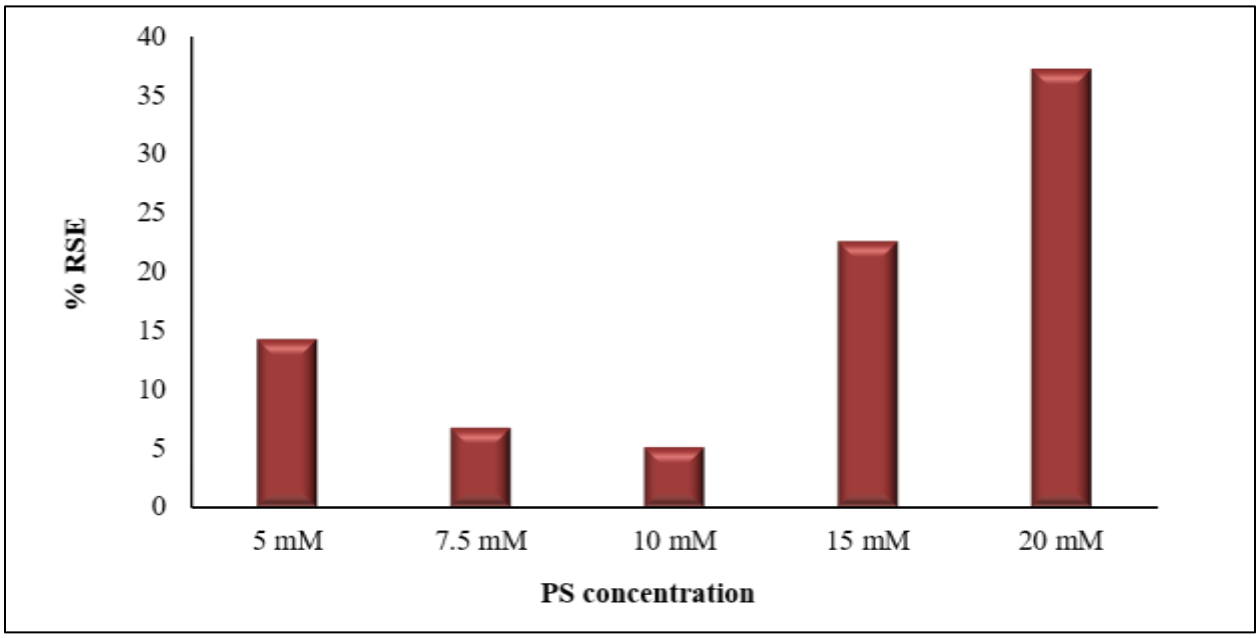

Figure 30: Reaction stoichiometric efficiencies during the TCPy degradation with different concentration of PS in heat activated PS system.

Effect of pH

Solution pH is an important factor which may significantly influence the degradation of pollutants as well as the formation of radicals [26]. Changing the solution media results in changing of the dominant oxidizing species. For example, it was reported that SRs are the primary reactive species in acidic condition, both SRs and HRs are present in natural pH systems, while in basic conditions all SRs are converted into HRs (Eq 3.6 and 3.7) [26].

$$SO_4^{\bullet-} + H_2O \rightarrow SO_4^{2-} + OH^{\bullet} + H^+ \quad (3.6)$$

$$SO_4^{\bullet-} + OH^- \rightarrow SO_4^{2-} + OH^{\bullet} \quad (3.7)$$

The change in normalized TCPy concentration over time at various initial solution pH values in the range of 3.0–12.0 is presented in Figure 31. As the solution pH increased from 3 to 10, the removal efficiency of TCPy increased. In basic conditions (pH =10) the oxidation of TCPy resulted in higher removal efficiency compared to that of acidic conditions (pH= 3). TCPy was successfully removed after 15 minutes at all solution pH values except pH 10, in which complete TCPy removal was achieved after 10 minutes. The results indicate that, with heat-activated PS, basic conditions are more favorable for TCPy oxidation than acidic conditions. Increasing the removal efficiency by increasing the solution pH is likely due to the increased presence of HRs at such pH, which have a higher redox potential than SRs. Additionally, in alkaline conditions the reactivity of SRs increases, and base-activated PS is used to successfully oxidize TCPy. In order to identify the predominant radical species responsible for TCPy oxidation at pH 10, additional experiments were performed by spiking the solution with two types of alcohol (ethanol [EtOH] and tert-butyl alcohol [TBA]). In each experiment, the alcohol was in great excess relative to PS and TCPy to ensure inhibition of the radicals.

In SR-AOPs, using alcohol such as EtOH and TBA as radical scavengers is common. EtOH with its α-H is known to scavenge sulfate radicals with a rate constant of 1.6-7.7× 10^7 M^{-1} s^{-1} and hydroxyl radicals with a rate constant of 1.2-2.8 × 10^9 M^{-1} s^{-1} [27] Conversely, TBA is an active reactant with hydroxyl radicals with a rate constant of 3.8-7.6 ×10^8 M^{-1} s^{-1}, which is higher than that with sulfate radicals (4.0-9.1 × 10^5 M^{-1} s^{-1}). Therefore, both EtOH and TBA were used to explore the involvement of the radical species in TCPy oxidation at pH 10.

As shown in Figure 32, in the quencher-free system complete removal of TCPy was achieved within 10 minutes, while treatment with either EtOH or TBA resulted in poor degradation efficiencies of 4.8% and 30.1%, respectively. In the TBA system, HRs were scavenged while SRs were responsible for TCPy degradation. However, both radicals (HR and SR) were scavenged in the EtOH system which results in the poor degradation efficiency. These results indicate that HR is the predominant species at pH 10 in the heat-activated PS system that oxidizes TCPy.

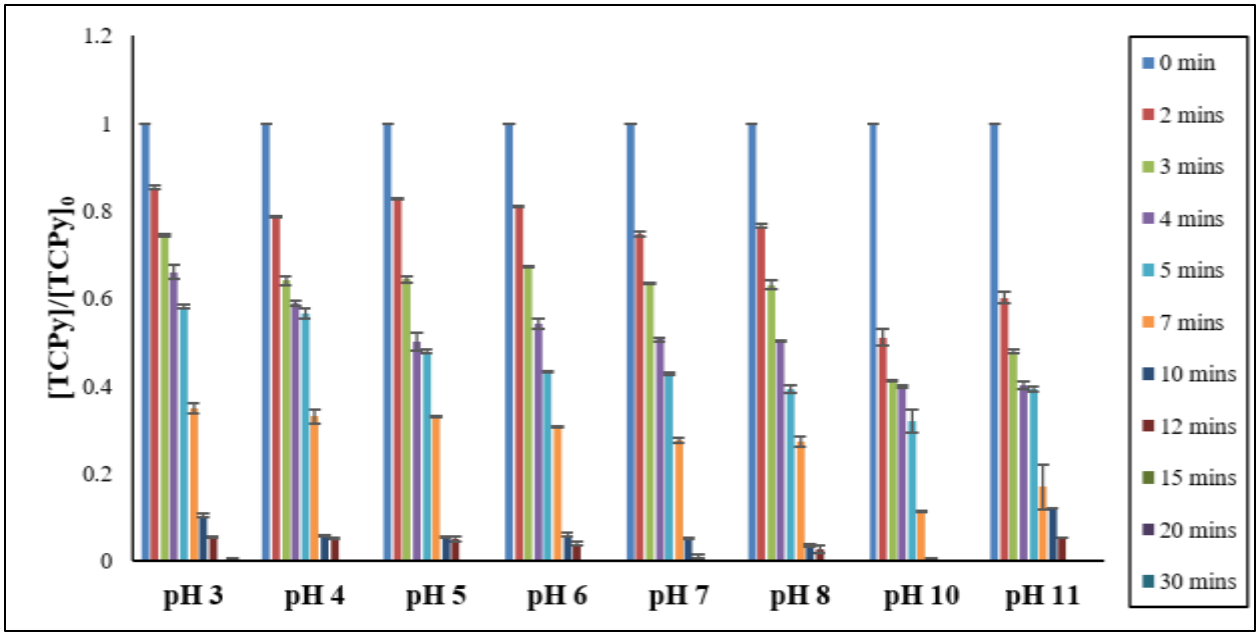

Figure 31: Oxidation of TCPy by heat activated PS at different pH. Experimental conditions: $[TCPy]_0$ = 50 µM; T= 70 °C; [PS] = 10 mM

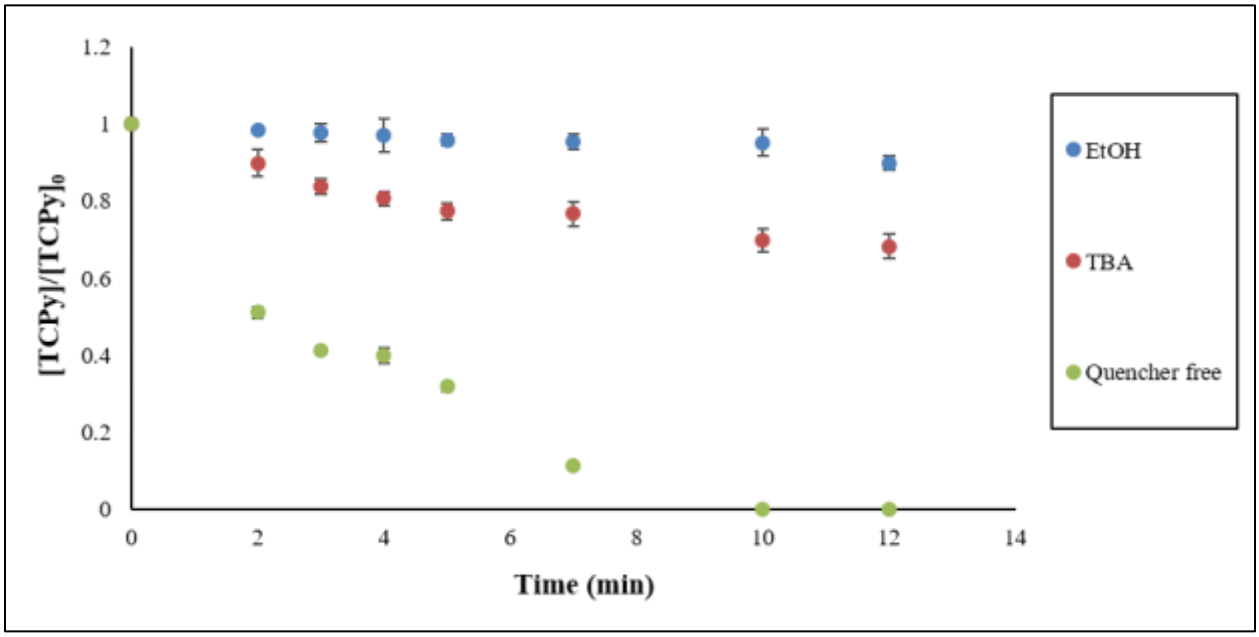

Figure 32: TCPy degradation in the absence and in the presence of radical scavengers at pH 10 in heat activated PS system.

Although at each solution pH from 3 to 8, TCPy was completely oxidized after 15 minutes, their degradation rates were slightly different. The normalized rate constants of TCPy removal at different solution pH (Figure 33) showed that TCPy removal exhibited pseudo-first-order kinetics (R^2 > 0.96 ± 0.03) at any applied pH value. As the solution pH increased from 3 to 10 the corresponding rate constant (k_{obs}) increased from 1×10^{-1} min^{-1} to 3.1×10^{-1} min^{-1}. However, as the solution pH further increased to 11 or 12, the k_{obs} decreased to 2.5×10^{-1} and 2.4×10^{-1}, respectively, which is likely due to the side reaction of HR with HR resulting in radical losses as described by Eq 3.8.

$$OH^{\bullet} + OH^{\bullet} \rightarrow H_2O_2 \qquad (3.8)$$

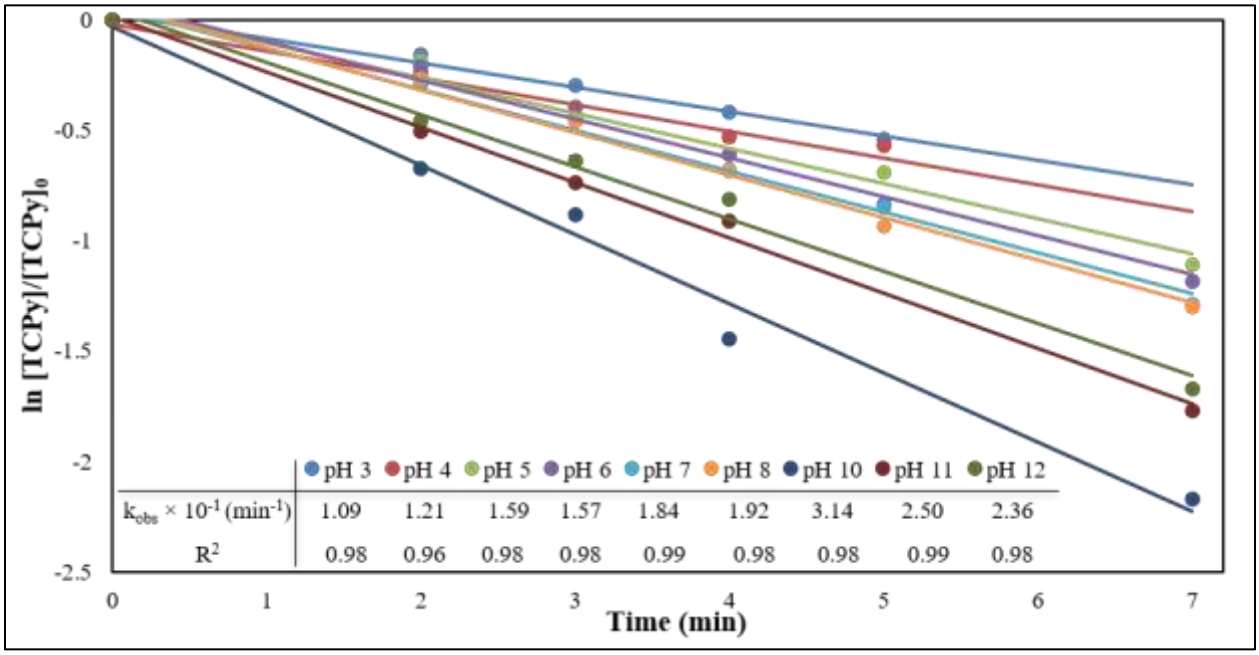

Figure 33: Pseudo-First-Order kinetics of TCPy degradation in heat activated PS system at different pH.

Regression Model Representation

The mineralization of TCPy by heat activated PS after 30 minutes treatment was chosen as an appropriate measure for assessing the combined effect of the selected parameters in this study by RSM. The experimental design matrix using the three factors (T, [PS], and solution pH) each on three levels and the responses (TCPy mineralization) based on experimental runs proposed by BBD are presented in Table 8. According to the Design Expert software, the quadratic model is suggested to be the most applicable model for the degradation of TCPy by heat-activated PS due to its higher correlation coefficient (R^2) value as well as lower standard deviation relative to other models. The final predicted model in terms of coded parameters is described by the following Eq:

$$Y = 77.18 + 13.45\ A + 16.96\ B + 20.76\ C - 5.83\ AB + 4.63\ AC - 6.90\ BC - 19.27\ A^2 - 11.59\ B^2 + 2.46\ C^2 \quad (3.9)$$

Where Y represents the % mineralization of TCPy at 30 min. A, B, and C are the coded values of the initial concentration of PS, pH, and the concentration of T, respectively.

Table 8: The BBD design matrix and experimental results for TCPy degradation by heat activated PS.

Run	Independent variables (coded)			TOC removal (%)	
	PS (mM)	pH	T (°C)	Exp.	Pred.
1	0	-1	-1	22.3	25.30
2	1	1	0	69	70.50
3	-1	0	-1	30	81.97
4	-1	1	0	51	70.50
5	0	0	0	76.6	42.56
6	1	0	-1	44.9	70.50
7	0	0	0	75	72.84
8	-1	0	1	66.6	70.50
9	0	0	0	76.4	75.30
10	1	-1	0	53.3	70.50
11	0	1	-1	76.6	49.12
12	0	0	0	83.2	18.21
13	0	0	0	74.7	3.66
14	-1	-1	0	12	27.19
15	0	-1	1	73.3	8.01
16	0	0	1	100	6.24
17	1	1	1	100	31.89

Statistical Analysis (ANOVA)

The statistical significance and the adequacy of the BBD model was evaluated by ANOVA and the results are presented in Table 9. As shown in this table, the model exhibited F-value of 40.93, indicating the model is significant. Coefficients having p-values less than 0.05 imply significance of that term. Therefore, in this study A, B, C, BC, A^2 and B^2 are statistically significant model terms with p-values less than 0.0001. The obtained correlation coefficient of 0.98 indicates good agreement between the experimental data and the model. The obtained adequate precision (Adeq Precision) ratio of the model is 22.478 which is greater than the minimum value of 4 necessary to confirm that the model is adequate.

Table 9: ANOVA for response surface quadratic model of TCPy mineralization in heat activated PS system.

Source	Sum of Squares	df	Mean Square	F-value	p-value	
Model	9845.20	9	1093.91	40.93	< 0.0001	significant
A-PS	1447.22	1	1447.22	54.15	0.0002	
B-pH	2301.81	1	2301.81	86.12	< 0.0001	
C-T	3448.65	1	3448.65	129.03	< 0.0001	
AB	135.72	1	135.72	5.08	0.0589	
AC	85.56	1	85.56	3.20	0.1167	
BC	190.44	1	190.44	7.13	0.0320	
A^2	1562.70	1	1562.70	58.47	0.0001	
B^2	565.59	1	565.59	21.16	0.0025	
C^2	25.48	1	25.48	0.9534	0.3614	
Residual	187.09	7	26.73			

R^2	0.9814
Adjusted R^2	0.9574
Predicted R^2	0.7708
Adeq Precision	22.4778
Std. Dev.	5.17
Mean	63.82
C.V. %	8.10

To further validate this model, residual analysis was used in this study including a normal probability plot and the plot of predicted responses versus actual responses. The normal probability plot of the residuals showed approximately a straight line which means this condition is satisfied, according to Teh, *et al.* [29] (Figure 34) The plot of predicted responses against actual responses showed that the residuals are well-distributed around the mean response, which confirmed good predictability (Figure 35).

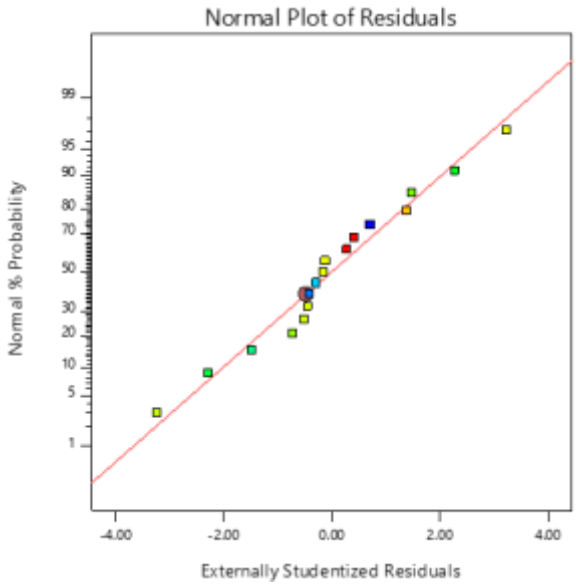

Figure 34: Normal probability plot of the residuals in heat activated PS system.

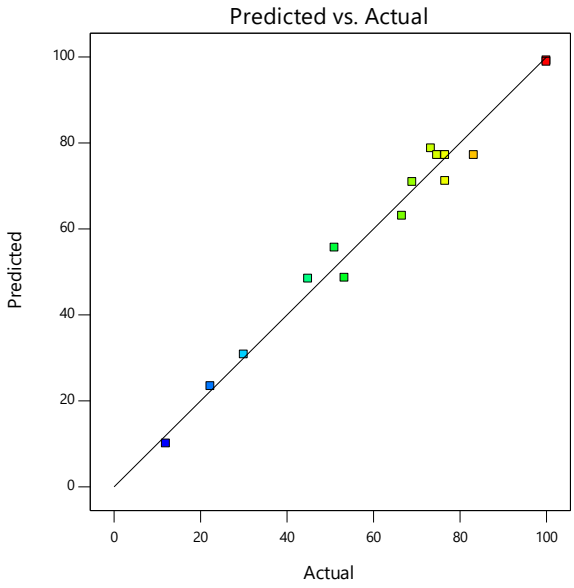

Figure 35: Predicted response versus actual response for TCPy mineralization in heat activated PS system.

One Factor Effect on TCPy Mineralization

The effect of one factor on TCPy mineralization by heat activated persulfate while keeping all other factors constant is established based on the quadratic model. The influence of persulfate concentration on the mineralization efficiency of TCPy at 70 °C and pH 7 is presented in Figure 36. Increasing the persulfate concentration up to 15 mM enhanced the efficiency of TCPy mineralization. However, further increasing persulfate concentration reduced the mineralization efficiency. While 90% of TCPy was predicted to be mineralized at an initial persulfate concentration of 15 mM, 85% of TCPy was mineralized with a higher persulfate concentration (20 mM). In the heat-activated persulfate system, PS is the source for producing sulfate radicals. Therefore, increasing the concentration of PS enhanced the mineralization efficiency. However, as the concentration of PS increased, more sulfate radicals are produced in the system causing

radical loss due to side reactions between the radicals and persulfate as well as between two radicals (Eqs 3.10 and 3.11).

$$SO_4^{\bullet -} + S_2O_8^{2-} \rightarrow SO_4^{2-} + S_2O_8^{\bullet -} \quad (3.10)$$

$$SO_4^{\bullet -} + SO_4^{\bullet -} \rightarrow S_2O_8^{2-} \quad (3.11)$$

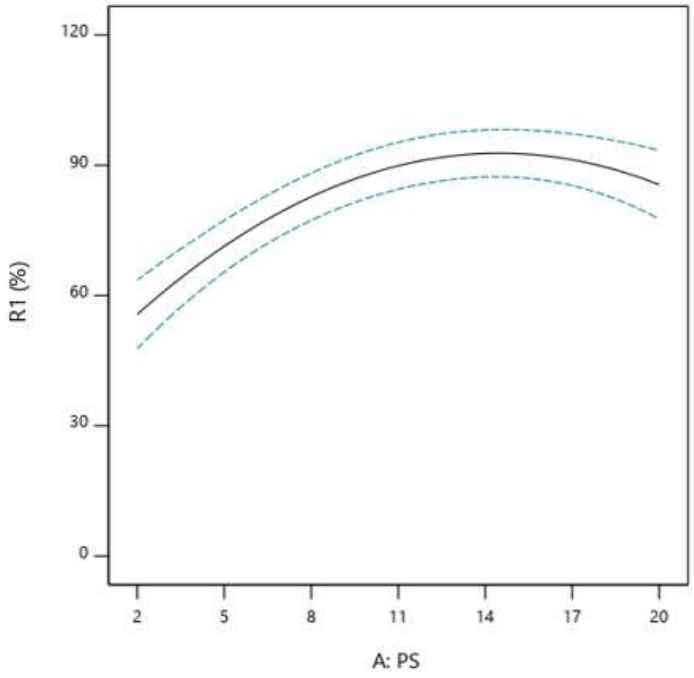

Figure 36: Effect of persulfate concentration on TCPy mineralization.

The influence of temperature on TCPy mineralization in the heat-activated persulfate system at constant PS concentration (11 mM) and at constant pH 7 is illustrated in Figure 37. As shown in this figure, enhancement of TCPy mineralization was observed with increasing

temperature. At higher temperatures, more sulfate radicals are produced which oxidize more TCPy compared to lower temperatures. This result indicated that the mineralization of TCPy is proportionally associated with increasing applied temperature.

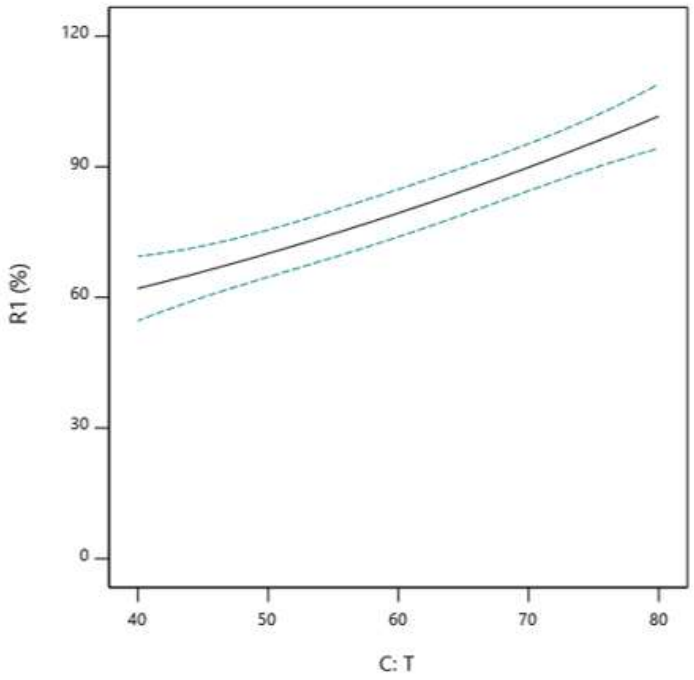

Figure 37: Effect of temperature on TCPy mineralization.

The influence of pH on TCPy mineralization in the heat-activated persulfate system at 70 °C with an initial persulfate concentration of 11 mM is shown in Figure 38. As the solution pH was increased from low (3) to high (8), the TCPy mineralization efficiency was increased; however, higher solution pH (8-9) plateau the mineralization of TCPy. At pH > 9 the mineralization was slightly decreased. In this case, where the temperature and the concentration of PS were kept constant, the presence of different reactive species as the solution pH changed influenced the TCPy mineralization. The identification of the reactive species (sulfate radicals and

hydroxyl radicals) produced by thermally-activated persulfate at different pH levels was investigated by Liang, C. & Su, H. W. [27]. The results of that study demonstrated the presence of sulfate radicals at pH < 7, both radicals are present at pH 9, while hydroxyl radical is present at higher pH (e.g., pH 12). The presence of hydroxyl radicals at higher solution pH enhanced the mineralization efficiency of TCPy due to its higher redox potential compared to sulfate radicals. The presence of an excessive amount of hydroxyl radicals at more basic pH reduces the mineralization efficiency of TCPy due to radical-radical reactions which result in radical loss (Eq 3.8).

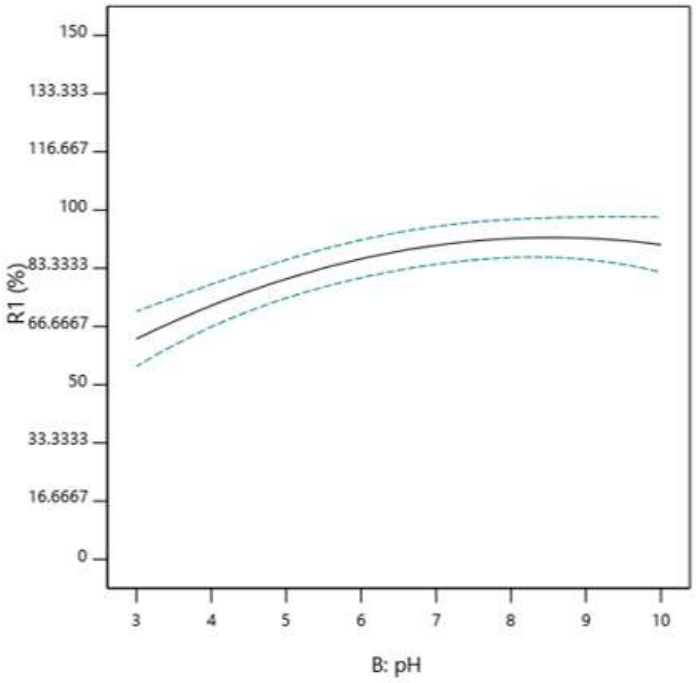

Figure 38: Effect of solution pH on TCPy mineralization.

Response Surface Plotting for TCPy Mineralization

A set of 3D response surface plots with their corresponding contour plots were generated by using the developed second-order polynomial model (Eq 3.4) to demonstrate the significant interactions between experimental variables by varying two parameters at a fixed value while keeping the other parameter at constant level [30].

Figure 39 demonstrates the significant interaction between [PS] (A) and temperature (C) for TCPy mineralization at constant pH (pH = 7). The interaction between [PS] and T showed that the mineralization efficiency of TCPy increased with increasing T and a higher mineralization efficiency was achieved with higher T at any specific concentration of PS. For example, at 40 °C, the mineralization efficiency of TCPy was 37.6% at [PS] of 2.5 mM. However, increasing the T to 80 °C led to 68.4% TCPy mineralization at the same concentration of PS. On the other hand, at 40 °C, the predicted response of TCPy mineralization increased slightly from 37.6% to 62.9% when the PS concentration increased from 2.5 to 15 mM. However, further increment of [PS] to 20 mM decreased the mineralization efficiency of TCPy to 51.7%. Similarly, at 80 °C, increasing the [PS] up to 15 mM improved the TCPy mineralization, however, further increasing PS concentration to 20 mM lowered the mineralization efficiency. This observation can be explained by the fact that higher concentrations of PS generate more SRs which could be scavenged by SR itself or by PS (Eq 3.10 and 3.11) [23-24].

Although 20 mM PS successfully removed TCPy with the highest rate of reaction, this concentration is not as effective for complete TCPy mineralization.

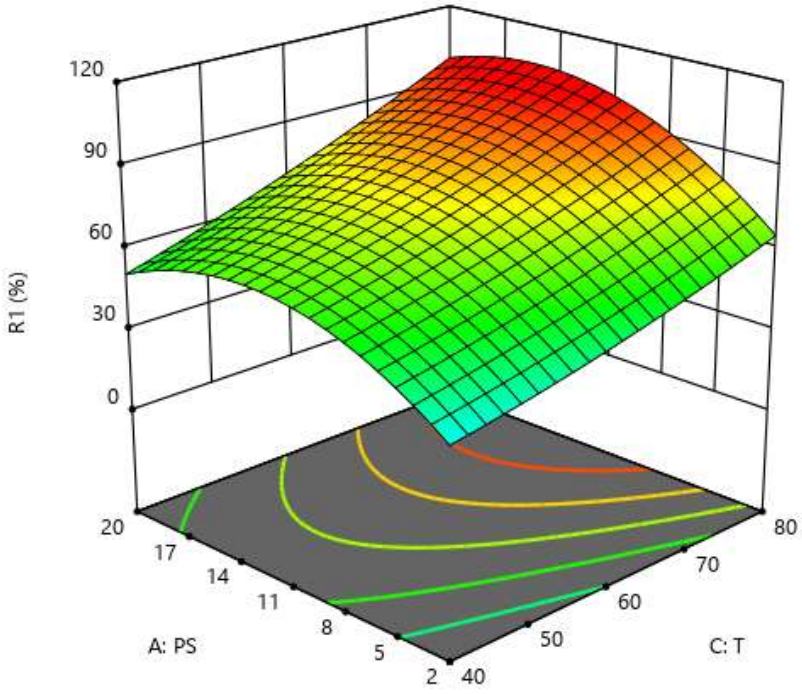

Figure 39: 3D-surface effect plots showing the effect of PS and temperature

The 3D response surface plot in Figure 40 shows the combined effects of pH and PS concentration at constant T (T= 70 °C). Increasing pH and the concentration of PS improved the mineralization efficiency of TCPy, however, above certain levels of PS concentration ([PS] > 14.3 mM), the mineralization efficiency decreased even at higher pH. For instance, at constant PS concentration ([PS]=2.5 mM), 26% of TCPy was mineralized at pH 3. However, the TCPy mineralization increased to 63% as the solution pH was increased to 10. This is likely due to the presence of more hydroxyl radicals at basic pH, which have a higher redox potential than sulfate radicals thus enhancing the mineralization efficiency of TCPy.

On the other hand, at constant pH (pH=10), as the PS concentration increased from 2.5 mM to 14.3 mM, the mineralization efficiency of TCPy increased from 63 % to 91.8 %, However, further increasing the PS concentration to 20 mM decreased TCPy mineralization to 81.6 %. This is likely due to the generation of more sulfate radicals at higher PS concentrations, which leads to radical quenching (Eq 3.10 and 3.11).

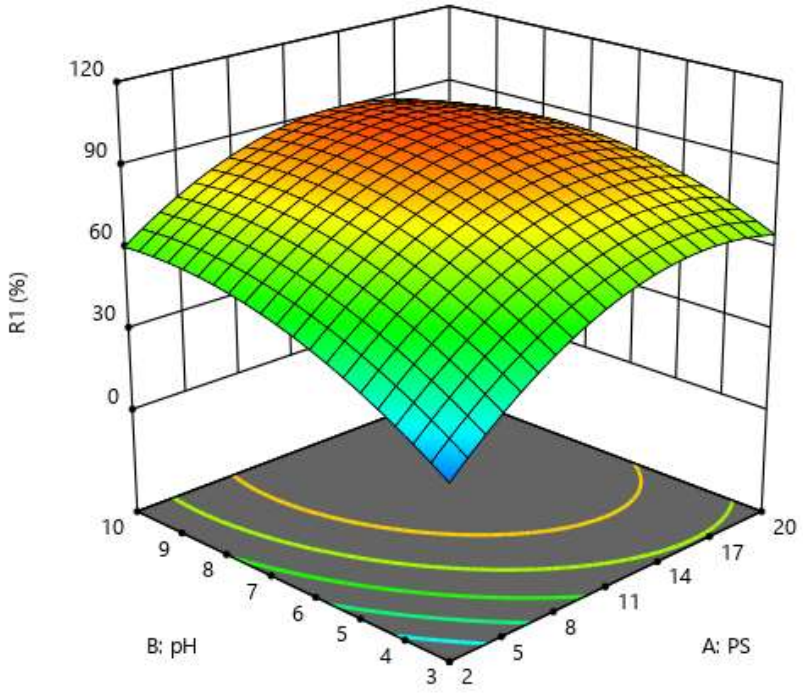

Figure 40: 3D-surface effect plots showing the effect of pH and persulfate.

The 3-D plot of the combined effects of temperature and solution pH at constant PS concentration ([PS]= 11 mM) is shown in Figure 41. At any specific solution pH, increasing the T from 40 °C to 80 °C increased the oxidization efficiency of TCPy. For instance, at pH 3 as T was increased from 40 °C to 80 °C, the mineralization efficiency increased from 24.1% to 79.3%.

Similarly, at pH 10, the TCPy oxidation efficiency increased from 71.1% to 98.8 % by increasing the applied T from 40 °C to 80 °C. On the other hand, at lower T (T=40 °C), increasing the solution pH enhanced the oxidation of TCPy. At all applied T (40 °C – 80 °C), the highest mineralization efficiency was observed around pH 8.3. However, increasing the solution pH to 10 decreased the mineralization efficiency. This trend can be attributed to the presence of more hydroxyl radicals at pH 10, which could be quenched by other hydroxyl radicals thus lowering the mineralization efficiency (Eq 3.8).

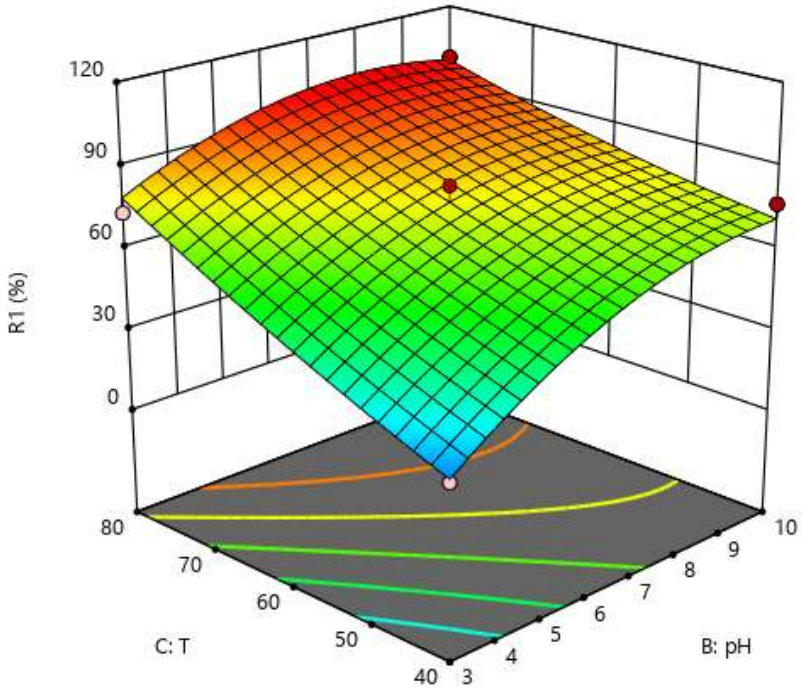

Figure 41: 3D-surface effect plots showing the effect of temperature and pH.

Optimization of the Removal Efficiency Using Desirability Function

The desirability function is a technique that has been widely used in industry since 1980 to simultaneously determine the optimum performance levels of input variables for multiple responses. The ideal case of this function is that the whole response desirability value (D), which can be obtained from Eq 3.12, as well as all individual response desirability values (d_i) are equal to 1 [32].

$$D = (d_1 \times d_2 \times d_3 \times. \ldots\ldots\ldots \times d_i)\ 1/n\ = (\prod_{i=1}^{n} d_i\ ) \tag{3.12}$$

That is, when all responses achieve the target, the overall desirability is 1.

Numerical optimization was used in order to determine the optimum conditions for maximum mineralization of TCPy. In the Design Expert software, all parameters (T, $[PS]_0$, and pH) were selected to be within the experimental range, while the response (percent TCPy mineralized) was set to the target of 100. Figure 42 represents a desirability ramp for numerical optimization of the system. Using the desirability function, the optimal operating conditions for the maximum TCPy mineralization were found to be a temperature of 77.1 °C, an initial PS concentration of 12.2 mM, and pH of 9.1, with the overall desirability of 1.000. Under these conditions, TCPy was predicted to be completely mineralized. To validate the prediction, an additional experiment was performed in triplicate using the predicted optimal conditions. The mean value of TCPy mineralization obtained in this experiment was 95+/-5%. The close agreement between the obtained experimental values and the predicted response indicate the validity of this prediction.

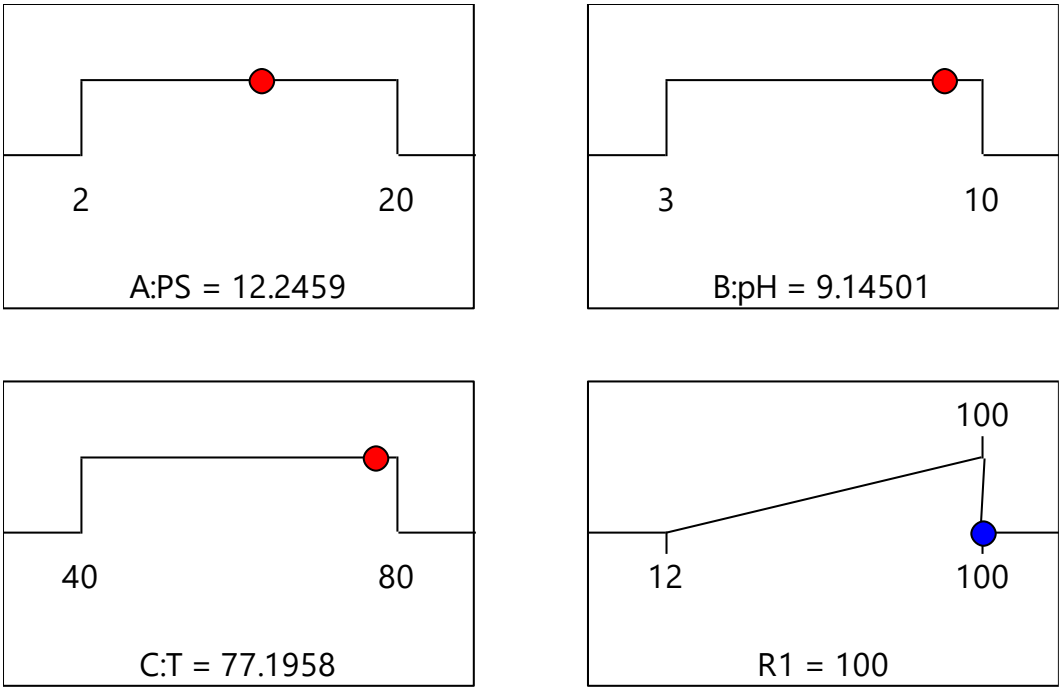

Figure 42: Desirability ramp for numerical optimization of the TCPy mineralization in heat activated PS system.

The degradation of TCPy by thermally activated PS under the optimum conditions suggested by RSM was studied and the results are presented in Figure 43. Complete TCPy removal was achieved after seven minutes of reaction and the TCPy removal exhibited pseudo-first-order kinetics with k_{obs} of 4.7×10^{-1} min^{-1} (Figure 44).

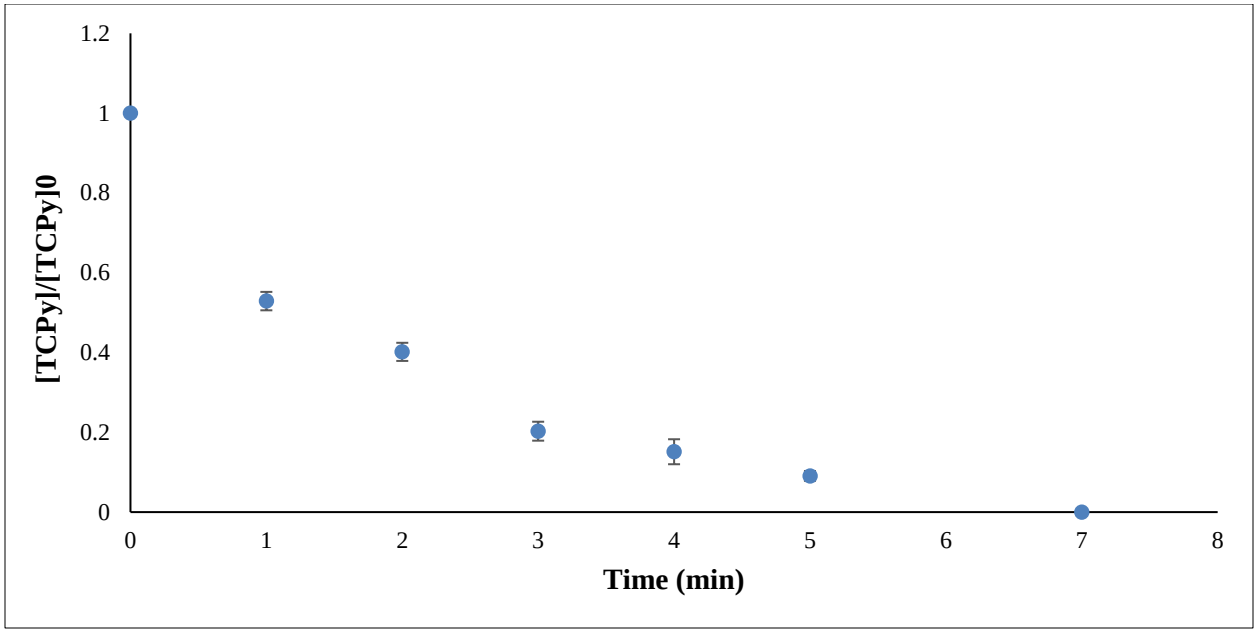

Figure 43: TCPy oxidation by heat activated PS at optimal condition.

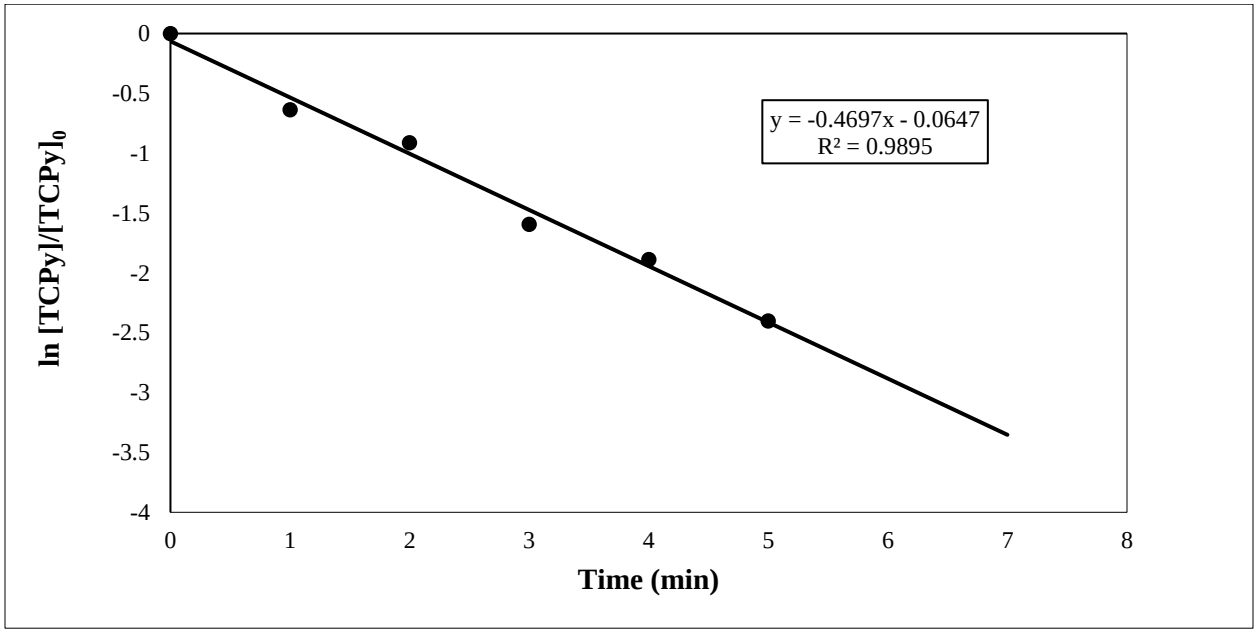

Figure 44: Pseudo-First-Order kinetics of TCPy degradation at optimum condition in heat activated PS system.

Effect of Inorganic Ions on TCPy Degradation

Effect of chloride ion

It has been found that the chloride ion has a dual function in the degradation of OCs using SR-based AOPs. The effect of Cl^- on the degradation efficiency is pH- and concentration-dependent. Several studies have shown that the presence of Cl^- results in poor removal efficiency due to the reaction of SR with Cl^- which forms radicals such as $Cl^\bullet$ and $Cl_2^{\bullet-}$, which are less reactive toward OCs than SR. On the other hand, PS may react with Cl^- generating active chlorine species (HOCl /Cl_2) which may increase the oxidation capacity with respect to organic compounds [33].

Figure 45 presents the results of the oxidation of TCPy by using a heat-activated system in the presence and absence of Cl^-. The addition of 0.1- 10 mM Cl^- showed no effect on TCPy oxidation. As we found in this study, both SR and HR are present in the solution. The reaction of SR with Cl^- results in the formation of less reactive species ($Cl^\bullet$) which could further react with Cl^- forming $Cl_2^{\bullet-}$ (Eq 3.13 and 3.14). The reaction of chloride radicals ($Cl^\bullet$ and $Cl_2^{\bullet-}$) with water leads to the formation of $HOCl^{-\bullet}$ which subsequently undergoes rapid decomposition to give HR and Cl^- (Eqs 3.15 and 3.16). Also, reaction of $Cl^\bullet$ with water leads to the formation of $H_2OCl^\bullet$ (Eq 3.18) which can be deprotonated to $HOCl^{-\bullet}$ (the pKa for $H_2OCl^\bullet$ is 5.1). Since the reverse reaction of Eq 3.17 (k= 4.3 x 10^9 M^{-1} s^{-1}) is suppressed by the fast forward reaction (k = 6.1 x 10^9 s^{-1}), the reaction of chloride anion with HR can be neglected [34-35]. This could explain our observation of the effect of Cl^- on TCPy degradation.

$$SO_4^{\bullet-} + Cl^- \rightarrow SO_4^{2-} + Cl^\bullet \quad (3.13)$$

$$Cl^\bullet + Cl^- \rightarrow Cl_2^{\bullet-} \quad (3.14)$$

$$Cl^{\bullet} + H_2O \rightarrow HOCl^{\bullet -} + H^+ \quad (3.15)$$

$$Cl_2^{\bullet -} + H_2O \rightarrow HOCl^{\bullet -} + H_2 + Cl^- \quad (3.16)$$

$$HOCl^{\bullet -} \leftrightarrow OH^{\bullet} + Cl^- \quad (3.17)$$

$$Cl^{\bullet} + H_2O \rightarrow (HOClH)^{\bullet} \quad (3.18)$$

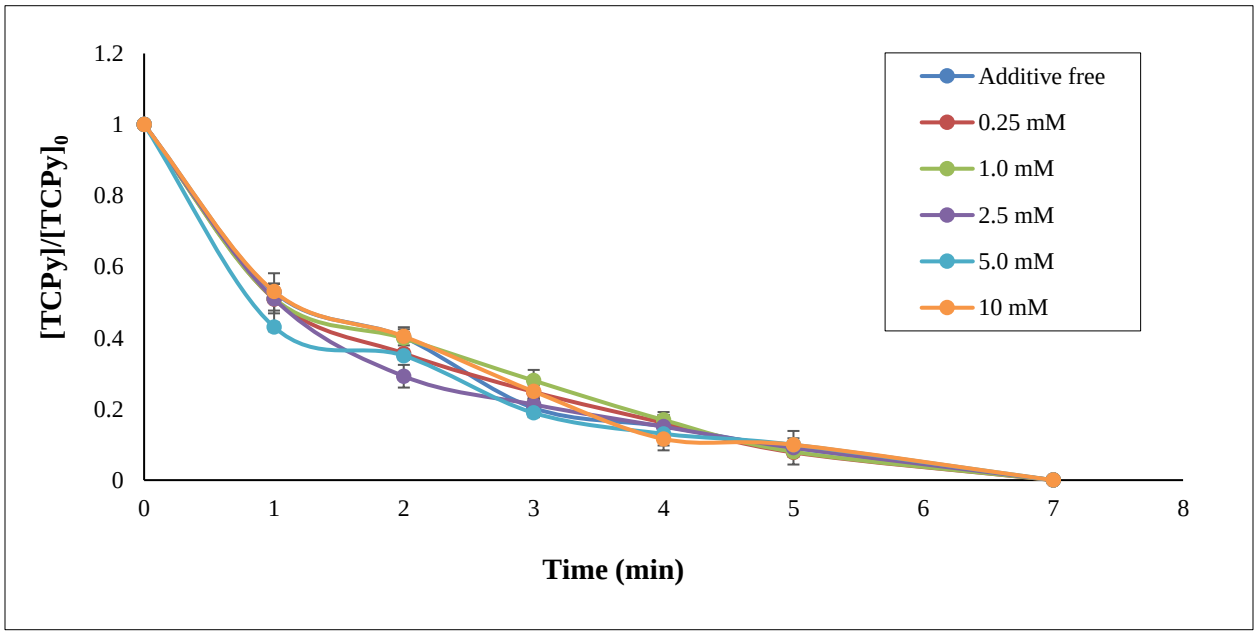

Figure 45: TCPy degradation using heat activated PS oxidation under different chloride concentrations.

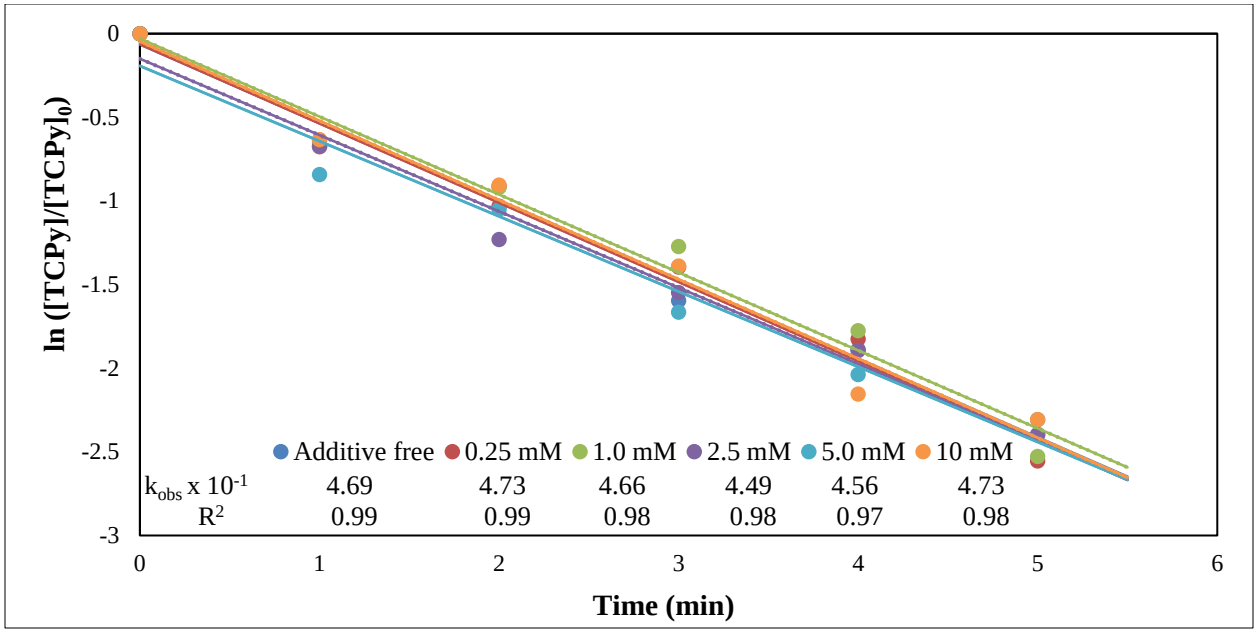

Figure 46: Pseudo-first-order rate constants TCPy degradation using heat activated PS oxidation under different chloride concentrations.

Effect of phosphate

The effect of the phosphate ($[PO_4^{3-}]_0$ = 0.1- 10 µM) on TCPy oxidation was also investigated. Varying the concentration of phosphate up to 10 µM showed no effect on TCPy degradation and in all systems TCPy was completely removed after 10 minutes. As presented in Figure 47, the reaction followed pseudo-first-order kinetics with respect to TCPy for any specific PO_4^{3-} dosage ($R^2 > 0.96$). The corresponding k_{obs} for TCPy removal is presented in Figure 48. Under the experimental conditions, both SR and HR are present in the solution. The reaction of these radicals with PO_4^{3-} and HPO_4^{2-} may produce less reactive species ($PO_4^{\bullet 2-}$ and $HPO_4^{\bullet 2-}$) (Eq 3.19 -3.23).

$$SO_4^{\bullet -} + HPO_4^{2-} \rightarrow SO_4^{2-} + HPO_4^{\bullet -} \qquad k = 1.2 \times 10^6\ M^{-1}\ s^{-1} \qquad (3.19)$$

$$OH^{\bullet} + HPO_4^{2-} \rightarrow OH^- + HPO_4^{\bullet-} \qquad k= 1.5 \times 10^5\ M^{-1}\ s^{-1} \qquad (3.20)$$

$$SO_4^{\bullet-} + PO_4^{3-} \rightarrow SO_4^{2-} + PO_4^{\bullet 2-} \qquad (3.21)$$

$$OH^{\bullet} + PO_4^{3-} \rightarrow OH^- + PO_4^{\bullet 2-} \qquad (3.22)$$

$$HPO_4^{\bullet-} \rightarrow H^+ + PO_4^{\bullet-} \qquad \text{pKa of } 8.9 \pm 0.1 \qquad (3.23)$$

However, the slow kinetics of SR and HR reaction with phosphate species (Eq 3.19 and 3.20) compared to the fast kinetics between SR and OCs (k ~1.0 × 10^9 M^{-1} s^{-1}) make the scavenging reactions of SR and HR by phosphate species negligible [36]. Therefore, the presence of PO_4^{3-} and HPO_4^{2-} is not worthy of consideration.

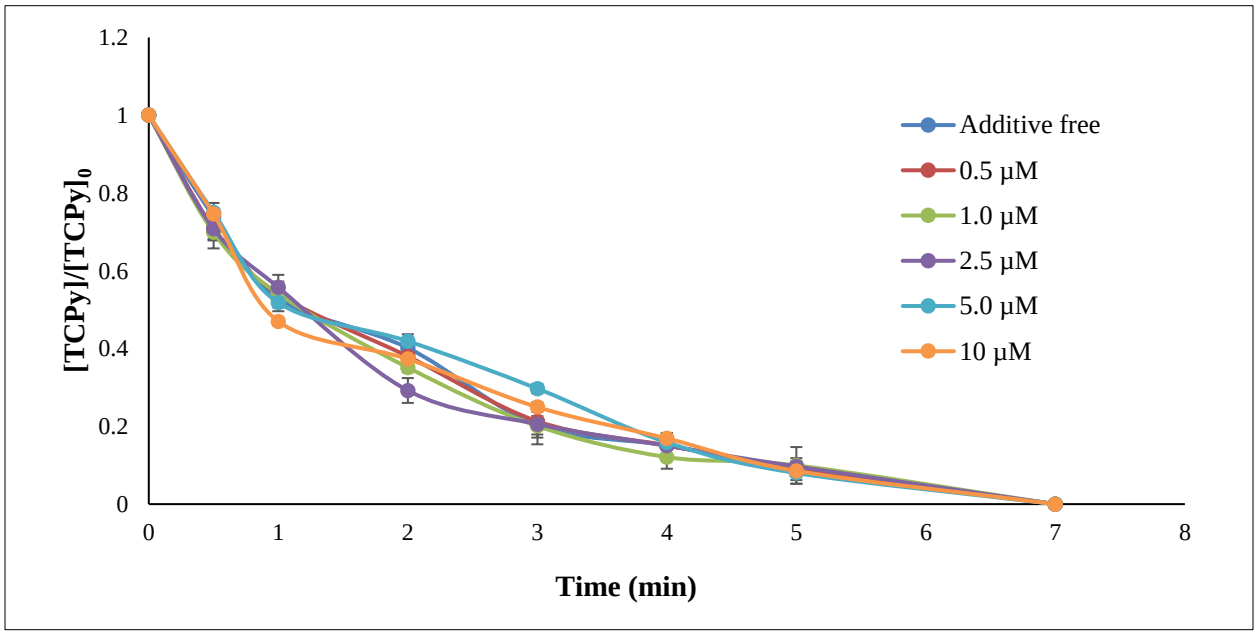

Figure 47: TCPy degradation using heat activated PS oxidation under different phosphate concentrations.

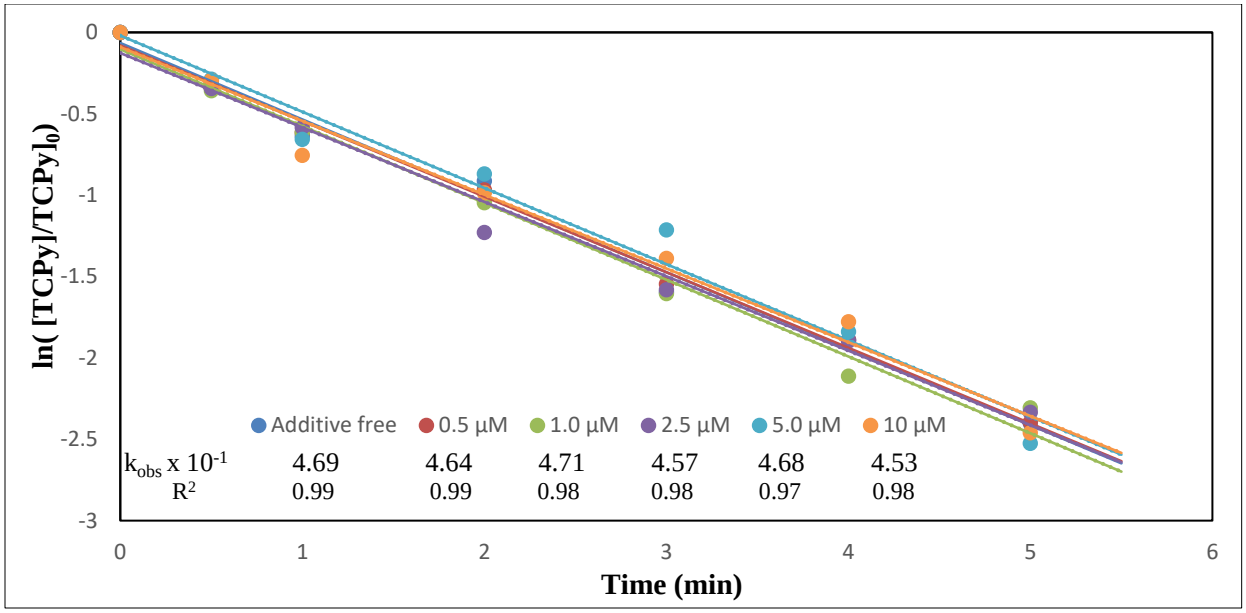

Figure 48: Pseudo-first-order rate constants TCPy degradation using heat activated PS oxidation under different phosphate concentrations.

Effect of sulfate

The effect of the presence of SO_4^{2-} (0.1-10 mM) on TCPy oxidation was investigated (Figure 49). The oxidation of TCPy was not affected by SO_4^{2-} . The normalized plots of [TCPy] vs time in the absence and presence of SO_4^{2-} almost overlap. The k_{obs} of TCPy removal with and without the addition of SO_4^{2-} showed close values (Figure 50). Since SO_4^{2-} didn't react with SRs, the TCPy oxidation was not affected by the presence of SO_4^{2-}. This observation is in accordance with other studies [36-38].

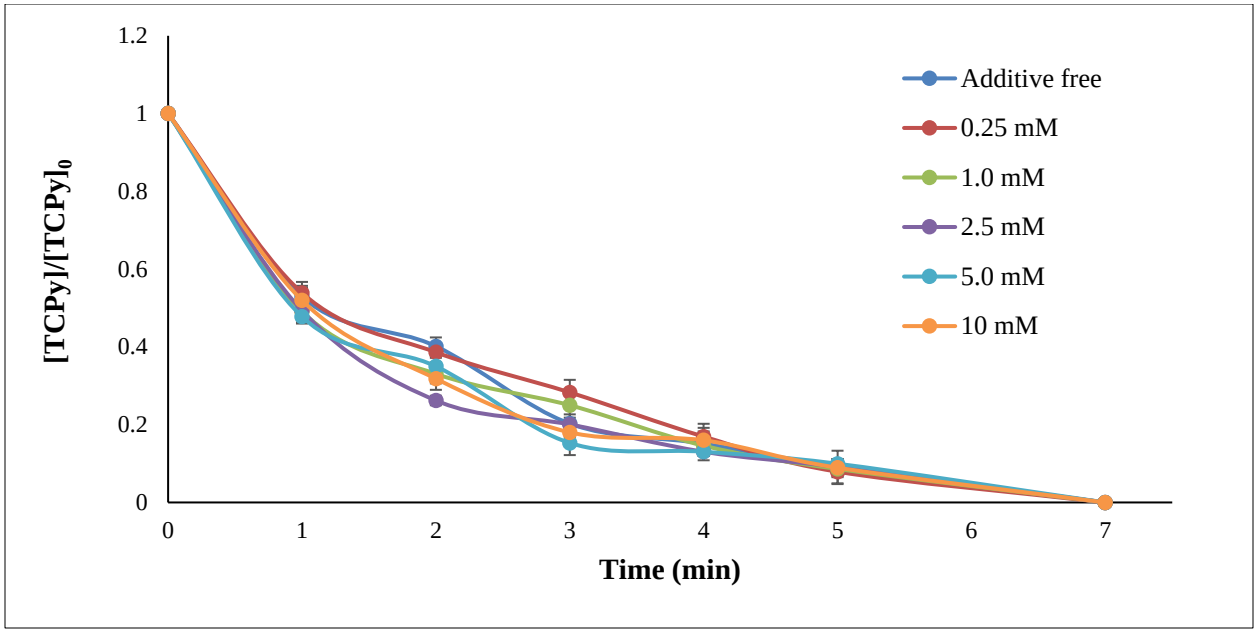

Figure 49: TCPy degradation using heat activated PS oxidation under different sulphate concentrations.

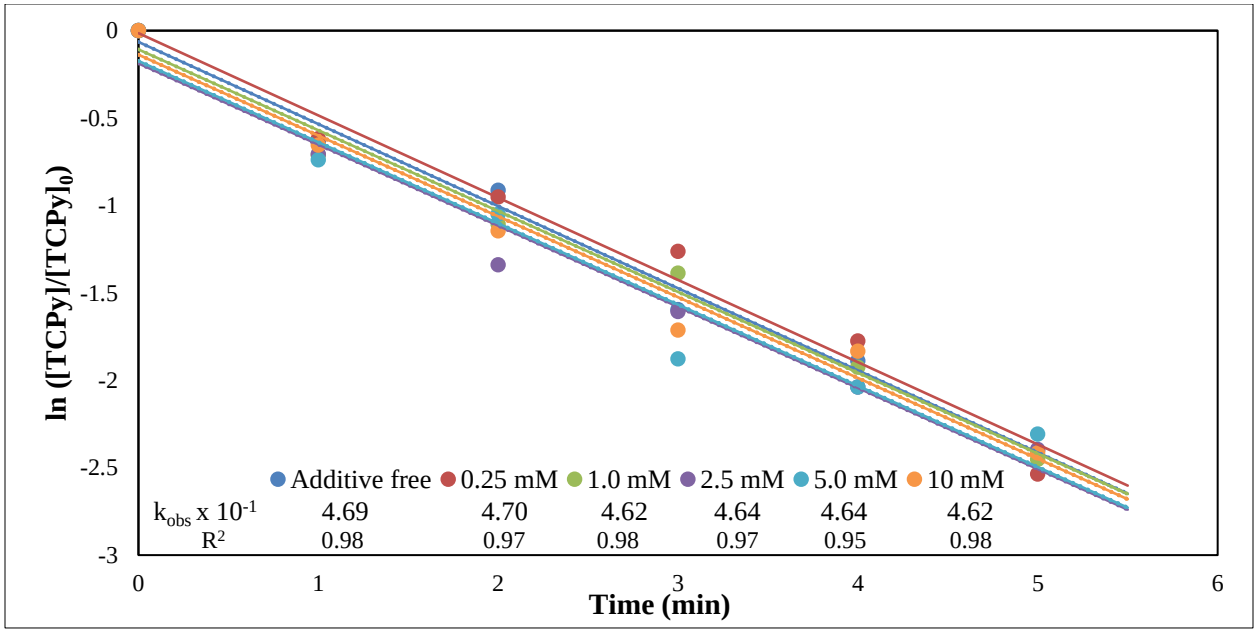

Figure 50: Pseudo-first-order rate constants TCPy degradation using heat activated PS oxidation under different sulfate concentrations.

Conclusion

Thermally-activated persulfate is an effective method for degradation of TCPy in water. Increasing the temperature and the concentration of PS increases the rate of TCPy removal. Basic pH is more favorable toward the TCPy degradation rate than acidic pH. TCPy degradation in heat-activated persulfate exhibited a pseudo-first-order kinetics pattern as a function of T, [PS], and pH.

Box-Behnken design and Response Surface Methodology were used to optimize the experimental factors (T, [PS], and pH). The desirability function was calculated to determine the optimum conditions for the system at maximum TCPy mineralization (100%). The optimum process conditions were found to be (T= 77.1 °C, 12.2 mM PS concentration, and an initial pH of 9.2). The values of predicted optimum conditions were further validated by performing triplicate experiments and the results agree with model predictions. The kinetics of the optimized conditions were investigated and showed that the oxidation of TCPy under these conditions is well fitted to a pseudo-first-order model (R=0.98) with removal rate (k_{obs}) of 4.7 x 10^{-1} min^{-1}. The presence of chloride, phosphate and sulfate showed no effect on the oxidation of TCPy in thermally-activated PS. Therefore, the interference of these anions on TCPy degradation could be negligible.

CHAPTER FOUR: EXPERIMENTAL INVESTIGATION OF REACTION ORDERS OF 3,5,6-TRICHLORO-2-PYRIDINOL UNDER THERMALLY ACTIVATED PERSULFATE

Introduction

Chlorpyrifos (CP), which is a broad-spectrum organophosphorous insecticide, has received great attention because of its potential environmental and health effects. The extensive use of CP as an insecticide causes widespread contamination of soil and water around the application site. The hydrolysis of CP results in the formation of 3,5,6-trichloro-2-pyridinol (TCPy) as its primary byproduct. The EPA identified TCPy as a persistent pollutant which has been detected in the places where CP was applied, and the higher water solubility of TCPy compared to CP results in more contamination of surface water and ground water.

In situ chemical oxidation (ISCO) is an effective remediation technology for the degradation of organic contaminants. There are many oxidants that are commonly used for ISCO including hydrogen peroxide, permanganate, ozone, and persulfate. Among them, persulfate has gained great attention as an effective and persistent oxidant.

Previous chapters indicated that heat-activated persulfate effectively degrades TCPy and the results indicated that the oxidation of TCPy in the presence of thermally-activated PS followed a pseudo-first-order kinetic model. However, to effectively apply ISCO in the field for soil and groundwater remediation, knowledge of reaction kinetics would be useful. Therefore, this chapter provides comprehensive investigations of the kinetic behavior of persulfate oxidation of TCPy in a heat-activated PS system. Kinetic parameters such as reaction order and rate constants were investigated.

Experimental

Chemicals

Neat TCPy, and ammonium acetate ($C_2H_7NO_2$, ≥ 98%) were purchased from Sigma Aldrich (USA). Sodium persulfate ($Na_2S_2O_8$, ≥ 98.0%) and the HPLC grade solvents acetonitrile (CH_3CN, >99.9%) and formic acid (HCOOH, ≥99.5 %) were purchased from Fisher Scientific.

Experimental Procedure

These experiments were conducted in 20 mL amber glass vials. Appropriate volumes of the prepared stock solution of TCPy and deionized water (DI) were added together into vials. Vials were immersed into a thermo-regulated water bath until reaching the working temperature. Then, appropriate volumes of the stock solution of PS were transferred into the vials to achieve a predetermined TCPy to PS ratio. All experiments were conducted at 70 ˚C. At designated time points, samples were removed from the water bath and quenched in an ice bath.

Analysis

Analysis of the TCPy was performed on an Agilent 6230 TOF LC-MS with an Agilent Zorbax SB-C18 analytical column. A mixture of acetonitrile (ACN) and water was used as the mobile phase at an ACN:H_2O ratio of 60:40 (v:v) and a flow rate of 1.0 mL/min.

Results and Discussion

Reaction Order and Kinetics

The chemical reaction rate of the reaction: xA + yB → products under constant temperature is defined as:

$$r = -\frac{dA}{dt} = k\,[A]^{\alpha}[B]^{\beta} \tag{4.1}$$

Based on the degradation of TCPy in the thermally-activated PS system, the reaction rate law of PS oxidation of TCPy may be related to the PS concentration and TCPy concentration as follow:

$$\mathrm{r} = -\frac{d[TCPy]}{dt} = \mathrm{k}\,[\mathrm{TCPy}]^{\alpha}[\mathrm{PS}]^{\beta} \tag{4.2}$$

where $r = -\frac{d[TCPy]}{dt}$ is the rate equation for TCPy degradation; k is the overall reaction rate constant; α and β are the reaction orders of TCPy and PS, respectively. In order to investigate the reaction orders, experiments were performed with an excess amount of the oxidant (PS) to ensure that the concentration of PS remains almost constant (*i.e.* $[PS]_0 \ggg [TCPy]_0$) during the reaction. Therefore, the kinetic equation (Eq 4.2) can be simplified as follows:

$$r = -\frac{d[TCPy]}{dt} = k_a[TCPy]^{\alpha} \tag{4.3}$$

where $k_a = k[PS]^{\beta}$.

Effect of TCPy concentration under fixed PS concentration

In order to investigate the reaction order of TCPy (α), experiments were conducted by fixing $[PS]_0$ to 11 mM while varying $[TCPy]_0$ from 0.1 to 0.8 mM to ensure the molar ratio of the oxidant to the contaminant ($[PS]_0/[TCPy]_0$) is greater than 10 as recommended by Espenson where one of the reactants remains essentially unchanged [39]. Collecting the experimental data points at the beginning of the reaction is an efficient way that is also recommended by Espenson to obtain an accurate kinetics study [39]. This is beneficial to minimize the side reaction between the oxidative species and the byproducts. Additionally, the method of half-lives based on the time required for the initial concentration of the reactant to be reduced to half its initial concentration, is also employed.

This method was successfully used to determine the reaction order of the degradation of ibuprofen and trichloroethylene by a heat-activated PS system [40,41]. Therefore, in this study the data points were collected in the early stage of the reaction with $[PS]_0/[TCPy]_0$ molar ratios from 110 down to 13.75. Table 10 summarizes the experimental matrix for TCPy oxidation by heat-activated PS undertaken at 70 °C and pH 7.0.

The normalized TCPy concentrations during the reaction are presented in Figure 51. A polynomial regression analysis was used for all experimental data analysis. As shown in Figure 51 the results exhibited an excellent correlation coefficient (R^2) greater than 0.99.

Table 10: Kinetic parameters for the determination of reaction orders for thermally activated persulfate oxidation of TCPy at 70 ˚C with respect to TCPy

$[TCPy]_0$ (mM)	$[PS]_0$ (mM)	$[PS]_0$ / $[TCPy]_0$	Half-life $t_{1/2}$ (min)	k_a x 10^{-2} ($mM\ min^{-1}$)
0.1	11	110	4.7	1.06
0.2	11	55	6.8	1.47
0.4	11	37.5	12.5	1.6
0.5	11	22	19	1.31
0.6	11	18.3	24	1.25
0.8	11	13.75	35	1.14

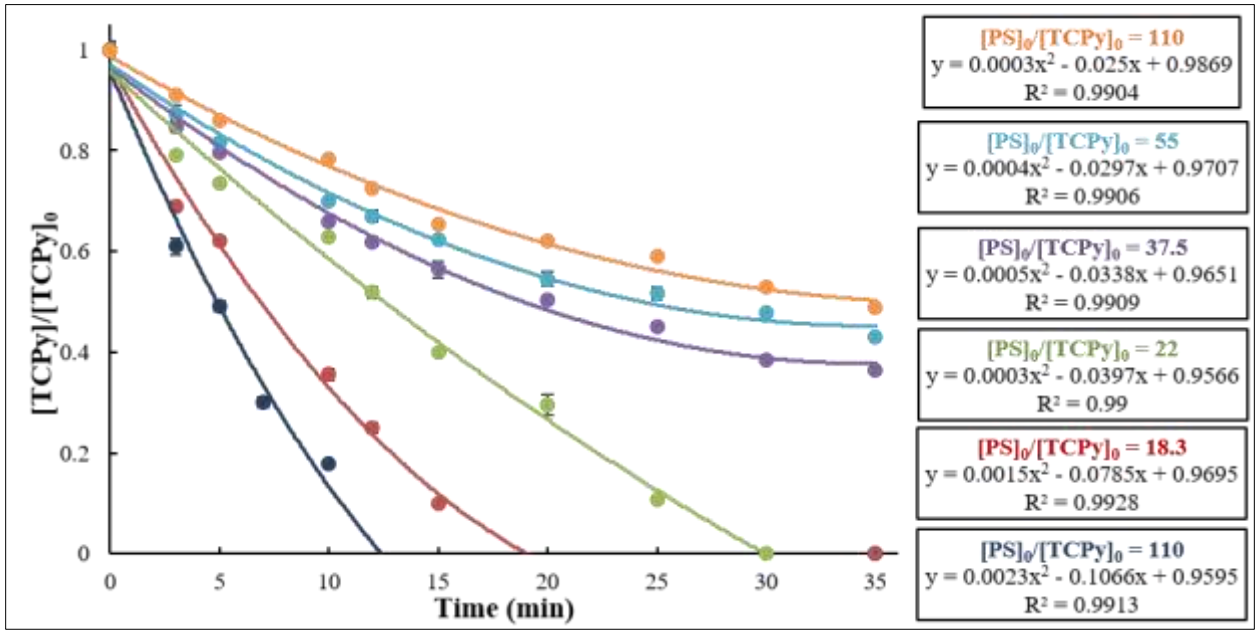

Figure 51: Normalized measured TCPy concentrations and fits of the polynomial regression analysis. Experimental conditions: pH= 7, temperature = 70 °C, $[PS]_0$ = 11 mM. $[TCPy]_0$= 0.1- 0.8 mM.

The polynomial equations were used to calculate the half-lives ($t_{1/2}$) as shown in Table 10.

The integration of Eq 4.3, with initial concentration of TCPy ($[TCPy]=[TCPy]_0$) when t=0, gives [42]:

$$t = \frac{1}{k_a\ (\alpha - 1)}\ \left[\frac{1}{[TCPy]} - \frac{1}{[TCPy]_0^{\alpha-1}}\right] \tag{4.4}$$

$$t = \frac{1}{k_a\ [TCP_y]_0^{\alpha-1}}\ \left[\left(\frac{[TCPy]_0}{[TCPy]}\right)^{\alpha-1} - 1\right] \tag{4.5}$$

The half-life of TCPy is the time required for [TCPy] to drop to half of its initial concentration:

$t = t_{1/2}$ When $[TCPy]= ½\ [TCPy]_0$

Substituting for [TCPy] in Eq 4.5 and rearranging:

$$t_{1/2} = \frac{2^{\alpha-1} - 1}{K_a(\alpha - 1)}\ \left[\frac{1}{[TCPy]_0^{\alpha-1}}\right] \tag{4.6}$$

Taking the natural log for both sides:

$$ln\, t_{1/2} = ln\ \frac{2^{a-1} - 1}{(\alpha - 1)K_a} + (1 - \alpha)\ln[TCPy]_0 \tag{4.7}$$

Rearrangement of Eq 4.7 :

$$t_{1/2} = \{2^{(\alpha-1)} - 1\}/\{k_\alpha(\alpha - 1)[TCPy]^{(\alpha-1)}\} \tag{4.8}$$

By assuming $a \neq 1$, this Eq can be further simplified as part of a function of $[TCPy]_0$ as follows:

$$t_{1/2} = F(\alpha, k_\alpha)/\ \{[TCPy]_0^{(\alpha-1)}\} \tag{4.9}$$

By taking the natural logarithm of both sides

$$\ln(t_{1/2}) = \ln\{\ F(\alpha, k_\alpha)\} - (\alpha - 1)\ln[TCPy]_0 \tag{4.10}$$

Where F (α, k_a) = (2^{a-1}- 1 / (α-1) k_a) as expressed in Eq 4.8.

Accordingly, the reaction order α can be obtained by plotting ln ($t_{1/2}$) as summarized in Table 10 against ln [TCPy]. As shown in Figure 52, the results showed excellent linearity with a correlation coefficient R^2 = 0.9612, and a slope of 0.97±0.001. The slope is equal to α+1. Therefore, the results showed that the reaction order α with respect to TCPy is -0.03, which is approximately pseudo-zeroth-order (*i.e.*, α = 0.0).

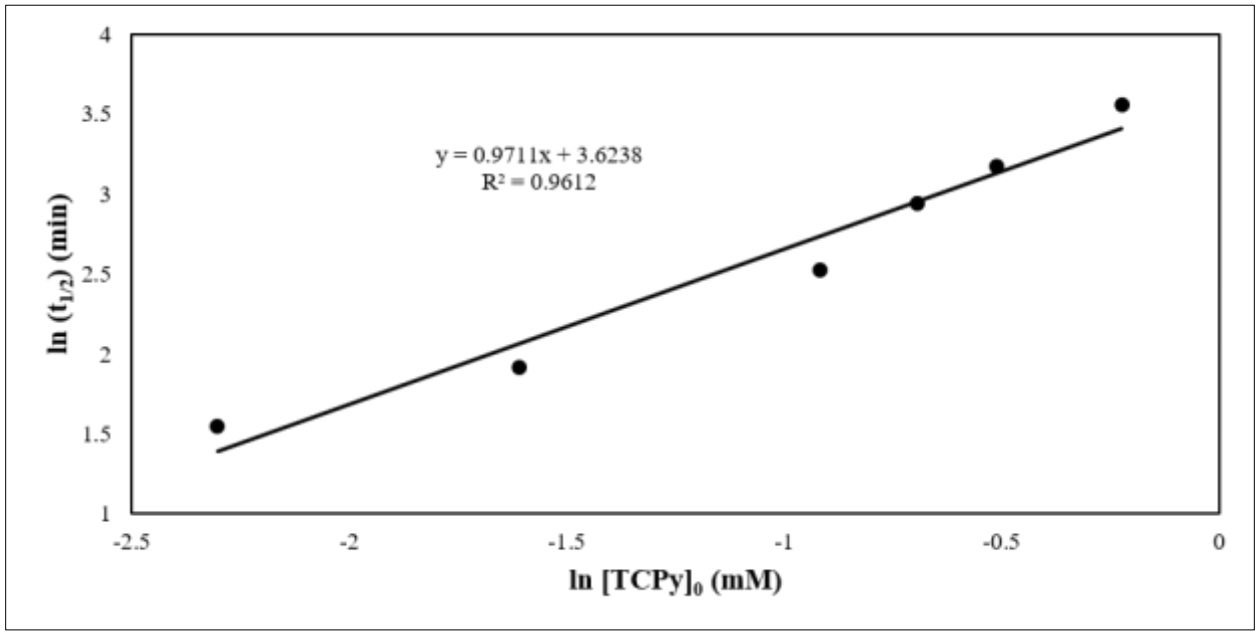

Figure 52: Plot of ln ($t_{1/2}$) versus ln $[TCPy]_0$. A slop of 0.97= -(α-1).

As shown in previous chapters, the oxidation of TCPy in a thermally-activated PS system depends on the generation of SR. The results of studying the oxidation of different TCPy concentrations at fixed [PS] and T indicated that the generation of SRs during the reaction would be stable, thus occurring at fixed rate. For instance, applying the same concentration of PS to degrade different TCPy concentration exhibited that the reaction time for TCPy removal was

reduced by decreasing the concentration of TCPy. This is likely due to the fact that the same amount of SRs are generated with fixed PS concentration. These radicals are oxidizing the same moles of TCPy during specific time. As shown in Table 10 the values of calculated pseudo-zero-order reaction rates using Eq 4.11 indicates that these values are independent of the initial concentration of TCPy when the initial concentration of PS is kept constant.

$$k_\alpha = \frac{[TCPy]_0}{2t_{1/2}} \tag{4.11}$$

Effect of PS concentration under fixed TCPy concentration

In order to determine the reaction order of PS (β), the second set of experiments was conducted by varying the concentration of PS from 11 mM to 88 mM while keeping the concentration of TCPy fixed at 0.8 mM.

The following relationships can be obtained by rearrangement of Eqs 4.2 and 4.3:

$$k_\alpha = k[S_2O_8^{2-}]_t^{\ \beta} \approx k[S_2O_8^{2-}]_{t=0}^{\ \beta} \tag{4.12}$$

Taking the natural logarithm of both sides yields:

$$\ln k_\alpha = \ln k + \beta \ln[PS]_{t=0} \tag{4.13}$$

The normalized $[TCPy]_t/[TCPy]_0$ at different PS/TCPy molar ratios over time is presented in Figure 53. As shown in this figure, an excellent polynomial regression fitting was obtained with correlation coefficient $R^2 > 0.99$. The k_a values which were calculated using Eq 4.11 are summarized in Table 11.

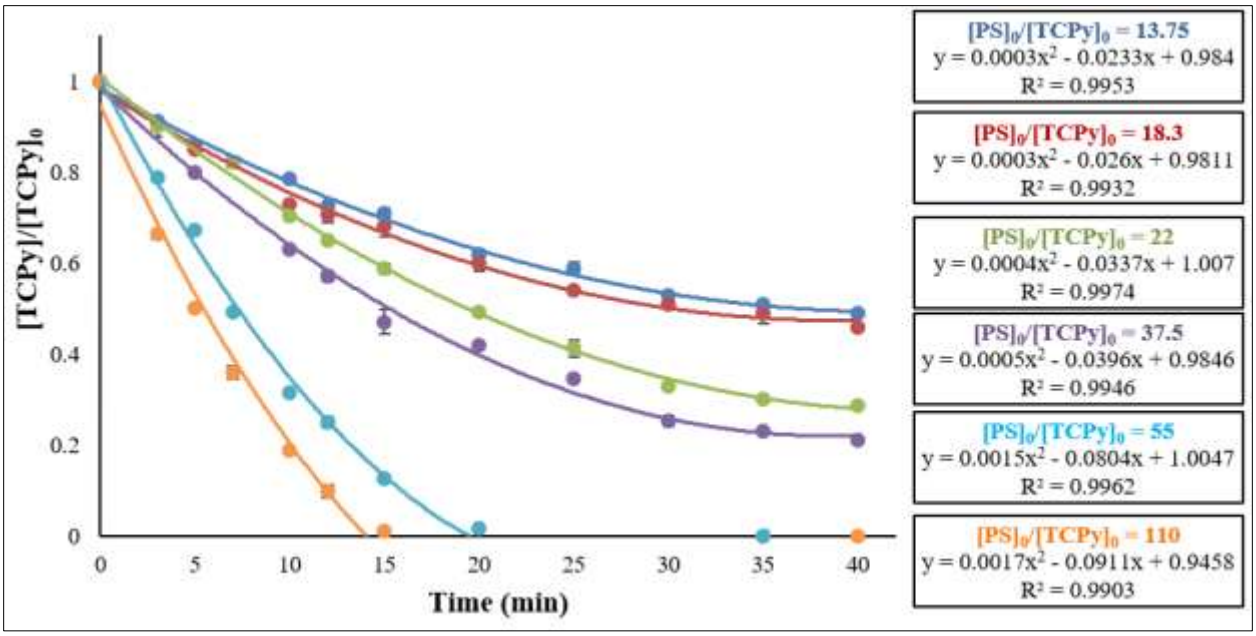

Figure 53: Normalized measured TCPy concentrations and fits of the polynomial regression analysis. Experimental conditions: pH= 7, temperature = 70 °C, $[TCPy]_0$= 0.8 mM, $[PS]_0$ = 11- 88 mM.

Table 11: Kinetic parameters for the determination of reaction orders for thermally activated persulfate oxidation of TCPy at 70 °C with respect to PS.

$[TCPy]_0$ (mM)	$[PS]_0$ (mM)	$[PS]_0$ / $[TCPy]_0$	Half-life $t_{1/2}$ (min)	k_a x 10^{-2} (mM min^{-1})
0.8	11	13.75	35	1.1
0.8	14.64	18.3	30	1.3
0.8	17.6	22	19	2.1
0.8	30	37.5	15	2.7
0.8	44	55	7.3	5.5
0.8	88	110	5.2	7.7

An excellent linearity (R^2 = 0.994) was obtained by plotting ln (k_{α}) vs. ln $[PS]_0$ (Figure 54). The straight slope obtained (slope = 0.99) corresponds to the reaction order β with respect to PS according to Eq 4.13. Therefore, the reaction order of TCPy oxidation by PS is first order.

Increasing the concentration of PS enhanced the removal efficiency of TCPy as shown in Figure 53. Since PS is the source of SRs, higher PS concentration generate more SRs which oxidized more TCPy.

In this study, the reaction orders with respect to TCPy and PS were found to be 0 and 1, respectively. The overall rate constant of the reaction (k_a) can be obtained from the y intercept (Figure 54) which is equal to 1.01×10^{-3} $mM^{1-(\alpha+\beta)}$ min^{-1}. Consequently, the reaction law between PS and TCPy would be expressed by the following equation:

$$r = -d[TCPy]/dt = k[TCPy]^{\alpha}[PS]^{\beta} = (1.01\times10^{-3} mM^{1-(\alpha+\beta)} min^{-1})\times [TCPy]^{\alpha=0}[PS]^{\beta=1}$$

This law could be used to describe the TCPy degradation rate under specific conditions described in this chapter.

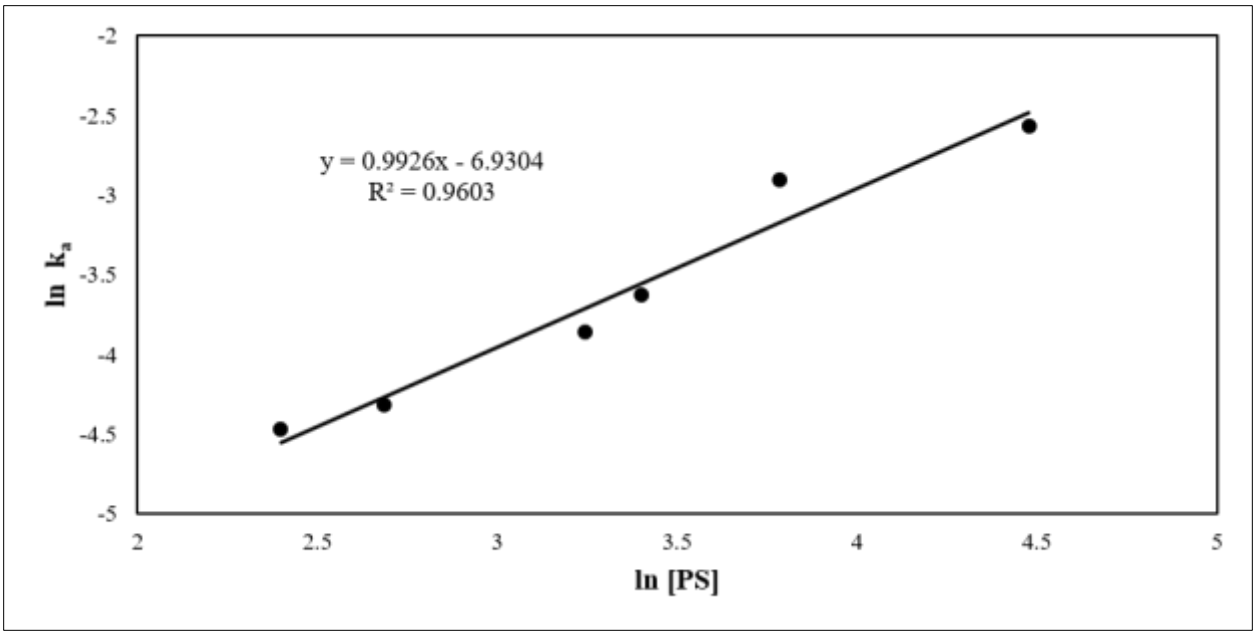

Figure 54: Plot of ln(k_α) vs. ln[PS]. The slope obtained (0.9926) is the reaction order in PS. All data are relative to experiments undertaken in Figure 53. Experimental conditions: pH= 7, temperature = 70 °C, $[TCPy]_0$= 0.8 mM, $[PS]_0$ = 11- 88 mM.

Conclusion

The kinetics of TCPy oxidation by heat-activated persulfate were investigated at a temperature of 70 °C and pH 7. Two sets of experiments were carried out to determine the reaction orders with respect to TCPy (α) and PS (β). The half-lives method was applied to determine the reaction order with respect to TCPy and the results demonstrated that the oxidation of TCPy exhibited pseudo-zeroth–order kinetics with respect to TCPy in the heat-activated PS system. This result indicates that, at fixed initial concentrations of PS, varying TCPy concentrations would result in the same TCPy degradation rate. Moreover, the observation of first–order kinetics with respect to PS indicates that increasing the concentration of PS for a fixed concentration of TCPy would result in a faster TCPy degradation rate. The degradation rate of TCPy by persulfate in the heat-activated PS system can be described by the kinetic rate equation:

$$-d[TCPy]/dt = k[TCPy]^{\alpha}[PS]^{\beta} = (1.01\times10^{-3} mM^{1-(\alpha+\beta)} min^{-1}) \times [TCPy]^{0}[PS]^{1}$$

The results of this study serve as a starting point to describe the kinetic behavior of the PS/TCPy system under the specific experimental conditions of this study.

CHAPTER FIVE: DEGRADATION PATHWAY OF 3,5,6-TRICHLORO-2-PYRIDINOL By ZERO VALENT IRON- AND THERMALLY - ACTIVATED PERSULFATE

Introduction

Chlorpyrifos (O,O-diethyl-O-3,5,6-trichloro-2-pyridyl phosphorothionate; CP) has been used worldwide as an agricultural insecticide since 1965, though it has been banned for residential use in the United States since 2000 [3]. Despite the significant contribution of CP to maintaining world food production levels, its widespread use has caused many concerns to the environment and human health [20]. CP enters the environment through agricultural application, industrial runoff, and improper disposal [8]. Once in the environment, the P-O bond of CP is hydrolyzed to form 3,5,6-trichloro-2-pyridinol (TCPy), which was identified as a persistent pollutant by the United States Environmental Protection Agency (USEPA) [10]. The higher water solubility of TCPy increases its capability to leach into surface water and groundwater, resulting in widespread contamination in soils, sediments and aquatic environments [11-12]. TCPy has been detected in golf course leachate near where CP was applied. Also, it was detected in wastewater streams from chlorpyrifos manufacturing plants [9].

Sulfate radical-based advanced oxidation processes (SR-AOPs) have been widely applied and effectively degrade a variety of persistent organic contaminants [17]. In this treatment method, persulfate (PS, E^0 =2.01 V) is activated by many methods to produce a more reactive species, the sulfate radical ($SO_4^{\bullet-}$, SR, E^0= 2.5-3.1 V), which significantly enhances oxidation efficiency. Sulfate radicals oxidize the original pollutants of concern to form various transformation byproducts and eventually produce carbon dioxide and water.

Recently, both experimental and theoretical studies have been performed to study the kinetics, catalytic mechanisms, and thermodynamics of the degradation of organic pollutants involving free radicals. For instance, Li and co-workers computationally investigated the role of hydroxyl and sulfate radicals on the oxidation of dibutylphthalate in the gas and aqueous phases by performing Density Functional Theory (DFT) calculations [43]. Moreover, the reaction mechanism of SR with gallic acid was investigated experimentally and theoretically using DFT by Caregnato, *et al.*[44]. Furthermore, DFT was applied to investigate the degradation mechanism of benzene by NO_3 radicals [45]. In addition, experimental and theoretical studies were performed to investigate the kinetics and mechanisms of the oxidation of dimethylphthalate by HR [46].

In previous chapters it was observed that both zero-valent iron-activated PS and thermally-activated PS systems can effectively oxidize TCPy in water. Based on the results of previous chapters, SR-AOPs are effective methods for the treatment of TCPy in water. While ZVI/PS exhibited a high mineralization rate of TCPy up to 81.1%, TCPy was completely mineralized in the heat-activated PS system. In order to completely evaluate the degradation efficiency of TCPy by SR-AOPs, the transformation intermediates and by-products of TCPy oxidation by ZVI- and heat-activated PS should be identified.

Therefore, this chapter studies the transformation products of TCPy by means of SR based AOPs using GC-MS. The favorable reaction sites of SR with TCPy are investigated by DFT. The degradation pathways of TCPy in both systems were proposed based on the identified products and the calculated ΔG values using DFT were compared with the proposed experimental pathway.

Experimental

Chemicals

Neat TCPy and N-tert-Butyldimethylsilyl-N methyltrifluoroacetamide (MTBSTFA (with 1% t-BDMCS)) were purchased from Sigma Aldrich (USA). Sodium persulfate ($Na_2S_2O_8$, ≥ 98.0%), and the HPLC grade solvents; acetonitrile (CH_3CN, >99.9%), formic acid (HCOOH, ≥99.5 %), tert-butyl alcohol (TBA) ($C_4H_{10}O$, > 99%) and chloroform ($CHCl_3$, 99.8%) were purchased from Fisher Scientific.

Experimental Procedure

To study the oxidation byproducts of TCPy in the ZVI/PS system, experiments were conducted in 20 mL amber glass vials. A predetermined mass of ZVI particles (1.5 g/L) was added to each of the vials, followed by the addition of TCPy stock solution to a final concentration of 80 mg L^{-1} and PS to 10 mM. Then, the vials were placed on a Thermo Scientific MaxO 4000 orbital shaker table operated at 200 rpm at room temperature for an appropriate amount of time. At designated time points, samples were removed from the shaker table and quenched in an ice bath.

To study the oxidation byproducts of TCPy in the heat-activated PS system, appropriate volumes of the prepared stock solution of TCPy and deionized water (DI) were added together into vials. Vials were immersed into a thermo-regulated water bath until reaching the working temperature (60 °C), appropriate volumes of the stock solution of PS were then transferred into the vials to achieve a final concentration of 80 mg L^{-1} TCPy and 10 mM PS. At designated time points, samples were removed from the water bath and quenched in an ice bath.

Analysis

The analysis of the TCPy was performed on an Agilent 5977 mass spectrometer (GC/MS) with an RTX-5 column (30 m, 0.25 mm i.d., 0.25 μm df). In order to facilitate the release of TCPy and its byproducts and avoid tailing of the chromatographic peaks, a derivative of TCP was prepared following a modified version of the approach by Li, Rui, *et al* [47]. The derivatization procedure at 50 ºC was proceed as follows:150 μM of MTBSTFA was added to 4 ml of the sample. After one hour, samples were extracted by addition of 5 mL chloroform with 10 mins of stirring, then the chloroform layer was analyzed by GC-MS. In GC/MS, an initial oven temperature of 55 °C was used, and then ramped at 5 °C /min up to 170 °C and hold for 1 min following by ramping at 5, 10 and 20 °C /min to 130, 160 and 260 °C, respectively. Ion chromatography was used to measure the release of chloride on DionexIonPac AS4A separation column (250mmx 4mm). A Shimadzu TOC-L Analyzer (Shimadzu Instruments, Kyoto, Japan) was used to determine the concentration of nonpurgeable (total) organic carbon (TOC).

Computational Method

In the DFT study, all geometries were optimized under B3LYP functional using Gaussian 09 molecular orbital calculation software package. The 6-31G++(d,p) basis set and the Polarizable Continuum Model (PCM) solvent model were applied to obtain satisfying accuracy. Unless specified, the Gibbs free energy is discussed in this research.

Results and Discussion

Chloride Ions Analysis

Ion chromatography was used to evaluate the release of chloride into solution during the degradation of TCPy. The released of chloride ions during the reaction was measured as presented in Figure 55. The data demonstrated that complete dechlorination of TCPy was achieved since the theoretical release of chloride from 10 mg/L of TCPy after complete dechlorination is 5.36 mg/L.

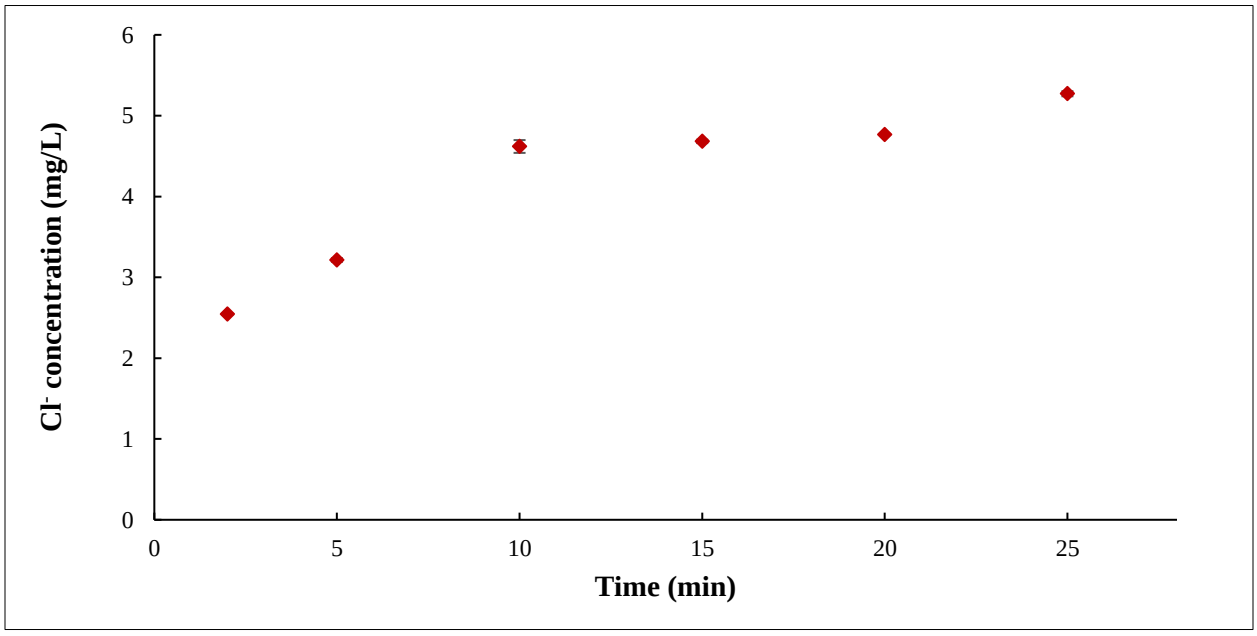

Figure 55: Chloride release during the oxidation of TCPy by ZVI/PS system.

The released of chloride ions during the reaction in the heat-activated PS system was measured and is presented in Figure 56. As shown in the figure, the release of chloride ions increased during the reaction. Complete dechlorination of TCPy was achieved after 15 minutes of reaction. TCPy dechlorination in heat-activated PS is faster than the ZVI/PS system.

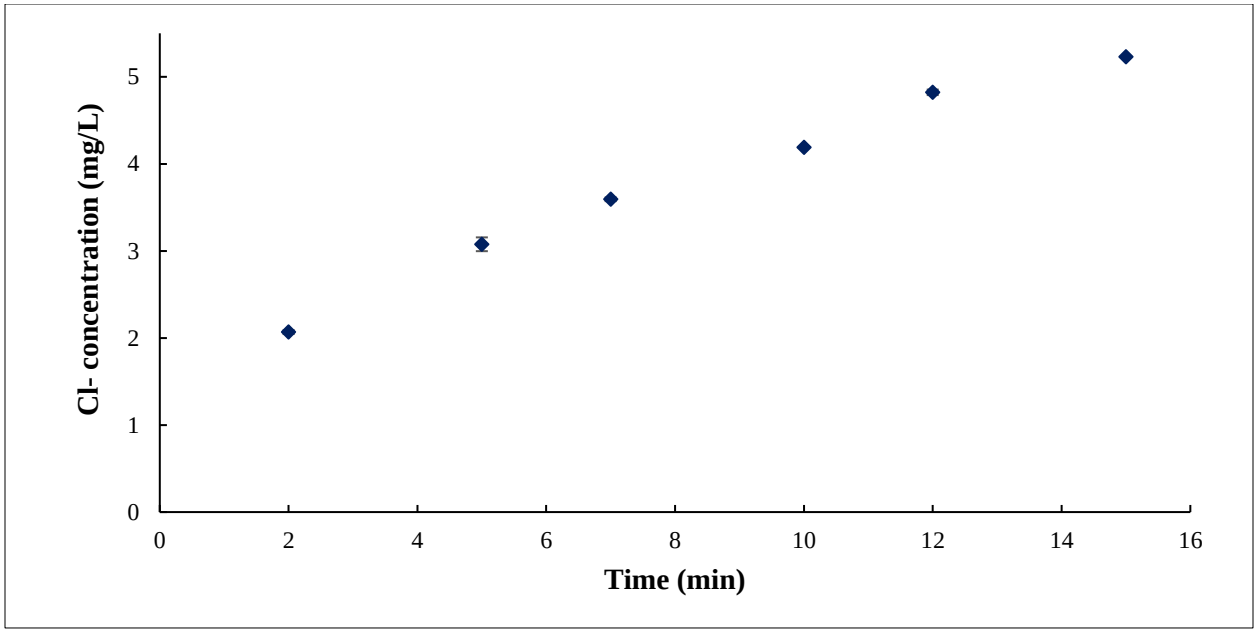

Figure 56: Chloride release during the oxidation of TCPy by heat activated PS.

Interaction of SR with TCPy

It was reported that the interaction of SR with aromatic compounds results in the formation of carbon-centered radicals by electron transfer from the organic compound to the SR [48]. Therefore, the reaction of sulfate radical with TCPy would involve an addition of sulfate radical to C_2- C_6 position in an unstable form. Then, the elimination of the sulfate group which is a good

leaving group, would result in the formation of the hydroxycyclohexadienyl-like radical, followed by hydroxylation through hydrolysis (Figure 57).

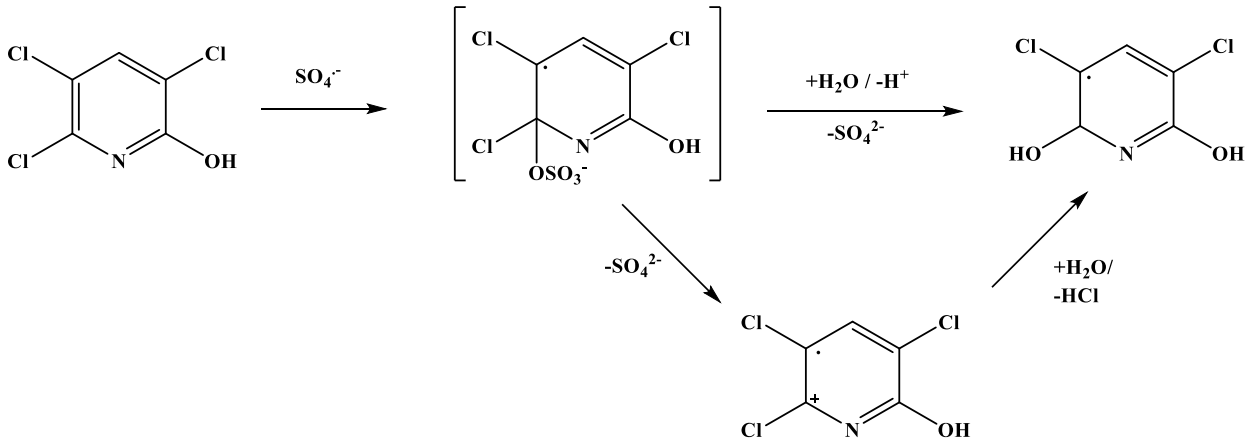

Figure 57: Sulfate radical attack on TCPy.

In order to understand the role of sulfate anion radicals in the reaction with TCPy, theoretical calculations were conducted to examine the free energies for the initial reaction step involving the addition of SR to the TCPy. There are five sites on the pyridine ring which SR can attack to form a hydroxycyclohexadienyl-like structure as shown as shown in Figure 58. The corresponding relative energies of the resulting five radicals are summarized in Table 12. The results indicate that SR additions *ipso* to Cl at the C_6, C_5, and C_3 positions are thermodynamically favorable with $\Delta G < 0$; their calculated free energy changes are -9.260645, -6.9432875, and -2.4830175 kcal mol^{-1}, respectively. According to the calculated free energies, the most preferred attack by SR is at the C_6 position. The observed result is in accordance with Dell'Arciprete, *et al.*, who studied the reaction of SR with substituted pyridines and concluded that the *para* and *ortho* positions to the substituent and to the nitrogen, respectively, are the preferred sites of SR attack to

the pyridine ring [49]. In TCPy, the addition of SR at the C_5 position is the second-most preferred position followed by SR addition in the C_3 position. However, the addition reactions of TCPy and SR in both the C_2 and the C_4 position are thermodynamically unfavorable with $\Delta G > 0$. The stability of the radicals formed according to the calculations follow the order I > II > IV> III > V.

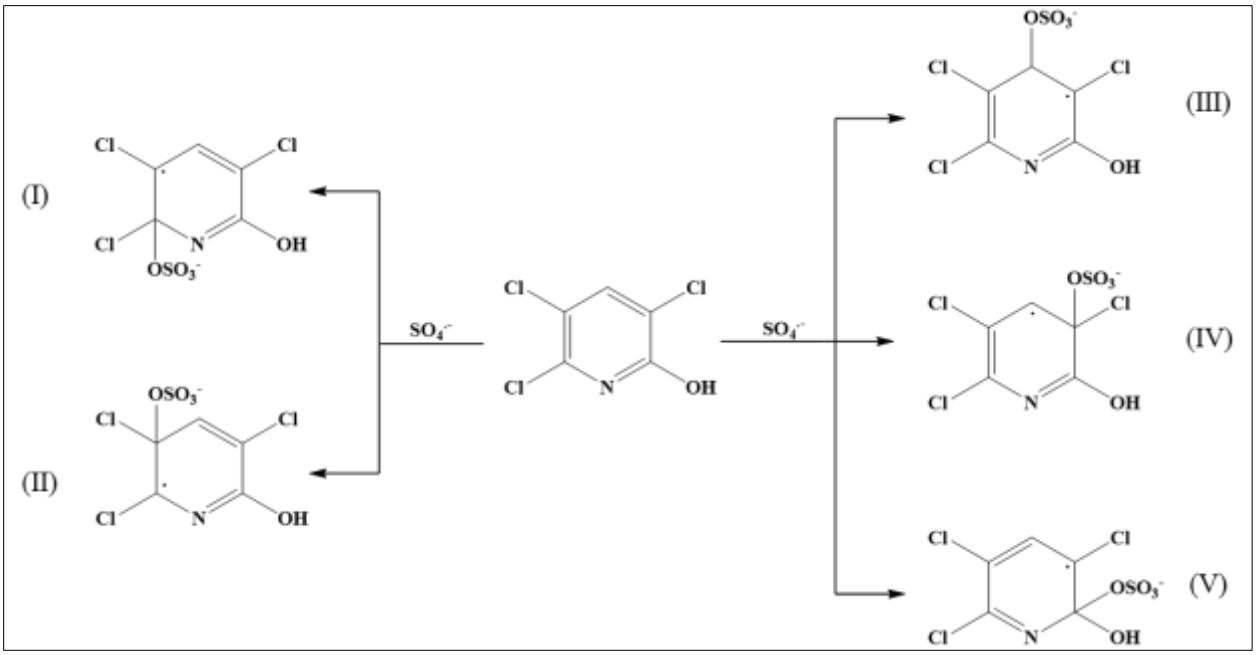

Figure 58: The initial step of SR addition to TCPy.

Table 12:The thermodynamic properties for the addition of SR to TCPy.

Position	ΔG (kcal mol^{-1})	ΔG (kJ mol^{-1})	ΔH (kcal mol^{-1})	ΔH (kJ mol^{-1})
I	-9.260645	-38.74653868	-58.8638925	-246.2865262
II	-6.9432875	-29.0507149	-17.372965	-72.68848556
III	15.27837	63.92470008	3.5391	14.8075944
IV	-2.4830175	-10.38894522	-12.5719625	-52.6010911
V	10.75786	45.01088624	-1.8442225	-7.71622694

The Degradation Pathway for TCPy by Heat and ZVI Activated PS Systems

As mentioned previously, the addition of SR to aromatic compounds leads to the formation of carbon-centered radicals through electron transfer from the organic compound to the SR[48]. Therefore, we predicted the formation of 3,5-dichloro-2,6-dihydroxypyridine, 3,6-dichloro-2,5-dihydroxypyridine or 5,6-dichloro-2,3-dihydroxypyridine as initial transformation products.

Experimentally, 5,6-dichloro-2,3-dihydroxypyridine was identified as one of the major transformation products. This compound was also detected as a byproduct in the photolytic and photocatalytic degradation of TCP in water by Žabar, *et al.* [9]. Feng, *et al.* also identified 3,5-dichloro-2,6-dihydroxypyridine and 3,6-dichloro-2,5-dihydroxypyridine in addition to 5,6-dichloro-2,3-dihydroxypyridine as byproducts of photolytic degradation of TCPy [50]. However, no experimental evidence for the formation of 3,5-dichloro-2,6-dihydroxypyridine or 3,6-dichloro-2,5-dihydroxypyridine was observed in this study. Since the latter compounds were not observed in this experiment, the formation of the observed 3,5-dichloro-2-hydroxypyridne and 3,6-dichloro-2-hydroxypyridne could be due to the hydrodechlorination of TCPy.

According to the experimentally identified byproducts, the possible degradation pathway of TCPy by ZVI/PS is proposed in Figure 59. Several possible pathways exist to produce the observed formamide and succinic acid. The reaction of TCPy with water (hydrolysis) results in the formation of 5,6-dichloro-2,3-dihydroxypyridine (II) via nucleophilic substitution on position C_3. The dechlorination of (II) on position C_6 results in the formation of 5-chloro-2,3-dihydroxypyridine (V) followed by dechlorination-hydroxylation processes to form (VI). The hydrodechlorination of (I) results in the formation of (III) and (IV), followed by sequential to form (VI). Also, (III) can be formed from hydrodechlorination of II. (VI) in turn is converted to succinic acid and formamide. While the detail of this mechanism is unclear, the formation of succinic acid and formamide suggests a possible retrograde [4+2] cycloaddition (i.e., reverse Diels-Alder) reaction. The formamide decomposes in water to produce formic acid and ammonia which converts to nitrate[51] while formic acid is further converted to carbon dioxide and water. Although (VI) was not observed in ZVI/PS system, it was observed in heat activated PS system. Based on that and on the calculation study, it was predicted to be formed in ZVI/PS before the ring cleavage.

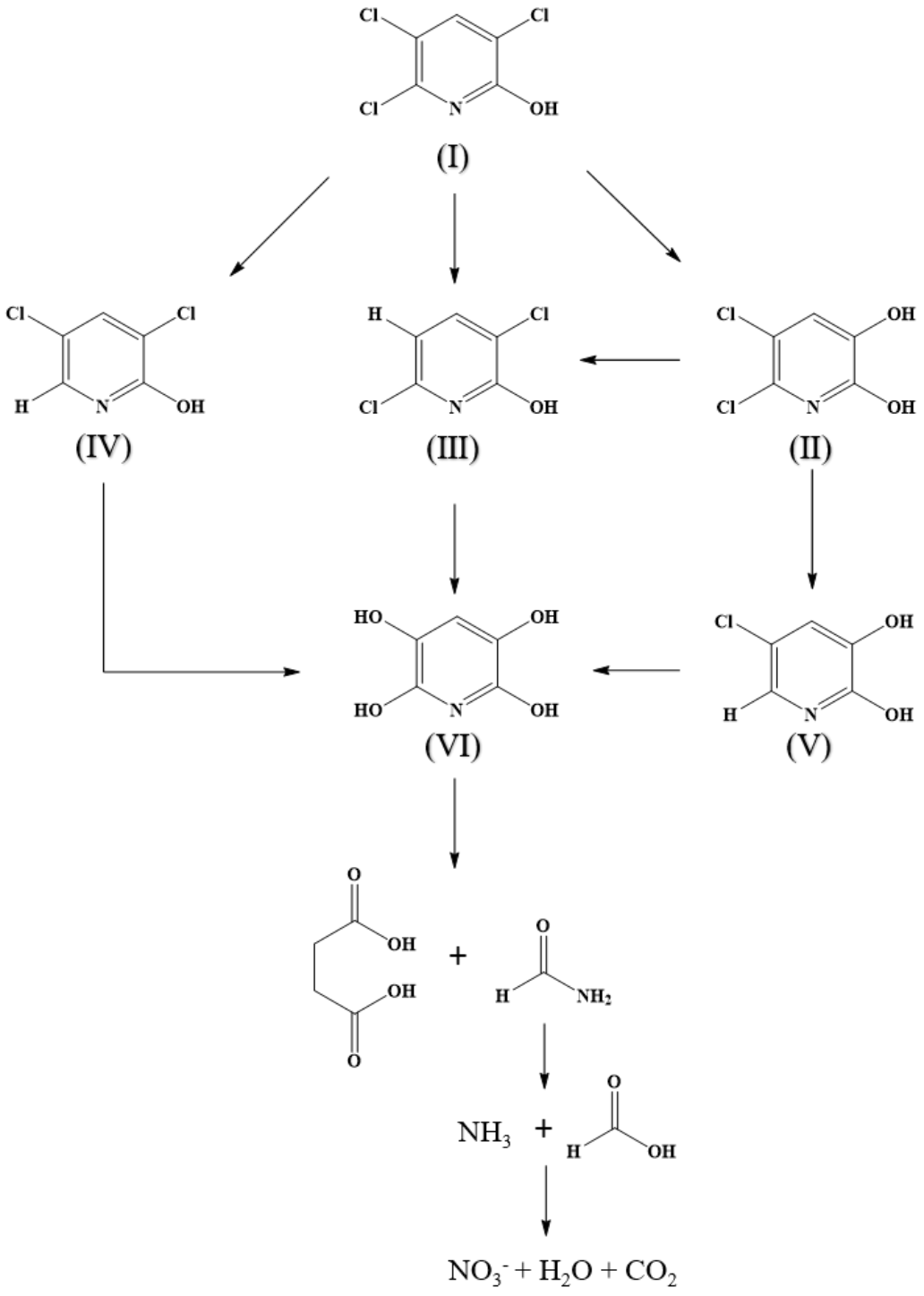

Figure 59: Degradation pathway of TCPy in ZVI/PS system.

Gaussian 09 molecular orbital calculation software with B3LYP functional was used to calculate the free energies (ΔG) of the reaction to track the oxidation pathways of TCPy by SR before ring cleavage. The results of calculated ΔG as presented in Table 13 agree with the experimental pathway. According to the calculated free energy, the main pathway of the degradation of TCPy is (I→III→VI) since it has the lowest ΔG values compared to other pathways.

Table 13: ΔG data of the reaction calculated with Gaussian 09 software with B3LYP method for TCPy and its degradation products in ZVI/PS system.

Reactant → Product	ΔG (kcal/mol)
I→II	-16.3
I→III	-28.3
I→IV	-26.3
II→V	-24.9
II→III	-11.9
V→VI	-7.5
III→VI	-20.4
IV→VI	-22.4

In the heat-activated PS system, there was no detectable formation of 3,5-dichloro-2,6-dihydroxypyridine, 3,6-dichloro-2,5-dihydroxypyridine, or succinic acid. Therefore, the degradation pathway of TCPy by the heat-activated PS system is slightly different than the ZVI/PS system. The hydrolysis of TCPy results in the formation of 5,6-dichloro-2,3-dihydroxypyridine (II) via nucleophilic substitution on position C3, followed by sequential hydrolysis steps to form

III which in turn is converted to fumaric acid and formamide. Although formamide was not observed in this system, the formation of formic acid is predicted as a result of formamide hydrolysis. While the detail of this mechanism is unclear, the formation of fumaric acid suggests a possible retrograde [4+2] cycloaddition (*i.e.*, reverse Diels-Alder) reaction. Formamide decomposes in water to produce formic acid and ammonia, which converts to nitrate,[51] while formic acid is further converted to carbon dioxide and water. The proposed degradation pathway of TCPy by heat activated persulfate is presented in Figure 60.

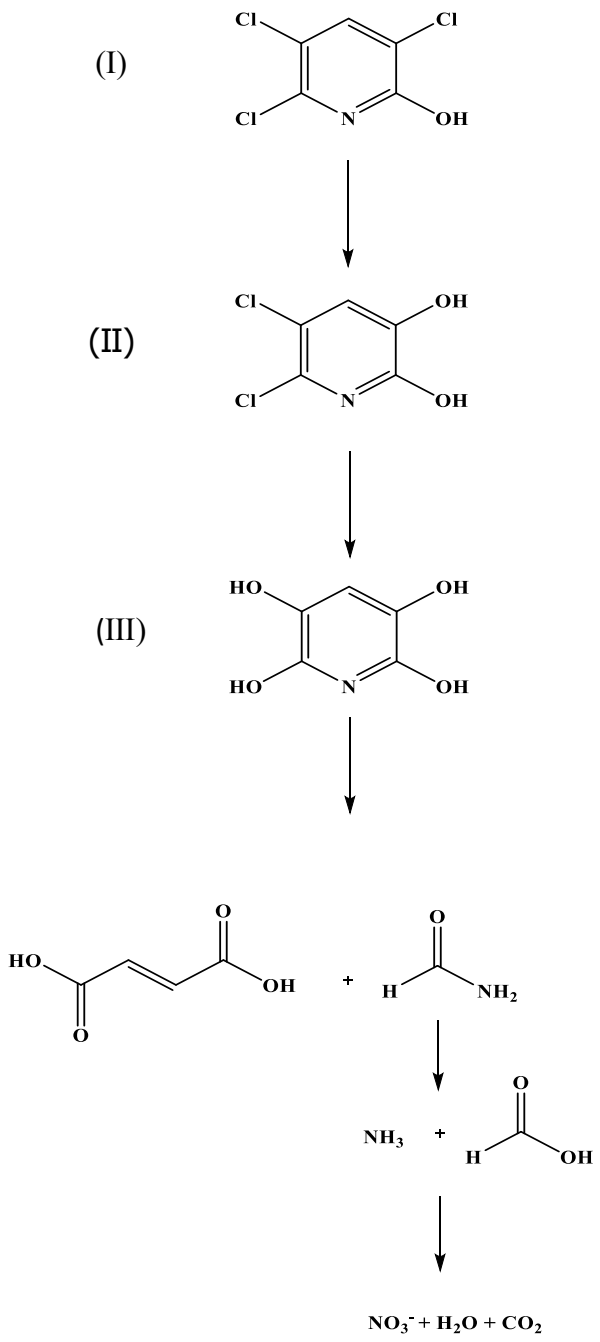

Figure 60: Degradation pathway of TCPy by heat activated PS system.

Conclusion

Transformation products during the degradation of TCPy by heat- and iron-activated persulfate systems were identified by GC-MS. Results show the number of transformation products detected during TCPy degradation in the ZVI/PS system was higher compared to the transformation products observed in the heat-activated PS system. Gaussian 09 molecular orbital calculation software with B3LYP functional was used to calculate the free energies (ΔG) of the reaction to track the oxidation pathways of TCPy by SR. The transformation intermediates and by-products of TCPy oxidation by ZVI/PS and thermally-activated persulfate were proposed and showed agreement with the theoretical DFT calculations of the free energy values for oxidation reactions of the systems. The initial reaction step involving the addition of SR to TCPy was investigated based on theoretical calculations. Results indicate that the SR addition *ipso* to Cl in the C_6, C_5, or C_3 position is thermodynamically favorable with $\Delta G < 0$. However, the addition reactions of TCPy and SR at both the C_2 and C_4 positions are thermodynamically unfavorable with $\Delta G > 0$. The release of chloride ions during the reaction in both systems was measured and results indicated that complete dechlorination of TCPy was achieved.

APPENDIX A: SUPPORTING INFORMATION FOR CHAPTER TWO

Table 14: The BBD design matrix and experimental results for TCPy degradation by ZVI/PS after 25 minutes reaction.

Run	Independent variables (coded)			Response	
	PS (mM)	pH	ZVI (g/L)	TCPy removal (100%)	Mineralization (ΔTOC) (%)
1	0	1	-1	32.6	7.80
2	0	0	0	54.3	28.1
3	0	-1	-1	100	32.1
4	0	0	0	53.9	28.4
5	1	0	1	33.4	15.3
6	0	0	0	54.6	27.6
7	1	-1	0	100	31.2
8	0	0	0	54.1	28.6
9	0	-1	1	96.7	31.4
10	0	0	0	54.7	28.3
11	0	1	1	85.6	13.2
12	1	1	0	20.9	8.02
13	-1	1	0	25.5	5.7
14	1	0	-1	48.5	17.2
15	-1	0	1	51.2	4.0
16	-1	0	-1	47.8	5.80
17	-1	-1	0	88.1	9.30

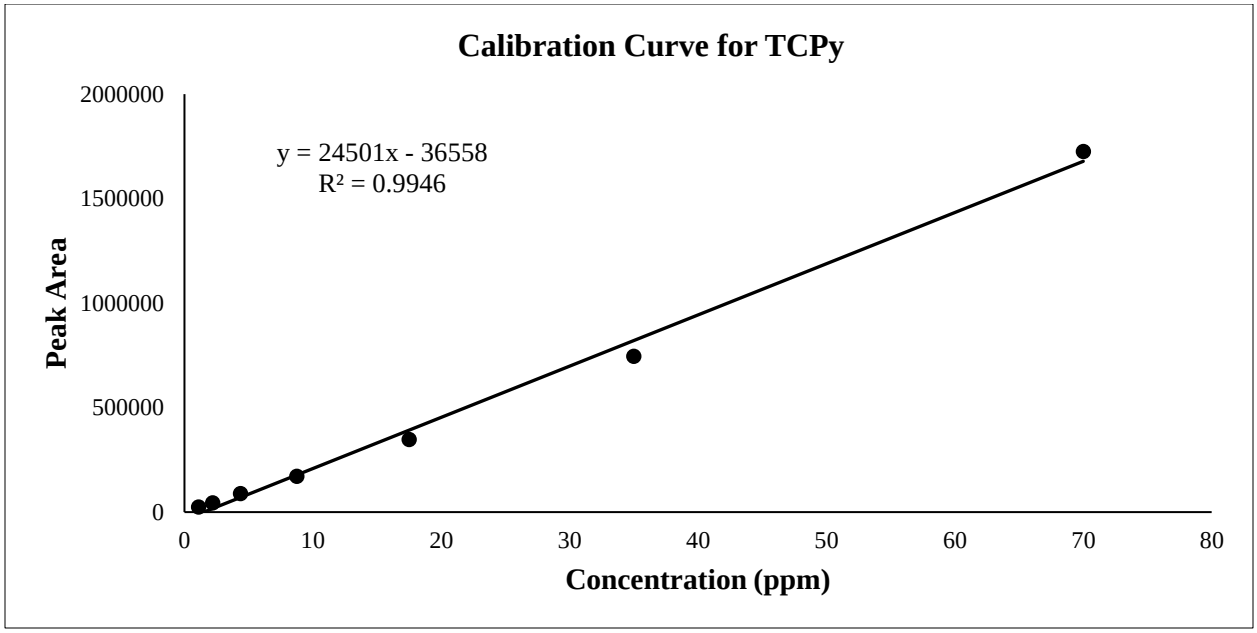

Figure 61: Calibration curve for TCPy.

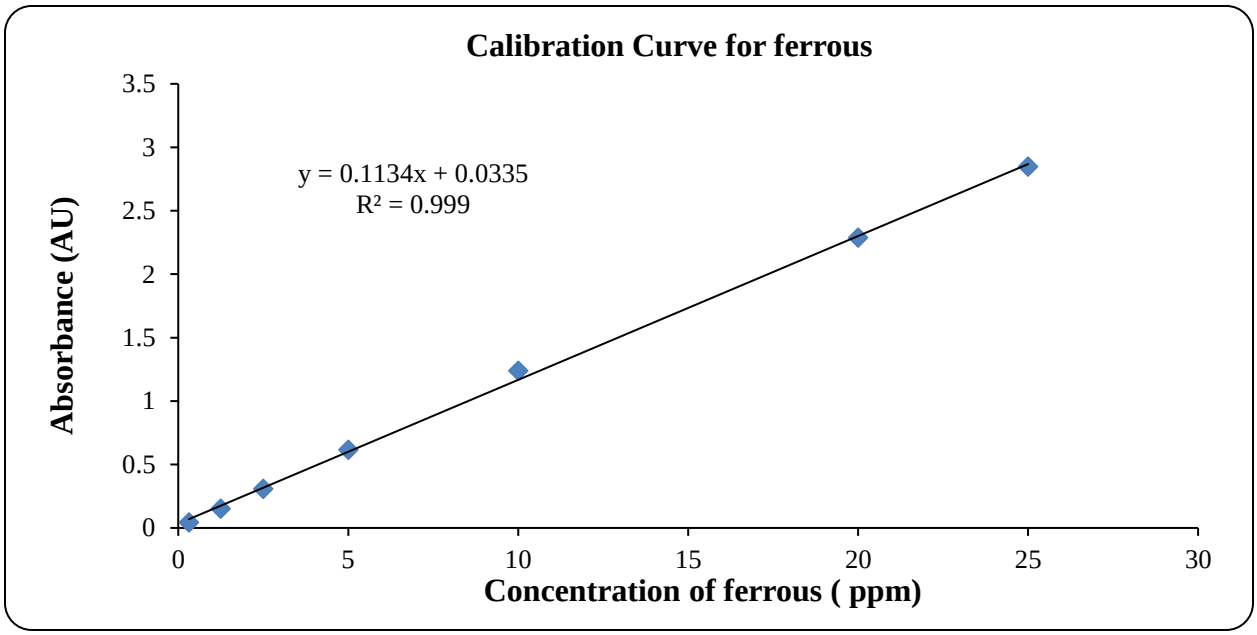

Figure 62: Calibration curve for ferrous.

APPENDIX B: SUPPORTING INFORMATION FOR CHAPTER THREE

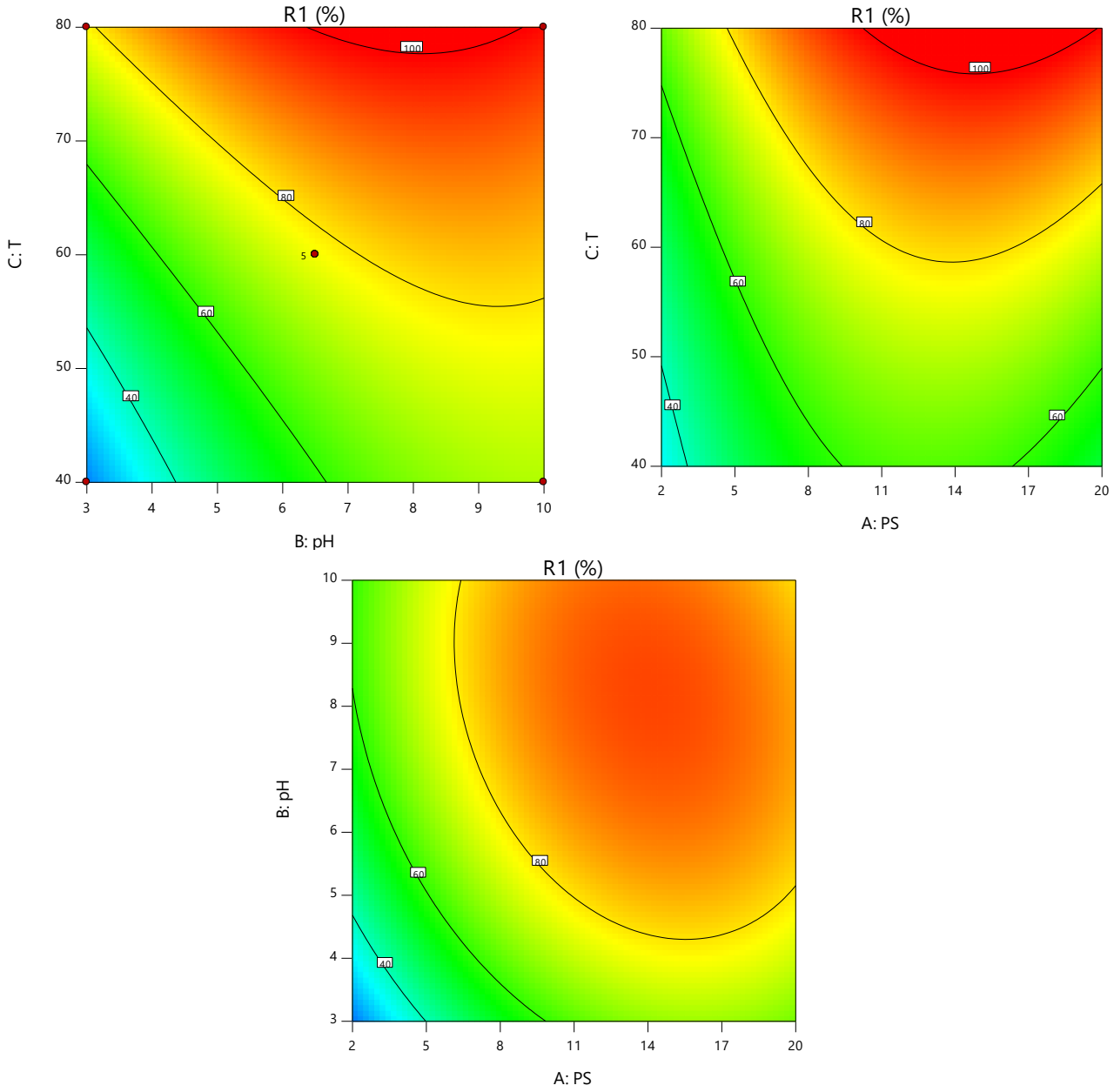

Figure 63: Contour plots of TCPy mineralization at 30 min reaction: the effect of T and pH, T and PS, and pH and PS.

APPENDIX C: SUPPORTING INFORMATION FOR CHAPTER FIVE

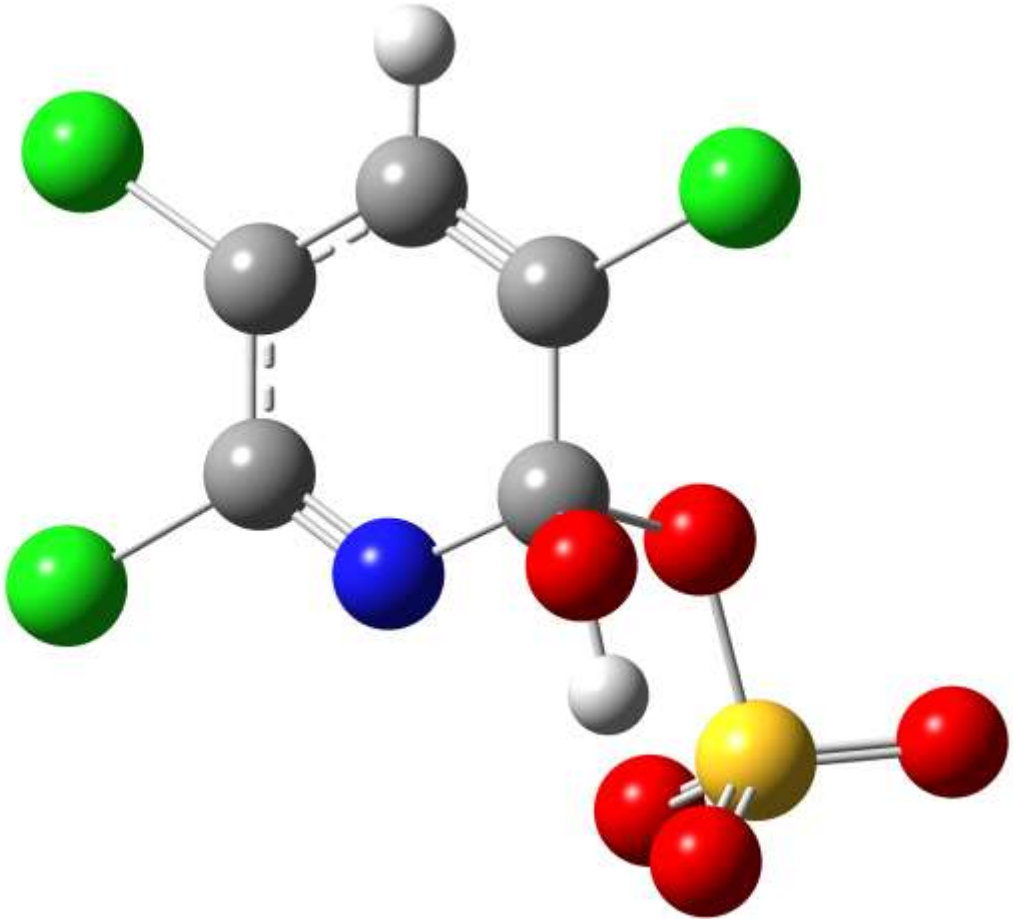

Figure 64: Optimized confirmation of TCPy with sulfate radical in C2.

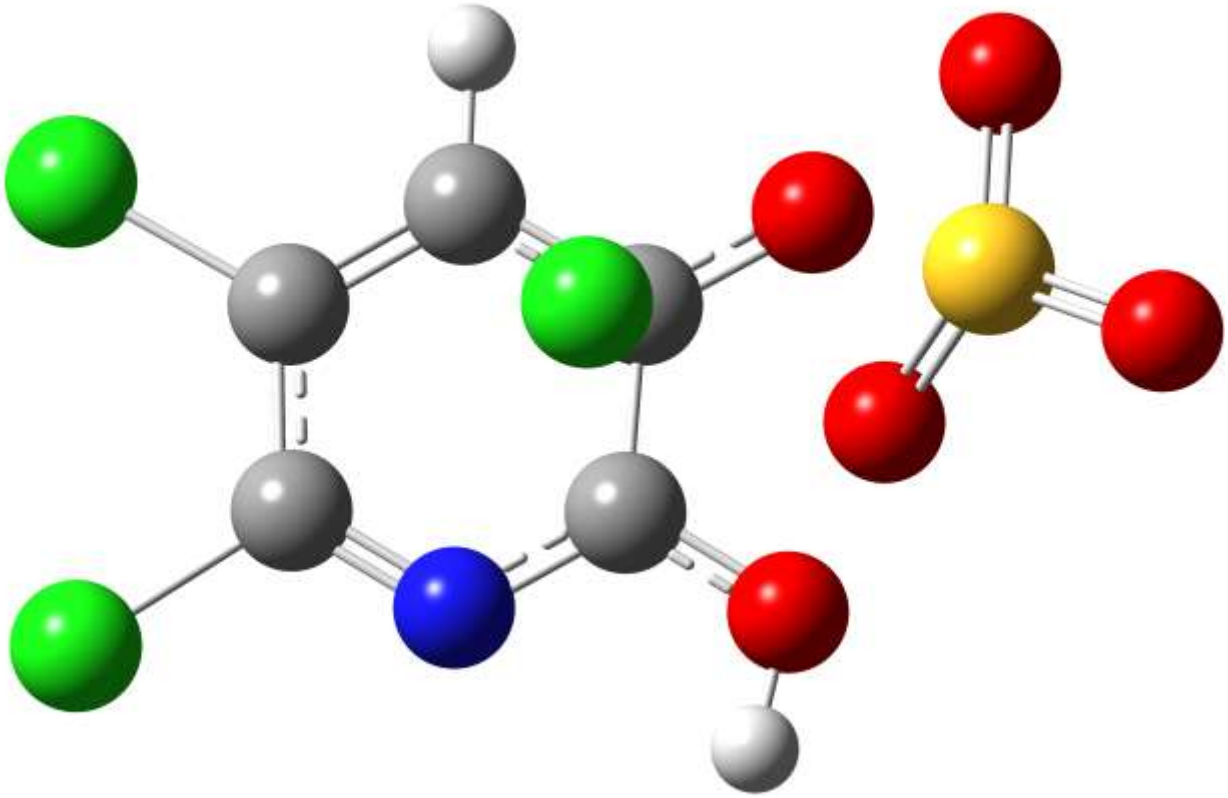

Figure 65: Optimized confirmation of TCPy with sulfate radical in C3.

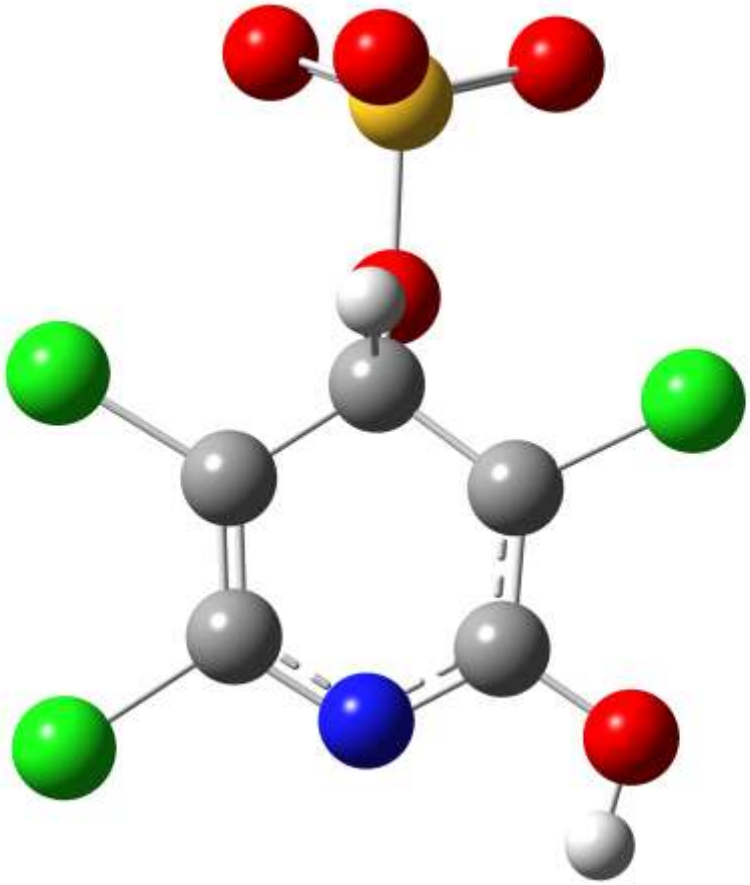

Figure 66: Optimized confirmation of TCPy with sulfate radical in C4.

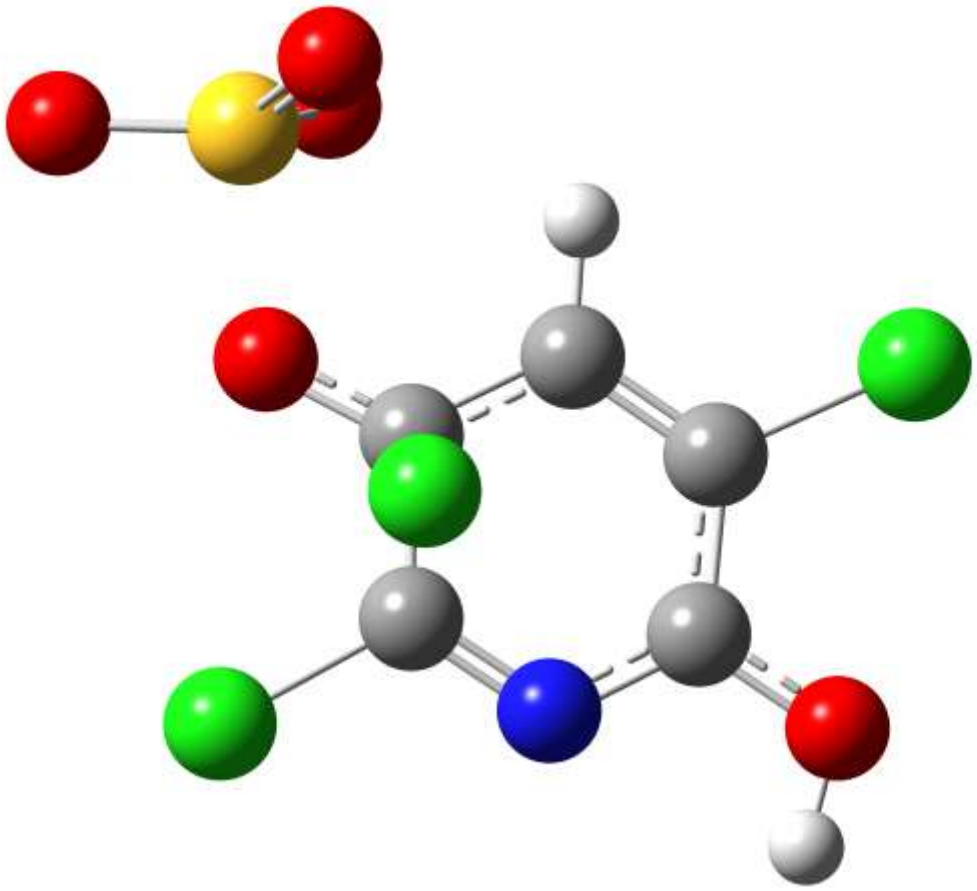

Figure 67: Optimized confirmation of TCPy with sulfate radical in C5.

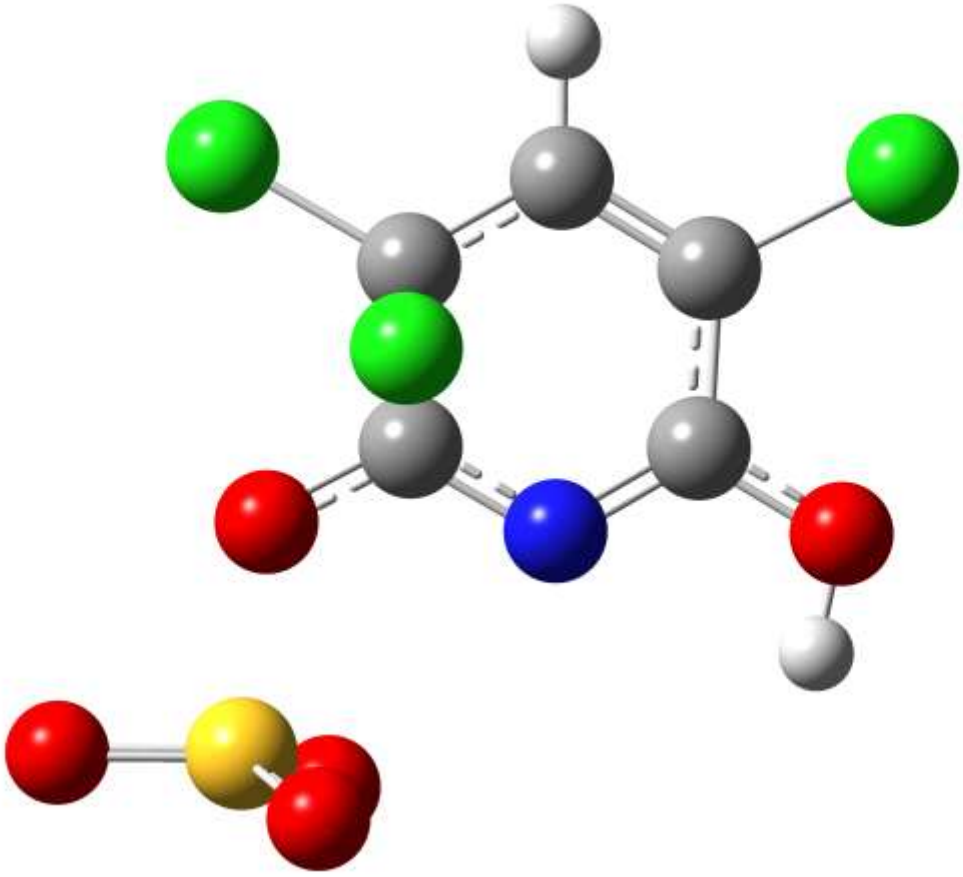

Figure 68: Optimized confirmation of TCPy with sulfate radical in C6.

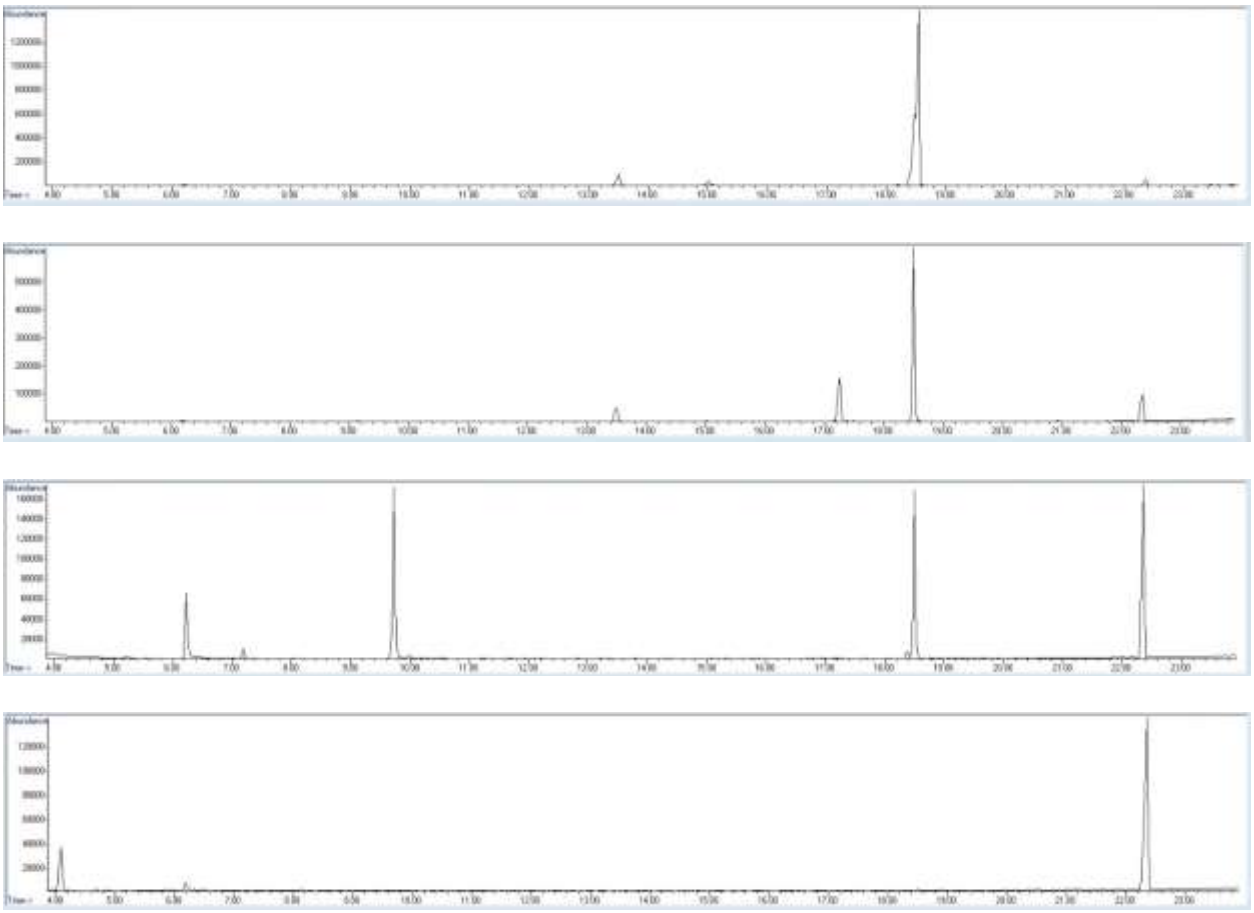

Figure 69: GC-MS chromatogram after one hour, two hours, three hours and six hours of TCPy treatment with ZVI/PS.

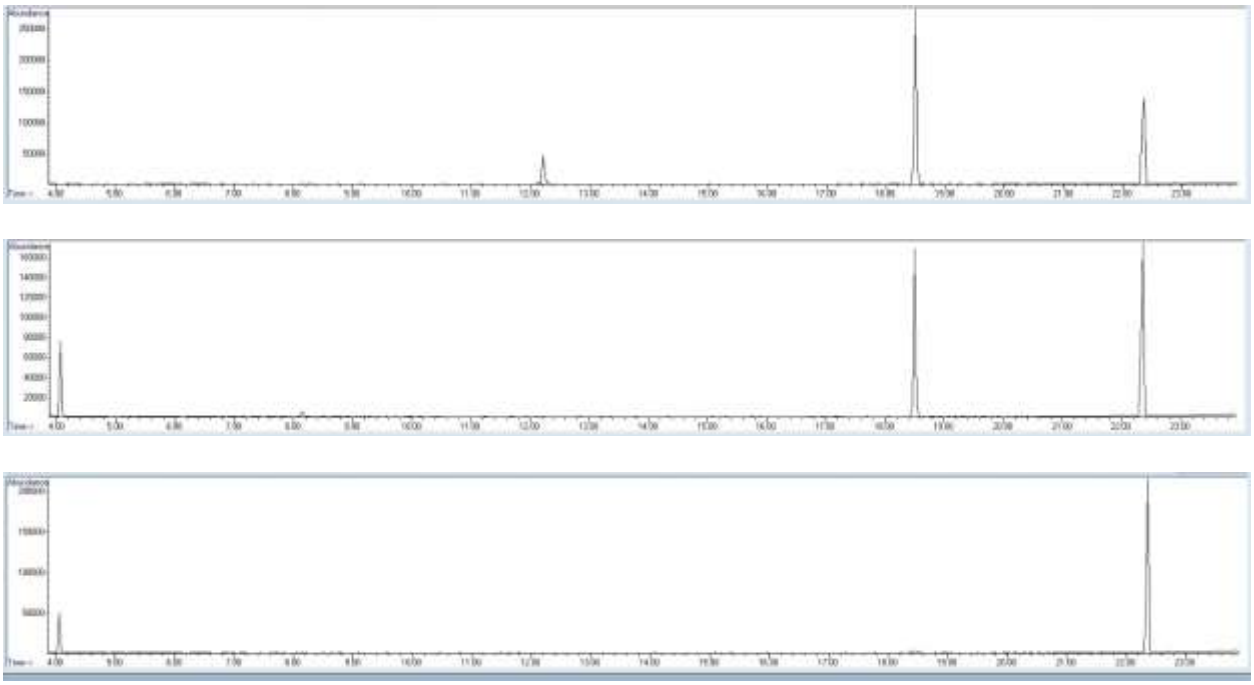

Figure 70: GC-MS chromatogram after 30 minutes, one hour and three hours for TCPy treatment with heat activated PS.

REFERENCES

1. Minton, N. A.; Murray, V. S., A review of organophosphate poisoning. *Medical toxicology and adverse drug experience* **1988,** *3* (5), 350-375.

2. AChE, D. R., Organophosphate Insecticides.

3. Grube, A.; Donaldson, D.; Kiely, T.; Wu, L., Pesticides industry sales and usage. *US EPA, Washington, DC* **2011**.

4. Organization, W. H., Organophosphorus insecticides: a general introduction. **1986**.

5. Alavanja, M. C.; Samanic, C.; Dosemeci, M.; Lubin, J.; Tarone, R.; Lynch, C. F.; Knott, C.; Thomas, K.; Hoppin, J. A.; Barker, J., Use of agricultural pesticides and prostate cancer risk in the Agricultural Health Study cohort. *American journal of epidemiology* **2003,** *157* (9), 800-814.

6. Lee, W. J.; Blair, A.; Hoppin, J. A.; Lubin, J. H.; Rusiecki, J. A.; Sandler, D. P.; Dosemeci, M.; Alavanja, M. C., Cancer incidence among pesticide applicators exposed to chlorpyrifos in the Agricultural Health Study. *Journal of the National Cancer Institute* **2004,** *96* (23), 1781-1789.

7. EPA, Chlorpyrifos: Revised Human Health Risk Assessment for Registration Review. **2016**.

8. Khalid, S.; Hashmi, I.; Khan, S. J., Bacterial assisted degradation of chlorpyrifos: The key role of environmental conditions, trace metals and organic solvents. *Journal of environmental management* **2016,** *168*, 1-9.

9. Žabar, R.; Sarakha, M.; Lebedev, A. T.; Polyakova, O. V.; Trebše, P., Photochemical fate and photocatalysis of 3, 5, 6-trichloro-2-pyridinol, degradation product of chlorpyrifos. *Chemosphere* **2016,** *144*, 615-620.

10. USEPA, Interim Registration Eligibility Decision for Chlorpyrifos. United States Environmental Protection Agency
2002; Vol. 738-R-01-007.

11. Amer, S. M.; Aly, F. A., Cytogenetic effects of pesticides. IV. Cytogenetic effects of the insecticides Gardona and Dursban. *Mutation Research/Genetic Toxicology* **1992,** *279* (3), 165-170.

12. Van Emon, J. M.; Pan, P.; van Breukelen, F., Effects of chlorpyrifos and trichloropyridinol on HEK 293 human embryonic kidney cells. *Chemosphere* **2018,** *191*, 537-547.

13. Affam, A. C.; Chaudhuri, M., Degradation of pesticides chlorpyrifos, cypermethrin and chlorothalonil in aqueous solution by TiO2 photocatalysis. *Journal of environmental management* **2013,** *130*, 160-165.

14. Gupta, V. K.; Eren, T.; Atar, N.; Yola, M. L.; Parlak, C.; Karimi-Maleh, H., CoFe2O4@ TiO2 decorated reduced graphene oxide nanocomposite for photocatalytic degradation of chlorpyrifos. *J. Mol. Liq.* **2015,** *208*, 122-129.

15. Zhang, Y.; Xiao, Z.; Chen, F.; Ge, Y.; Wu, J.; Hu, X., Degradation behavior and products of malathion and chlorpyrifos spiked in apple juice by ultrasonic treatment. *Ultrason. Sonochem.* **2010,** *17* (1), 72-77.

16. Samet, Y.; Agengui, L.; Abdelhédi, R., Electrochemical degradation of chlorpyrifos pesticide in aqueous solutions by anodic oxidation at boron-doped diamond electrodes. *Chem. Eng. J.* **2010,** *161* (1-2), 167-172.

17. Ike, I. A.; Linden, K.; Orbell, J. D.; Duke, M., Critical review of the science and sustainability of persulphate advanced oxidation processes. *Chem. Eng. J.* **2018**.

18. Tsitonaki, A.; Petri, B.; Crimi, M.; Mosbæk, H.; Siegrist, R. L.; Bjerg, P. L., In situ chemical oxidation of contaminated soil and groundwater using persulfate: a review. *Critical Reviews in Environmental Science and Technology* **2010,** *40* (1), 55-91.

19. Ji, Y.; Shi, Y.; Kong, D.; Lu, J., Degradation of roxarsone in a sulfate radical mediated oxidation process and formation of polynitrated by-products. *Rsc Advances* **2016,** *6* (85), 82040-82048.

20. Uniyal, S.; Sharma, R. K., Technological advancement in electrochemical biosensor based detection of Organophosphate pesticide chlorpyrifos in the environment: A review of status and prospects. *Biosens. Bioelectron.* **2018**.

21. Liang, C.; Huang, C.-F.; Mohanty, N.; Kurakalva, R. M., A rapid spectrophotometric determination of persulfate anion in ISCO. *Chemosphere* **2008,** *73* (9), 1540-1543.

22. APHA, *Standard Methods for the Examination of Water and Wastewater*. 20 ed.; American Public Health Association: Washington, DC, 1998.

23. Wei, X.; Gao, N.; Li, C.; Deng, Y.; Zhou, S.; Li, L., Zero-valent iron (ZVI) activation of persulfate (PS) for oxidation of bentazon in water. *Chem. Eng. J.* **2016,** *285*, 660-670.

24. Ghauch, A.; Ayoub, G.; Naim, S., Degradation of sulfamethoxazole by persulfate assisted micrometric Fe0 in aqueous solution. *Chem. Eng. J.* **2013,** *228*, 1168-1181.

25. Hussain, I.; Zhang, Y.; Huang, S.; Du, X., Degradation of p-chloroaniline by persulfate activated with zero-valent iron. *Chem. Eng. J.* **2012,** *203*, 269-276.

26. Matzek, L. W.; Carter, K. E., Activated persulfate for organic chemical degradation: a review. *Chemosphere* **2016,** *151*, 178-188.

27. Liang, C.; Su, H.-W., Identification of sulfate and hydroxyl radicals in thermally activated persulfate. *Ind Eng Chem Res* **2009,** *48* (11), 5558-5562.

28. Wang, Y.; Chen, S.-y.; Yang, X.; Huang, X.-f.; Yang, Y.-h.; He, E.-k.; Wang, S.; Qiu, R.-l., Degradation of 2, 2′, 4, 4′-tetrabromodiphenyl ether (BDE-47) by a nano zerovalent iron-activated persulfate process: The effect of metal ions. *Chem. Eng. J.* **2017,** *317*, 613-622.

29. Teh, C. C.; Ibrahim, N. A.; Yunus, W. M. Z. W., Response surface methodology for the optimization and characterization of oil palm mesocarp fiber-graft-poly (butyl acrylate). *BioResources* **2013,** *8* (4), 5244-5260.

30. Kusic, H.; Peternel, I.; Koprivanac, N.; Loncaric Bozic, A., Iron-activated persulfate oxidation of an azo dye in model wastewater: influence of iron activator type on process optimization. *J Environ Eng* **2010,** *137* (6), 454-463.

31. Li, J.; Liu, J.; Shen, W.; Zhao, X.; Hou, Y.; Cao, H.; Cui, Z., Isolation and characterization of 3, 5, 6-trichloro-2-pyridinol-degrading Ralstonia sp. strain T6. *Bioresour. Technol.* **2010,** *101* (19), 7479-7483.

32. Nam, S.-N.; Cho, H.; Han, J.; Her, N.; Yoon, J., Photocatalytic degradation of acesulfame K: Optimization using the Box–Behnken design (BBD). *Process Safety and Environmental Protection* **2018,** *113*, 10-21.

33. Yuan, R.; Ramjaun, S. N.; Wang, Z.; Liu, J., Effects of chloride ion on degradation of Acid Orange 7 by sulfate radical-based advanced oxidation process: implications for formation of chlorinated aromatic compounds. *J. Hazard. Mater.* **2011,** *196*, 173-179.

34. Lutze, H. V.; Kerlin, N.; Schmidt, T. C., Sulfate radical-based water treatment in presence of chloride: formation of chlorate, inter-conversion of sulfate radicals into hydroxyl radicals and influence of bicarbonate. *Water Res.* **2015,** *72*, 349-360.

35. Alegre, M. L.; Gerones, M.; Rosso, J. A.; Bertolotti, S. G.; Braun, A. M.; Martire, D. O.; Gonzalez, M. C., Kinetic study of the reactions of chlorine atoms and Cl2•-radical anions in aqueous solutions. 1. Reaction with benzene. *The Journal of Physical Chemistry A* **2000,** *104* (14), 3117-3125.

36. Ma, J.; Yang, Y.; Jiang, X.; Xie, Z.; Li, X.; Chen, C.; Chen, H., Impacts of inorganic anions and natural organic matter on thermally activated persulfate oxidation of BTEX in water. *Chemosphere* **2018,** *190*, 296-306.

37. Deng, J.; Shao, Y.; Gao, N.; Deng, Y.; Zhou, S.; Hu, X., Thermally activated persulfate (TAP) oxidation of antiepileptic drug carbamazepine in water. *Chem. Eng. J.* **2013,** *228*, 765-771.

38. Qi, C.; Liu, X.; Ma, J.; Lin, C.; Li, X.; Zhang, H., Activation of peroxymonosulfate by base: implications for the degradation of organic pollutants. *Chemosphere* **2016,** *151*, 280-288.

39. Espenson, J. H., *Chemical kinetics and reaction mechanisms*. Citeseer: 1995; Vol. 102.

40. Ghauch, A.; Tuqan, A. M.; Kibbi, N., Ibuprofen removal by heated persulfate in aqueous solution: a kinetics study. *Chem. Eng. J.* **2012,** *197*, 483-492.

41. Liang, C.; Bruell, C. J., Thermally activated persulfate oxidation of trichloroethylene: experimental investigation of reaction orders. *Ind Eng Chem Res* **2008,** *47* (9), 2912-2918.

42. Fogler, H. S., Elements of chemical reaction engineering. **1999**.

43. Li, H.; Zhang, Y.; Wan, J.; Xiao, H.; Chen, X., Theoretical investigation on the oxidation mechanism of dibutyl phthalate by hydroxyl and sulfate radicals in the gas and aqueous phase. *Chem. Eng. J.* **2018,** *339*, 381-392.

44. Caregnato, P.; David Gara, P. M.; Bosio, G. N.; Gonzalez, M. C.; Russo, N.; Michelini, M. d. C.; Mártire, D. O., Theoretical and experimental investigation on the oxidation of gallic acid by sulfate radical anions. *The Journal of Physical Chemistry A* **2008,** *112* (6), 1188-1194.

45. Qu, X.; Zhang, Q.; Wang, W., Degradation mechanism of benzene by NO3 radicals in the atmosphere: A DFT study. *Chem. Phys. Lett.* **2006,** *426* (1-3), 13-19.

46. An, T.; Gao, Y.; Li, G.; Kamat, P. V.; Peller, J.; Joyce, M. V., Kinetics and mechanism of• OH mediated degradation of dimethyl phthalate in aqueous solution: experimental and theoretical studies. *Environ. Sci. Technol.* **2013,** *48* (1), 641-648.

47. Li, R.; He, L.; Zhou, T.; Ji, X.; Qian, M.; Zhou, Y.; Wang, Q., Simultaneous determination of chlorpyrifos and 3, 5, 6-trichloro-2-pyridinol in duck muscle by modified QuEChERS coupled to gas chromatography tandem mass spectrometry (GC-MS/MS). *Anal Bioanal Chem* **2014,** *406* (12), 2899-2907.

48. Anipsitakis, G. P.; Dionysiou, D. D.; Gonzalez, M. A., Cobalt-mediated activation of peroxymonosulfate and sulfate radical attack on phenolic compounds. Implications of chloride ions. *Environ. Sci. Technol.* **2006,** *40* (3), 1000-1007.

49. Dell'Arciprete, M. L.; Cobos, C. J.; Furlong, J. P.; Mártire, D. O.; Gonzalez, M. C., Reactions of sulphate radicals with substituted pyridines: a structure–reactivity correlation analysis. *ChemPhysChem* **2007,** *8* (17), 2498-2505.

50. Feng, Y.; Minard, R. D.; Bollag, J. M., Photolytic and microbial degradation of 3, 5, 6-trichloro-2-pyridinol. *Environmental Toxicology and Chemistry: An International Journal* **1998,** *17* (5), 814-819.

51. Low, G. K.; McEvoy, S. R.; Matthews, R. W., Formation of nitrate and ammonium ions in titanium dioxide mediated photocatalytic degradation of organic compounds containing nitrogen atoms. *Environ. Sci. Technol.* **1991,** *25* (3), 460-467.